

# FEEDBACKS BETWEEN VEGETATION AND RAINFALL IN THE AMAZON BASIN

## A complex network approach

### DISSERTATION

zur Erlangung des akademischen Grades

Doctor rerum naturalium

(Dr. rer. nat.)

im Fach Geographie

eingereicht an der

Mathematisch-Naturwissenschaftlichen Fakultät

der Humboldt-Universität zu Berlin

von

**Dipl.-Agr.-Ing. Delphine Clara Zemp**

Präsident der Humboldt-Universität zu Berlin:

Prof. Dr. Jan-Hendrik Olbertz

Dekan der Mathematisch-Naturwissenschaftlichen Fakultät:

Prof. Dr. Elmar Kulke

Gutachter/innen:

1. PD Dr. Dieter Gerten
2. Dr. Gilvan Sampaio de Oliveira
3. Prof. Dr. A.J. (Han) Dolman

Tag der Abgabe: 20.10.2015

Tag der mündlichen Prüfung: 19.04.2016

## Acknowledgements

Firstly, I would like to express my sincere gratitude to Anja Rammig, my research supervisor, for her continuous support and valuable advice during my PhD studies and for her constructive suggestions to improve the different chapters in this thesis. I would like also to thank Gilvan Sampaio for advice and support during my stay at the National Institute for Space Research in Brazil and for being a referee for this thesis. I am grateful to the other members of my PhD committee: Patrick Hostert, Dieter Gerten, Han Dolman and Christoph Schneider.

Carl-Friedrich Schlessner deserves very special thanks for initially designing this PhD project, for valuable contributions to this thesis and for continuous guidance over three years. Special thanks should also be given to Ruud van der Ent, who developed the atmospheric moisture tracking model used in this thesis and who shared with me his script. My grateful thanks are also extended to Henrique Barbosa for fruitful discussions at the University of Sao Paulo, for being always responsive despite his busy agenda and for giving me the opportunity to visit the Amazonian Tall Tower Observatory in the middle of the rainforest for a few days, an experience that I will never forget. I would also like to thank Marina Hirota for sharing her thoughts and knowledge on so many different topics and for welcoming me to the University of Santa Catarina in Florianopolis. I thank Marc Wiederman, Jonathan Donges and Arie Staal for their valuable contributions to the different chapters. I would also like to thank Line Gordon, Lan Wang-Erlandsson and Patrick Keys for welcoming me during a short visit to the Stockholm Resilience Center and for insightful discussions. I thank Carlos Alberto Afonso for his patience and good humor during Portuguese classes. I also thank Kirsten Thonicke and the members of the ECOSTAB group for the great atmosphere in the office and for continuous support.

I was part of the IRTG1740 “Dynamical Phenomena in Complex Networks” funded by the German Research Foundation and led by Jürgen Kurths, which provided me excellent conditions to achieve this multidisciplinary and international research project. Assistance provided by David Hansmann was greatly appreciated. I am also grateful for financial support from the EU-FP7 ROBIN project under grant agreement 283093 for a period of three months.

I wish to thank Liubov Tupikina for inspiring discussions on cascade dynamics and all the rest. I wish to deeply thank Pierre Manceaux for showing me that design can be fun and useful, for his patience and great support but most of all, for being just what he is. Finally, I thank my parents and my sister who are always supportive. I am so glad to have them around me.

## Abstract

The distribution of rainfall and vegetation are closely interconnected in the Amazon basin. Rainforests maintain atmospheric humidity by evapotranspiration, which eventually contributes to regional rainfall but also to rainfall over subtropical South America. A comprehensive understanding of the complex interactions between the terrestrial and atmospheric components of the hydrological cycle that occur as moist air is transported by winds over land is missing. The first aim of this thesis is to fill this gap in knowledge by means of complex network analysis of water fluxes from the sources to the sinks of rainfall on the continent. Using this novel approach, the concept of “cascading moisture recycling” is introduced, defined as moisture recycling on the continent involving “re-evaporation cycles” (evaporation of precipitating moisture in the same location) along the way. A methodological framework is developed to quantify the importance of cascading moisture recycling and to identify key regions where re-evaporation cycles are taking place. Applied to several combinations of observation-based gridded climate data for South America, it reveals, for instance, that the southern part of the Amazon basin is not only a direct source of rainfall for the La Plata basin (as previously thought) but also an intermediary region that re-distributes moisture evaporating from the entire Amazon basin towards the subtropics. This new concept lays the foundation for evaluating the vulnerability of the Amazon forest to environmental perturbations, which is the second aim of this thesis. Land-use and rainfall variability are expected to be intensified at the end of the twenty-first century and may push the south-eastern part of the Amazon forest towards a grass-dominated ecosystem. Such a forest loss would reduce local dry-season evapotranspiration and the resulting moisture supply for down-wind rainfall. In turn, this might erode the resilience of the remaining forest and lead to further forest losses. Using a complex network approach, the concepts of forest resilience and cascading moisture recycling are combined in a data-driven modeling framework. Key regions are identified where deforestation would greatly destabilize the remaining forest, as well as tipping points in dry-season intensification for large-scale self-amplified Amazon forest loss. The findings highlight the need to maintain the diversity and connectivity of forest patches in order to sustain the ecological integrity of the largest remaining tropical forest on Earth.

## Zusammenfassung

Im Amazonasgebiet sind die Verteilung von Niederschlag und Vegetation eng miteinander verknüpft. Die Regenwälder des Amazonasbeckens geben über den Prozess der Evapotranspiration große Mengen Wasserdampf an die Atmosphäre ab. Die erhöhte Luftfeuchtigkeit trägt zu regionaler Niederschlagsbildung und durch Feuchtigkeitstransport auch zu Regenfällen im subtropischen Südamerika bei. Bisher fehlt jedoch ein detailliertes Verständnis für das komplexe Wechselspiel zwischen Biosphäre und Atmosphäre und wie der Transport von feuchter Luft die hydrologischen Prozesse beeinflusst. Daher ist das erste Ziel dieser Arbeit, eine umfassende Analyse der Wasserflüsse durchzuführen und Quellen und Senken des kontinentalen Niederschlags zu identifizieren. Als Analysemethoden werden komplexe Netzwerke verwendet, ein Ansatz, mit dessen Hilfe das neuartige Konzept des "cascading moisture recycling" (CMR) eingeführt wird. CMR wird als vielfache Verdunstung von Niederschlag während des Feuchtigkeitstransports über bewaldeten Gebieten definiert. Dieses Verfahren ermöglicht es, den Anteil von CMR an der Menge des regionalen Niederschlags zu quantifizieren und Schlüsselregionen des CMR zu identifizieren. Die Analyse verschiedener gitterbasierter Klimadaten für Südamerika zeigt, dass der südliche Bereich des Amazonasbeckens nicht nur eine direkte Quelle für Niederschlag im La-Plata Becken ist, sondern auch als "Brückenregion" dient, über die die verdunstete Feuchtigkeit des ganzen Amazonasbeckens auf dem Weg in die Subtropen transportiert wird. Diese Ergebnisse zeigen, dass eine Neubewertung der Vulnerabilität des Amazonasregenwalds unter Umweltveränderungen unabdingbar ist. Dies ist das zweite Ziel der vorliegenden Arbeit. Man nimmt an, dass die zunehmende Intensivierung der Landnutzung, aber auch eine verstärkte Variabilität des Niederschlags gegen Ende des 21. Jahrhunderts, zu tiefgreifenden Ökosystemveränderungen vor allem im südöstlichen Teil des Amazonasgebietes führen könnten. Durch diese Veränderungen könnten große Teile des Regenwaldes in eine Savanne umgewandelt werden. Die damit einhergehenden Verluste an Waldfläche würden die Evapotranspiration während der Trockenzeit stark verringern, und damit auch die vom Wind transportierten Luftfeuchtigkeit. Dies würde wiederum den Niederschlag reduzieren und längere bzw. intensivere Trockenzeiten zur Folge haben, was sich negativ auf die Stabilität der verbleibenden Waldgebiete auswirken und ein Waldsterben verursachen kann. Für die Analyse dieser Zusammenhänge werden ebenfalls komplexe Netzwerke verwendet, um das Konzept der Ökosystem-Resilienz und CMR basierend auf Beobachtungsdaten zu kombinieren. Es werden die Schlüsselregionen, in denen Entwaldung zu einer Destabilisierung der verbleibenden Wald führt, identifiziert und die Möglichkeit eines großflächigen Absterbens des Regenwaldes aufgrund von verlängerter Trockenzeit untersucht. Die Ergebnisse der Untersuchung zeigen, dass die Diversität des Regenwaldes



und die durch den Feuchtigkeitstransport gegebene Konnektivität der Waldgebiete eine wichtige Rolle für die Stabilität und ökologische Integrität dieses Ökosystems spielen.



# Contents

<b>Acknowledgements</b>	<b>ii</b>
<b>Abstract</b>	<b>iii</b>
<b>Zusammenfassung (German)</b>	<b>iv</b>
<b>Contents</b>	<b>vi</b>
<b>List of Figures</b>	<b>xi</b>
<b>List of Tables</b>	<b>xiii</b>
<b>Abbreviations</b>	<b>xv</b>
<b>1 General introduction</b>	<b>1</b>
1.1 The vegetation-rainfall system in the Amazon basin . . . . .	3
1.1.1 Current rainfall and vegetation distribution . . . . .	3
1.1.2 The Amazon forest under threat of climate variability and defor- estation . . . . .	7
1.2 Moisture recycling from a complex network perspective . . . . .	11
1.2.1 Current understanding of moisture recycling in South America . .	11
1.2.2 A new concept: cascading moisture recycling . . . . .	11
1.2.3 The complex network approach to analyze cascading moisture re- cycling . . . . .	12
1.3 Critical transitions in vegetation-rainfall system . . . . .	13
1.3.1 Concepts and definitions . . . . .	13
1.3.2 Shifts in the bioclimatic equilibrium as simulated by coupled models	14
1.3.3 Critical transition in the vegetation with altered rainfall regime . .	15
1.4 Assessing potential cascade dynamics in the Amazon vegetation-rainfall system . . . . .	17
1.4.1 Combining the concepts of forest resilience and cascading moisture recycling . . . . .	17
1.4.2 A complex network approach to investigate the stability of the system . . . . .	18
1.4.3 The benefits and shortcomings of an empirical approach . . . . .	19
1.5 Research questions and structure of the thesis . . . . .	20

1.5.1	Chapter 2 and 3: Analysis of cascading moisture recycling in South America . . . . .	21
1.5.2	Chapter 4: Analysis of self-amplified Amazon forest . . . . .	22
<b>2</b>	<b>Node-weighted measures for complex networks with directed and weighted edges for studying continental moisture recycling</b>	<b>23</b>
2.1	Introduction . . . . .	24
2.2	Preliminaries . . . . .	25
2.3	Definition of measures . . . . .	26
2.3.1	Degree and strength . . . . .	27
2.3.2	Clustering coefficient and motifs . . . . .	27
2.4	Application 1: Benchmark network . . . . .	30
2.5	Application 2: Moisture recycling network . . . . .	31
2.6	Conclusion . . . . .	34
2.7	Acknowledgments . . . . .	35
<b>3</b>	<b>On the importance of cascading moisture recycling in South America</b>	<b>37</b>
3.1	Introduction . . . . .	38
3.2	Methods . . . . .	41
3.2.1	Building moisture recycling networks . . . . .	41
3.2.2	Basic assumptions . . . . .	44
3.2.3	Moisture recycling ratio . . . . .	45
3.2.4	Quantifying cascading moisture recycling . . . . .	49
3.2.5	Complex network analysis . . . . .	49
3.2.6	Similarities and differences between the presented measures . . . . .	51
3.3	Results and discussion . . . . .	51
3.3.1	Comparison of continental and regional moisture recycling ratios with other existing studies . . . . .	51
3.3.2	Importance of cascading moisture recycling . . . . .	53
3.3.3	Complex network analysis . . . . .	54
3.3.4	Moisture recycling from the Amazon basin to the La Plata basin . . . . .	54
3.3.5	Possible impact of land-cover change in the intermediary regions . . . . .	55
3.4	Conclusions . . . . .	56
3.5	Acknowledgements . . . . .	57
<b>4</b>	<b>Self-amplified Amazon forest loss with dry-season intensification</b>	<b>67</b>
4.1	Methods . . . . .	71
4.1.1	Modeling cascading forest loss . . . . .	71
4.1.2	Quantifying cascading effects . . . . .	72
4.1.3	Simple evapotranspiration model on a monthly time scale . . . . .	73
4.1.4	Dry-season intensification scenarios . . . . .	73
<b>5</b>	<b>General conclusion</b>	<b>79</b>
5.1	Achievements . . . . .	79
5.1.1	Complex network analysis for weighted and directed networks . . . . .	79
5.1.2	The new concept of cascading moisture recycling and associated methodological framework . . . . .	80
5.1.3	Cascade dynamics in the complex Amazon vegetation-rainfall system . . . . .	80

5.2	Answers to the research questions . . . . .	80
5.3	Potential further developments . . . . .	83
5.4	Potential further applications . . . . .	84
5.4.1	Effect of inter-annual variability . . . . .	84
5.4.2	Effect of land-use change in tropical South America on continental rainfall . . . . .	85
5.4.3	Continental feedback on oceanic moisture inflow . . . . .	85
5.4.4	Cascading moisture recycling in Eurasia and Africa . . . . .	85
5.4.5	Critical transition in the vegetation-rainfall equilibrium in the Sahara/Sahel . . . . .	86
5.4.6	Effect of temperature and atmospheric CO <sub>2</sub> concentration . . . . .	86
5.5	Perspectives and recommendations . . . . .	87
<b>A Glossary</b>		<b>89</b>
<b>B Supplementary information to the method in chapter 3</b>		<b>91</b>
B.1	Cascading moisture recycling ratios . . . . .	91
B.2	Robustness of the cascading moisture recycling ratios . . . . .	92
B.3	Quantifying cascading moisture recycling . . . . .	93
B.4	Complex network analysis . . . . .	94
B.4.1	Clustering coefficient associated with Middleman motifs . . . . .	94
B.4.2	Optimal pathway . . . . .	96
B.4.3	Betweenness centrality . . . . .	97
<b>C Supplementary figures to chapter 4</b>		<b>99</b>
<b>D Supplementary information to chapter 4</b>		<b>111</b>
D.1	Supplementary Methods . . . . .	111
D.1.1	Cascade model . . . . .	111
D.1.2	Simple empirical evapotranspiration model on a monthly time scale	113
D.1.3	Vegetation Resilience . . . . .	117
D.1.4	Moisture recycling . . . . .	119
D.2	Supplementary Discussion . . . . .	120
D.2.1	Comparison between fit evaluation and data . . . . .	120
D.2.2	Minimum evapotranspiration values . . . . .	121
D.2.3	Effect of deforestation on evapotranspiration . . . . .	121
<b>Bibliography</b>		<b>123</b>



# List of Figures

1.1	Climatology of rainfall, evapotranspiration and moisture recycling for tropical South America for the period 1989-1995 . . . . .	2
1.2	Scheme of structure of the thesis . . . . .	21
2.1	Zonal averages of the standard and n.s.i. versions of the normalized strength and the edge-weighted clustering coefficient applied to the benchmark network model . . . . .	31
2.2	Normalized n.s.i. in-strength and relative decrease of this measure compared to the standard version . . . . .	32
2.3	Normalized n.s.i. out-strength and relative decrease of this measure compared to the standard version . . . . .	33
2.4	N.s.i. edge-weighted and direct clustering coefficients associated with the different network motifs . . . . .	34
2.5	Relative decrease in the edge-weighted clustering coefficient after n.s.i. correction . . . . .	35
3.1	WAM-2layers input and output as calculated for the period 2001–2010 from MODIS and TRMM . . . . .	58
3.2	WAM-2layers input and output as calculated for the period 1990–1995 from LandFlux-EVAL and an average of four observation-based precipitation products . . . . .	59
3.3	Schematic representation of the moisture recycling network . . . . .	60
3.4	Schematic representation of the sink and source regions as quantified by the moisture recycling ratios . . . . .	60
3.5	Dependence and contribution to cascading moisture recycling . . . . .	62
3.6	Results of complex network analysis . . . . .	63
3.7	Direct and cascading source regions of precipitation over the La Plata basin . . . . .	64
3.8	Direct and cascading sink regions of evapotranspiration from the La Plata basin . . . . .	65
4.1	Continental precipitation recycling ratio, forest resilience and hot spots where deforestation would lead to a maximal impact on the resilience of the remaining forest . . . . .	74
4.2	Schematic representation of feedbacks between vegetation and rainfall, which may cause cascading forest loss . . . . .	75
4.3	Cascading forest loss for the historical rainfall regime and dry-season intensification experiments . . . . .	76
4.4	Effect of heterogeneity and connectivity . . . . .	77
5.1	Key results showing the importance of cascading moisture recycling. . . . .	81

---

5.2	Effect of a business-as-usual deforestation 2050 on continental rainfall during the dry-season and Amazon forest resilience . . . . .	84
B.1	Scheme explaining the removal of cascading moisture recycling . . . . .	93
B.2	Different cascading moisture recycling pathways and their contributions . . . . .	95
B.3	Betweenness centrality obtained for different thresholds . . . . .	96
C.1	Cascade model scheme . . . . .	100
C.2	Sensitivity of the results to mean resilience thresholds . . . . .	102
C.3	Vegetation resilience . . . . .	103
C.4	Results of dry-season intensification experiment with cascade-mode off . . . . .	104
C.5	Additional results on links removal experiments . . . . .	105
C.6	Rainfall regimes where forest and savanna are alternative stable states . . . . .	106
C.7	Frequency distribution of tree cover in tropical South America . . . . .	107
C.8	Relative difference between evapotranspiration from the Landflux-EVAL data and the fit evaluation . . . . .	108
C.9	Evapotranspiration from Landflux-EVAL data and the fit evaluation . . . . .	109
C.10	Effect of deforestation on evapotranspiration . . . . .	110



# List of Tables

2.1	Network motifs taxonomy, patterns and the associated quantities used in the calculation of the directed clustering coefficients . . . . .	28
3.1	Input data sets used for building moisture recycling networks . . . . .	40
3.2	Overview of regional precipitation recycling ratio in the Amazon basin as found in many studies . . . . .	47
3.3	Importance of direct moisture recycling and cascading moisture recycling	61



# Abbreviations

<b>SAMS</b>	South American Monsoon System
<b>ENSO</b>	El Niño Southern Oscillation
<b>SST</b>	Sea Surface Temperature
<b>GCM</b>	General Circulation Model
<b>CMIP5</b>	Phase 5 of the Coupled Model Intercomparison Project
<b>SALLJ</b>	South American Low Level Jet
<b>DGVM</b>	Dynamic Global Vegetation Model
<b>BUN</b>	Binary Undirected Network
<b>WDN</b>	Edge-Weighted Undirected Network
<b>WDN</b>	Edge-Weighted Directed Network
<b>BDN</b>	Binary Directed Network
<b>CMR</b>	Cascading Moisture Recycling
<b>DMR</b>	Direct Moisture Recycling
<b>SSE</b>	South-Southeastern



*Dedicated to the memory of Katia Djanaïeff.*



# Chapter 1

## General introduction

The forests located within the Amazon River watershed (Amazon forest or Amazonia) represent the largest natural tropical ecosystem on the Earth with a coverage exceeding 5 million km<sup>2</sup>. This ecosystem stores 150–200 Pg. of carbon in soils and living biomass [Feldpausch et al., 2012], which is equivalent to more than 10 years global fossil fuel emissions [Davidson et al., 2012]. The Amazon forest hosts an exceptional biodiversity [Hopkins, 2007] and regulates the global climate through atmospheric teleconnections [Werth and Avissar, 2002]. However, the Amazon forest is facing increasing disturbances from deforestation and climate variability. Perturbations in the forest cover might be accelerated through vegetation-rainfall feedback processes and interactions between land-use, drought and fire [Davidson et al., 2012]. As the future of the Amazon forest is uncertain, a better understanding of the interactions between vegetation and rainfall is needed to assess the risk and effects of a large-scale forest loss.

The first section of this introduction gives an overview of the current state of vegetation and rainfall distribution in the Amazon basin, followed by a description of the threats of deforestation and climate change affecting the Amazon forest. In a second section, interactions between the vegetation and the hydrological component of the atmosphere (involving evapotranspiration, moisture transport and rainfall) are described. The benefit of applying a complex network approach to study these interactions is discussed. In a third section, feedback processes leading to critical transitions in the vegetation-rainfall system are presented. The fourth section explains how cascade dynamics in the vegetation-rainfall system might arise from the interactions among these feedback processes. The approach adopted in this thesis to analyze such dynamics is also presented. Finally, the fifth section describes the research questions and organization of the thesis.

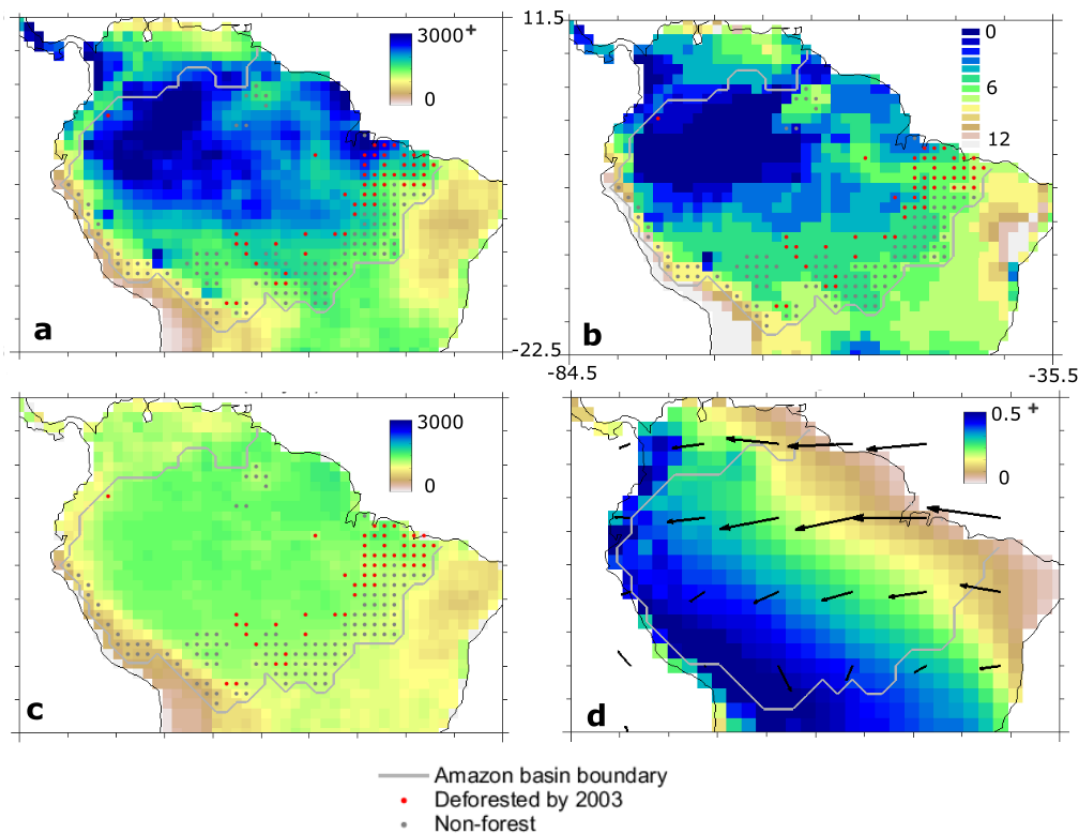


FIGURE 1.1 **Climatology of rainfall, evapotranspiration and moisture recycling for the tropical South America for the period 1989-1995.** **a**, Mean annual precipitation and **b**, number of months with less than 100 mm rainfall. Rainfall data were averaged from four observation-based products (CRU, GPCC, GPCP and CPC, see description in Chapter 3). **c**, Mean annual evapotranspiration obtained from the average of forty different products including observation-based data, land-surface model output and reanalysis data (LandFluxEval, Mueller et al. [2013]). The deforested (blue dots) and non-forest (gray dots) areas are obtained by up-scaling remote sensing data [Soares-Filho et al., 2006] to  $1^\circ$  longitude and latitude by selecting the most frequent value from the original dataset. **d**, Continental precipitation recycling ratio defined as the fraction of rainfall that comes from continental evapotranspiration [van der Ent et al., 2010]. The result is obtained using an atmospheric moisture tracking experiment by the Water Accounting Model - two layers (WAM-2layers, [van der Ent et al., 2014]) forced by the rainfall and evapotranspiration data together with vertically integrated moisture fluxes (black arrows) obtained from humidity and wind speed from ERA-Interim [Dee et al., 2011] at  $1.5^\circ$  longitude and latitude.



## 1.1 The vegetation-rainfall system in the Amazon basin

### 1.1.1 Current rainfall and vegetation distribution

#### 1.1.1.1 Rainfall distribution and variability

Mean annual rainfall is about 2,100 mm/year on average but large spatial variability is found across the Amazon basin. Annual rainfall exceeds 3,000 mm/year in the northwestern part of the basin, while the southern and eastern parts of the basin form the “dry belt” [Sombroek, 2001] with average annual rainfall below 1,800 mm/year (Fig. 1.1a). Moisture inflow from the tropical Atlantic Ocean is the most important source of rainfall over the Amazon basin. Another source of rainfall is provided by evaporation from the land surface and by transpiration from the vegetation (evapotranspiration) that release on average around 1,350 mm of moisture into the atmosphere every year (Fig. 1c and Fisher et al. [2009]). This atmospheric moisture returns to land and contributes to 25 to 50% of the total rainfall over the Amazon basin [Brubaker et al., 1993, Burde et al., 2006, Eltahir and Bras, 1994, Lettau et al., 1979, Trenberth, 1999].

The oceanic moisture inflow is provided by trade winds all year round but is enhanced by the establishment of the South American Monsoon System (SAMS). Low-level circulation changes associated with the SAMS arise from a complex interplay between differential heating of land and oceans, a southward displacement of the intertropical convergence zone and a reinforcement of the southward low-level jet stream east of the Andes [Marengo et al., 2012, Vera et al., 2006b]. Due to this complex climatological feature, distinct dry and wet seasons are found in tropical South America. The wet season lasts generally from December to February in southern Amazonia and southeastern Brazil, although it occurs later (March to May) in northwestern and central Amazonia [Marengo et al., 2012]. The length of the dry season (usually defined as the number of months with less than 100 mm rain [Sombroek, 2001]) varies widely across the Amazon basin. While dry seasons longer than 6 months are observed in the southeastern part of the Amazon basin, rainfall in the northwestern part is plentifully distributed throughout the year (Fig. 1.1b).

Besides intra-annual fluctuations, Amazonian rainfall is also characterized by inter-annual variability associated with anomalies of sea surface temperature (SST) in the Pacific and Atlantic Ocean resulting in large-scale atmospheric circulation changes. In the tropical Pacific, regular but infrequent alternations of warm and cold phases characterize the El Niño Southern Oscillation (ENSO). Reduced precipitation over the Amazon basin is usually found during the warm phase of ENSO (El Niño), while the opposite happens during its cold phase (la Niña) (Liebmann and Marengo [2001] and references

therein). In the last two decades, extreme hydrological events have become more frequent [Marengo et al., 2011]. In particular in 2005 and 2010, the Amazon basin experienced two “once-in-a-century” drought events. The 2005 event was not related to ENSO, but rather to a warming of the tropical North Atlantic ocean leading to a decrease of oceanic moisture inflow by trade winds [Marengo et al., 2008]. The drought in 2010 was initiated by El Niño and was reinforced by an anomalous warming of the tropical Atlantic [Marengo et al., 2011].

### 1.1.1.2 Vegetation distribution depending on rainfall regime

The amount of annual rainfall and dry season intensity are the most important drivers of natural vegetation distribution in the lowland (up to 600 m altitude) and non-flooded Amazon region [Ghazoul et al., 2010, Saatchi et al., 2000]. In very wet regions ( $> 2,200$  mm/year) without regular dry seasons, forests usually called “rainforest”, “wet forest” or “dense forest” are characterized by high tree density (500-800 trees per hectare), closed canopy cover and high biodiversity rates (150 - 300 species per hectare). Canopy height varies between 25 to 45 m and trees are mostly evergreen [Saatchi et al., 2000]. Where the dry season lasts six months or more, “dry forest” is dominated by deciduous vegetation that is well adapted to fire. While the canopy height average is about 50% that of wet forests, dry forests have usually a larger proportion of root biomass than wet forests [Murphy and Lugo, 1986], indicating an adaptation to seasonal drought. The number of tree species in dry forests is about half that found in wet dense forests. The transition from wet forests to dry forests is gradual. With declining rainfall, the abundance of grasses and other herbs increases [Ghazoul et al., 2010], and forests become semideciduous and more open, with gaps occupied by lianas, palms or bamboos indicating fire penetration [Saatchi et al., 2000].

Savannas are found mainly in the south-southeastern part of the Amazon basin, but defining a climatic zone for this biome is difficult. The transition between dry forest and savanna is usually very abrupt and controlled by other factors than rainfall alone, as will be explained later in this introduction. Savannas form a continuum of physiognomic types ranging from closed woodlands with a grass understory to treeless grasslands. While the herbaceous layer is dominated by C4 grasses, the woody component comprises fire-tolerant trees and shrubs [Huntley and Walker, 2012].

### 1.1.1.3 Forest adaptability to seasonal drought

The current understanding of the effect of seasonal drought on forest productivity has largely been achieved by the international research initiative Large-Scale Biosphere Atmosphere Experiment in Amazonia. Using eddy covariance measurements from flux towers installed in tropical South America, Von Randow et al. [2004], Da Rocha et al. [2009] and Restrepo-Coupe et al. [2013] showed that in contrast to vegetation types with lower tree density (e.g., savanna or pasture), tropical forests are able to maintain high evapotranspiration rates during the dry season. The dry-season evapotranspiration rate reaches up to 4 mm/day in wet forests and is as low as 2.5 mm/day in dry forests and 1mm/day in savannas [Da Rocha et al., 2009]. The absence of water limitation for evapotranspiration during seasonal drought in some forests is explained by tree root systems taking up soil water at depths of 8 meters or more [Bruno et al., 2006, Nepstad et al., 1994]. In addition, trees in central Amazonia are able to redistribute water from wet to dry regions in the soil profile overnight (hydraulic redistribution) [Oliveira et al., 2005].

An increase in forest evapotranspiration and productivity in some regions during the dry season correlated with increasing solar radiation (due to reduced cloud cover) and water vapor deficit has been reported using flux tower measurements [Da Rocha et al., 2009, Restrepo-Coupe et al., 2013] and satellite monitoring of the vegetation [Graham et al., 2003, Hilker et al., 2014, Huete et al., 2006]. This finding suggests that water is not the most limiting factor for forest productivity, although this affirmation is still under debate. An increase of canopy greenness observed during the dry season [Graham et al., 2003, Huete et al., 2006] has been attributed to an increase in leaf area or chlorophyll content [Samanta et al., 2012]. However, it has been suggested that the apparent greening of the forest is due to artifacts in sensors' geometry [Morton et al., 2014]. Correcting these artifacts, Morton et al. [2014] report that the forests maintain their photosynthetic activity during the dry season, while Hilker et al. [2014] and Guan et al. [2015] even show a slight increase in this activity given sufficient annual water supply.

Beside this debate, decline of evapotranspiration and photosynthetic activity during the dry season has been observed in southern and eastern part of the Amazon basin, suggesting potential water stress [Da Rocha et al., 2009, Guan et al., 2015]. This is explained by the insufficient subsurface water recharge during the preceding wet season in dry regions (below approximately 2,000 mm/year) being insufficient to supply enough water for the vegetation demand [Guan et al., 2015].

#### 1.1.1.4 Forest vulnerability to pronounced inter-annual drought

Despite the adaptability of some forests in the Amazon region to seasonal drought, they might be affected by pronounced inter-annual drought. The two extreme drought events in 2005 and 2010 affected the forests over a large spatial extent (1.9 million km<sup>2</sup> and 3.0 million km<sup>2</sup>, respectively). Carbon storage was reduced by 1.6 Pg.C in 2005 and 2.2 Pg.C in 2010 compared to normal years, mainly due to tree mortality, temporary cessation of biomass increase and carbon decomposition [Lewis et al., 2011, Phillips et al., 2009]. The vulnerability of forests to increasing rainfall deficit during the last decade has been confirmed by satellite data suggesting a widespread decline of Amazonian forest photosynthetic activity [Hilker et al., 2014, Lee et al., 2013, Xu et al., 2011]. This decline was partly explained by regulation of the stomatal aperture to avoid hydraulic failure during water stress [Lee et al., 2013]. In addition, Saatchi et al. [2013] showed an alteration of canopy structure and water content in particular in southwestern Amazonia (covering 40 thousand km<sup>2</sup>), with slow recovery after the drought in 2005, suggesting that frequent droughts (every 5-10 years) might permanently alter the forest canopy [Saatchi et al., 2013].

In rainfall exclusion experiments, in which 35–60% of the total rainfall was intercepted in the course of several years by plastic panels, tree mortality doubled, wood production declined by 30–60% and above-ground biomass was reduced by 18–25% [Brando et al., 2008, da Costa et al., 2010]. Mortality rates were greater in large trees (> 40 cm diameter) and low-wood-density trees, suggesting a possible shift of forest functional composition [Phillips et al., 2010]. A drought threshold was reached of 30% reduction of the plant-available water over 2.5 years beyond which forests suffered from drastic mortality [Nepstad et al., 2007]. The drought threshold is likely to vary among regions as forest susceptibility to drought varies according to rainfall regimes (total rainfall and seasonality), to soil properties (texture and depth), and to individual tree characteristics and adaptation to drought [Phillips et al., 2010]. Hence, effects of pronounced drought on forest cover are difficult to predict but structural changes in forests are expected with more frequent drought events, in particular in the less adapted forests [Maeda et al., 2015].

## 1.1.2 The Amazon forest under threat of climate variability and deforestation

### 1.1.2.1 Deforestation

From the late 1990s until 2004, the Amazonian forest was facing increasing deforestation rates, reaching 25,000 km<sup>2</sup> per year in 2004. In total, more than 20% of the original forest cover was converted to cattle pasture and soybean cropping favored by technological advances and good commodity market conditions [Morton et al., 2006]. Most of the deforestation took place along the southeastern border of the tropical forests, the so-called ‘arc of deforestation’ (red dots in Fig. 1). Not only does the direct conversion of forest to agricultural land contribute to forest degradation but also selective logging. Logging reduces up to 40-50% of canopy cover, increases the likelihood of fire and implies road building. Hence, logging is usually a first step towards complete deforestation. From 1999 until 2004, 32% of the logged forest was deforested within four years following logging (Cochrane and Laurance [2008] and references herein). Based on a “business-as-usual” scenario assuming that the trend of deforestation observed until 2005 would continue, new protected areas would not be created and road would be paved as scheduled, Soares-Filho et al. [2006] projected that more than 40% of the Amazon forest could be clear-cut in 2050.

Since 2005, deforestation rates decreased to reach around 6,000 km<sup>2</sup> per year in 2013. This sharp decline in deforestation was a consequence of several factors including law enforcement, a soy moratorium, restrictions on access to credit for farms located in deforested areas, and expansion of protected areas and indigenous territory encompassing 47% of the entire Brazilian Amazon region [Nepstad et al., 2014]. Despite these recent improvements, recent prospects suggest that deforestation might continue in the near-term future [Fearnside, 2015]. An expanding market for agricultural commodities, weak institutions and large infrastructure projects might potentially contribute to the return of high deforestation rates [Aguiar et al., 2014].

### 1.1.2.2 Current rainfall trends and future projections

Since the late 1970s, a gradual decrease in rainfall at the end of the dry season (September-November) in the Amazon basin has been recorded [Fu et al., 2013, Marengo et al., 2011]. This trend coincides with a tropical North Atlantic SST increase [Marengo et al., 2011], but a direct link to anthropogenic forcing of climate change is difficult to establish due to the poor understanding of the underlying processes [Fu et al., 2013].

Ensemble simulations from several global circulation models (GCMs) used in phase 5 of the Coupled Model Intercomparison Project (CMIP5) simulate a strengthening of the annual cycle of the SAMS at the end of the twenty-first century [Boisier et al., 2015, Joetzjer et al., 2013]. In particular, the simulations show a reduction of rainfall at the end of the dry season ( $-0.54 \pm 0.64$  mm/day in September–November) and a slight increase in rainfall during the wet season (December–February). Most GCMs agree that rainfall changes are expected due to a strengthening of the SST gradient between the northern and southern Pacific Ocean leading to northward displacement of the intertropical convergence zone. However, most GCMs used in the CMIP5 tend to under-estimate current precipitation in the Amazon basin, suggesting that the processes controlling rainfall, and in particular the feedbacks between land-surface latent heat flux and rainfall, are still poorly represented [Joetzjer et al., 2013, Yin et al., 2013]. Due to the poor representation of the processes controlling dry-season rainfall variability, the strengthening of seasonal drought in the future might be stronger than predicted by most GCMs [Boisier et al., 2015, Fu et al., 2013]. Implementing current rainfall trends in statistical analysis, Boisier et al. [2015] projected a stronger dry-season prolongation (June - November) compared to the GCMs simulations alone.

### 1.1.2.3 Simulated responses of forest cover to climate change

Dynamic global vegetation models (DGVMs) have been used to investigate Amazon forest response to climate change (e.g. Galbraith et al. [2010], Huntingford et al. [2013], Rammig et al. [2010]). DGVMs represent mechanisms of plant physiology and vegetation dynamics for different plant functional types and simulate vegetation distribution under changing climate conditions (e.g. Krinner et al. [2005], Sitch et al. [2003]). Different DGVM simulations display a great variety of projections for the Amazon region ranging from a large-scale decline of forest cover [Cramer et al., 2004, Galbraith et al., 2010, White et al., 1999] to no reduction in forest cover [Huntingford et al., 2013]. This variety is explained by different representations of the plant physiological processes. In particular, some DGVMs simulate that increasing atmospheric carbon dioxide concentration ( $[CO_2]$ ) enhances water-use efficiency and tropical tree growth (“ $CO_2$  fertilization effect”) [Huntingford et al., 2013, Rammig et al., 2010], a hypothesis that has been partly contradicted by tree-ring analysis [van der Sleen et al., 2014]. In addition, large uncertainties in the simulated response of the vegetation arise from the representation of the sensitivity of forests to water stress, making predictions of Amazon forest’s response to increasing drought very challenging [Galbraith et al., 2010, Joetzjer et al., 2014]. In fact, the uncertainties arising from the representation of the physiological processes are

larger than the uncertainties associated with different climate forcing data [Huntingford et al., 2013, Rammig et al., 2010].

Another approach to evaluate the potential effect of changing climate on vegetation distribution is the use of statistical models based on empirical relationships between climate variables and the distribution of natural vegetation. Most of these statistical models project a replacement of at least the southern and eastern part of the tropical forests by savanna as a result of a drier and warmer climate [Lapola et al., 2009, Malhi et al., 2009, Salazar et al., 2007, Zelazowski et al., 2011]. These models are limited by the assumption that climate exerts the dominant control on vegetation while other non-climatic factors (e.g., natural and anthropogenic disturbances) and ecological processes (e.g., migration and colonization) might also play an important role in determining the distribution of vegetation.

While the models described above focus purely on the impacts of climate on vegetation distribution, it is also important to consider feedbacks between vegetation and climate which may lead, for example, to amplification of drought with forest loss.

#### **1.1.2.4 Deforestation affecting regional rainfall**

As a result of reduced dry-season evapotranspiration due to deforestation, the amount of moisture available for local and downwind rainfall is also reduced. The local effect of deforestation on the atmosphere was investigated using flux tower measurements [Von Randow et al., 2004] showing that the evaporative fraction (ratio of latent heat to incoming solar radiation) is 24% lower in forests compared to pasture during the dry season. To evaluate the sensitivity of rainfall to forest cover, Spracklen et al. [2012] analyzed empirical relationships between remotely sensed vegetation cover and rainfall data along wind trajectories. In 60% of the tropical areas, air passing over extended vegetation produces at least twice as much rain as air passing over little vegetation. Extrapolating this finding to a business-as-usual deforestation scenario for 2050 leads to a rainfall reduction over the Amazon basin of 12% and 21% during the wet and dry seasons, respectively.

Rainfall changes after deforestation projected using climate models vary widely according to the structure of the models and their spatial resolution, which determine the processes represented. Most GCMs agree that complete deforestation of the Amazon forest would lead to warmer (0.1 - 3.8°C) and drier (140-540 mm/year, i.e., around 15% annual rainfall reduction) regional climate (Lawrence and Vandecar [2015] and references herein, e.g., Hasler et al. [2009], Nobre et al. [2009], Sampaio et al. [2007]). The simulated drying of the Amazon basin results from (1) reduced evapotranspiration and the

resultant downwind moisture transport and recycling and (2) weakening of the regional atmospheric circulation driving rainfall over the region. The second effect arises from changes in the ratio of sensible to latent heat flux that impacts the thermal stability of the atmospheric boundary layer due to increasing albedo (fraction of reflected short-wave solar radiation) and evapotranspiration, as well as a reduction of surface roughness altering low-level wind speeds [Bonan, 2008].

On the other hand, a regional climate model with higher spatial resolution (25 km grid) projected a much smaller decrease of regional rainfall (-62 mm/year) for a complete deforestation scenario [Medvigy et al., 2011]. Some regional models also show that low levels of deforestation (up to around 20%) increase rainfall over the deforested area as a result of a heterogeneous heating of the land surfaces, which increases mesoscale convection (“vegetation breeze”) and cloud formation [Medvigy et al., 2011, Walker et al., 2009]. However, the importance of this effect varies according to the considered size and pattern of the deforestation patches [Lawrence and Vandecar, 2015], as well as the model considered. For example, Bagley et al. [2014] found a rainfall reduction of 5% during the dry season (July-September) in the Amazon basin already under historical Amazon deforestation. This change was attributed to a local reduction of evapotranspiration (30% in July-September) and resultant moisture transport rather than changes in atmospheric circulation patterns. Most regional models agree that the effect of the vegetation breeze vanishes beyond a certain area of deforestation (around 30%) for which a decrease of regional rainfall especially during the dry season is expected (e.g., Walker et al. [2009]).

Several studies (e.g., Pires and Costa [2013], Sampaio et al. [2007]) suggest the existence of a threshold of deforestation (40% in Sampaio et al. [2007]) beyond which strong rainfall reduction would be observed regionally, potentially leading to a large-scale shift of the remaining forest towards a drier ecosystem. The existence of a so-called tipping point (see Sect. 1.3.1) is under debate, as Walker et al. [2009] showed that deforestation in the Amazon basin outside the current protected areas would not lead to an excessive regional drying and therefore would not affect the stability of the remaining forest. This question is further addressed in this thesis by an analysis of the feedbacks between vegetation and rainfall in the Amazon basin. It is worth noting that feedback processes involving changes in atmospheric circulation, which are still poorly understood as previously mentioned, will not be considered. Rather, the focus of this thesis will be on moisture recycling.



## 1.2 Moisture recycling from a complex network perspective

The process of evapotranspiration returning to the land as rainfall is called moisture recycling, which is a key process controlling stability of the Amazon forest and rainfall regulation in South America. This section will discuss how a complex network approach might open new perspectives to analyze moisture recycling in South America.

### 1.2.1 Current understanding of moisture recycling in South America

Early studies on the analysis of isotopic composition of water from the river system in the Amazon basin provided ground-based evidence of moisture recycling [Dall’Olio et al., 1979, Gat and Matsui, 1991, Salati et al., 1979, Victoria et al., 1991]. Using atmospheric bulk models (or recycling models), in which conservation of mass in a control volume of the atmosphere is applied using gridded data of water vapor flux and evapotranspiration, it has been estimated that moisture recycling contributes 25-50% of the total rainfall over the Amazon basin [Brubaker et al., 1993, Burde et al., 2006, Eltahir and Bras, 1994, Lettau et al., 1979, Trenberth, 1999].

More recently, numerical moisture tracking experiments have allowed investigation of the source and sink regions of precipitation over the South American continent. For example, Dirmeyer et al. [2009] and Martinez and Dominguez [2014] evaluated changes in humidity along backward trajectories (a Lagrangian approach), and showed that between 20 and 23% of the annual rainfall over the subtropical La Plata basin comes from the southern part of the Amazon basin. van der Ent et al. [2010] implemented tracers of moisture within an algorithm of water vapor balance on a grid cell basis (an Eulerian approach). They showed that around 50% of the evapotranspiration from the Amazon region returns to the continent as rain and 70% of rainfall over the La Plata basin has a continental origin, suggesting the possible source-sink linkage between these two regions. Using the same tracking model, Keys et al. [2012] identified the southern part of the Amazon basin as a source of rainfall for southern Argentina.

### 1.2.2 A new concept: cascading moisture recycling

So far, most of the studies on moisture recycling have only assessed the link between source and sink regions through “direct moisture recycling”. I introduce this term to refer to the transport of atmospheric water from the place of evapotranspiration (source) up to the place of precipitation (sink) without exchange between the vegetation

and the atmosphere on the way. However, precipitating water can be re-evaporated and transpired in the same location (“re-evaporation cycle”) and can be transported further downwind before it falls again as precipitation over land (see Fig.2 in Chapter 4). Therefore I introduce the concept of “cascading moisture recycling” to describe moisture transport on the continent from sources to sinks that involves re-evaporation cycles on the way. Such a concept is needed to better grab the complexity of the interactions between vegetation and rainfall in South America.

To my knowledge, only two previous studies analyzed cascading moisture recycling [Goessling and Reick, 2013, Numaguti, 1999]. Adding different types of tracers within a GCM, the authors counted the number of re-evaporation cycles that water molecules experienced since they evaporated from the ocean. Numaguti [1999] found that this number exceeds two in northern Eurasia during summer, while Goessling and Reick [2013] demonstrated that the distribution of re-evaporation cycles on the continents can be approximated by a Poisson process. Although these studies suggested the importance of cascading moisture recycling for continental rainfall, no quantitative estimates were provided for the South American continent using observation-based data.

### **1.2.3 The complex network approach to analyze cascading moisture recycling**

In this thesis, moisture recycling networks are built based on an Eulerian moisture tracking model [van der Ent et al., 2010, 2014] forced by observation-based climate data for South America (see Chapter 2). In the resulting networks, links represent the amount of moisture transported from source to sink of rainfall on the continent. Nodes represent grid cells covering the South American continent (Fig. 3.3). A complex network approach is applied in this thesis to explore the architecture and functioning of these moisture recycling networks.

The study of complex networks, i.e., networks with irregular, complex or dynamic structures, aims to link the description of the network’s topology with its dynamical and functional behavior. This approach has been widely applied in the course of the last decade in different domains including biology [Zhou et al., 2006], communication [Capocci et al., 2006], social science [Newman and Park, 2003], economy [Baskaran et al., 2011] and climatology [Donges et al., 2009b]. For example, linking grid cells over the Earth’s surface according to statistical correlations in climatic fields (e.g., temperature and rainfall) allowed identification of atmospheric teleconnections [Donges et al., 2009b] and predict ENSO [Ludescher et al., 2014] or extreme rainfall events in the central Andes [Boers

et al., 2014]. In this thesis, the links in the network do not represent statistical similarity measures as was done in previous climate network studies, but actual fluxes of atmospheric water on the continent, which is a significant methodological improvement.

Representing moisture recycling as a complex network opens new perspectives. For example, particular and recurrent network motifs detected in various systems (e.g., electronic circuits, food webs and gene regulation) throw light on the flow of information processing or functional organization of the system [Milo et al., 2002]. As shown in this thesis (chapter 2), such motifs are also found in moisture recycling networks, thereby providing information on moisture recycling pathways in South America. As another example, the betweenness centrality is a complex network measure that was originally developed to quantify the importance of an individual in a social network [Wasserman and Faust, 1994]. Applied in chapter 3, this measure allows regions to be identified where cascading moisture recycling pathways are channeled.

### 1.3 Critical transitions in vegetation-rainfall system

In the previous sections of this introduction, the interactions between vegetation and rainfall in the Amazon basin have been addressed. In this section, processes leading to critical transition in the vegetation-rainfall system will be described.

#### 1.3.1 Concepts and definitions

The question of whether the response of tropical forest cover to altered rainfall regime will be gradual or abrupt raised great interest among the scientific community in the last decade (e.g., Cox et al. [2000], Hirota et al. [2011], van Nes et al. [2014]). A theory suggests that forest cover might stay relatively constant over a range of rainfall changes until a threshold (“tipping point”) is reached, beyond which the forest cover suddenly drops to a new, qualitatively different state (“critical transition”). Such a dynamic arises when feedback processes accelerate ongoing changes. The proximity of a tipping point is estimated using the concept of forest resilience, defined as ‘the ability of a forest to absorb disturbances and re-organize under change to maintain similar functioning and structure’ [Scheffer, 2009]. In some cases, vegetation would remain in the new state after a critical transition even if rainfall increases at a much higher level than the initial one, a process known as “hysteresis”. This suggests that multiple equilibria (“alternative stable states”) in the vegetation exist for a given rainfall regime and the observed vegetation state is “path-dependent”, i.e., depends on the historical climate and disturbance regime [Scheffer and Carpenter, 2003, Scheffer et al., 2012]. Evidence from the past confirming

the theory of critical transition in the vegetation in the Amazon basin is difficult to provide and most analyses rely on modeling approaches (e.g., Oyama and Nobre [2003], van Nes et al. [2014]) or interpretation of current tree cover distribution in remotely sensed data [Hirota et al., 2011, Staver et al., 2011].

### **1.3.2 Shifts in the bioclimatic equilibrium as simulated by coupled models**

In section 1.1.2, I discussed how deforestation may reduce rainfall and how increasing drought affects forest cover. In the following, modeling studies integrating coupled feedback processes between vegetation and rainfall are reviewed.

Coupling an atmospheric GCM with a statistical vegetation model, Oyama and Nobre [2003] found distinct vegetation-climate equilibria in tropical South America under present-day climate conditions. In addition to the current state, a new equilibrium was simulated where the eastern Amazon forest is replaced by savanna (over more than 2 million km<sup>2</sup>) and semi-desert area appears in the driest region of northeast Brazil (over 0.3 million km<sup>2</sup>). This new equilibrium was found by initializing the model with a treeless state. Because the evapotranspiration rate for treeless states is smaller than for forests, the absence of trees weakens moisture recycling and reduces annual rainfall by up to 0.5 mm/day. This result suggests that forest loss induced by anthropogenic pressures (deforestation and climate change) might lead to shifts in the Amazon bioclimatic equilibrium.

A large-scale catastrophic forest loss (Amazon dieback) for the end of the twenty-first century was simulated as a result of changing climate amplified by a dynamic vegetation interacting with the atmosphere on the carbon and hydrological cycles through respiration, photosynthesis and evapotranspiration [Betts et al., 2004, Cox et al., 2000]. Results from an early version of the coupled model of the Hadley Centre HadCM3LC showed an amplification of carbon release (by 280 ppm of CO<sub>2</sub> concentration) accelerating climate change [Cox et al., 2000]. The enhancement of precipitation reduction was mainly attributed to a Niño-like SST warming pattern with increasing atmospheric CO<sub>2</sub> concentration. The increasing CO<sub>2</sub> concentration was mainly due to an exponential release of carbon by plant autotrophic respiration with temperature rise [Cox et al., 2004]. In addition to this biogeochemical feedback, Betts et al. [2004] showed that the Amazon dieback amplified rainfall reduction by 20% due to reduced evapotranspiration affecting the available moisture for regional rainfall. The dieback hypothesis is controversial as the simulated response of the vegetation-rainfall system to climate change is highly dependent on the structure of the model [Huntingford et al., 2013]. The new version of

Hadley Centre model HadGEM2-ES projected a minimal forest loss [Good et al., 2013] resulting, among other structural model improvements, from a better representation of plant respiration at high temperature. The improved Hadley Centre model displayed a limited carbon release, thereby lowering projected changes in dry-season length (7 months differences compared to the old version). In addition, the forest responded differently to drought as the net primary productivity was less drastically reduced. Hence, discrepancies among simulations show the difficulty in accurately representing the fully coupled vegetation-climate system in a process-based modeling approach. The Amazon dieback is still a plausible scenario and therefore further understanding of the feedbacks between vegetation and rainfall is needed [Good et al., 2013].

### **1.3.3 Critical transition in the vegetation with altered rainfall regime**

In the previous section, it has been shown that shifts in the bioclimatic equilibrium might result from alteration of large-scale vegetation-rainfall feedbacks. In the following, potential critical transitions in the vegetation resulting from other feedback processes are discussed.

#### **1.3.3.1 Forest and savanna as alternative stable states**

The analysis of remotely sensed tree-cover data distribution revealed the existence of three distinct high-frequency modes that were interpreted as three alternative stable states corresponding to forest (tree cover >60%), savanna (tree cover between 5 and 60%) and treeless (tree cover <5%) states [Hirota et al., 2011]. The cut-off levels in tree cover were defined according to the lowest frequency found in tree-cover data and are considered as unstable states. It has been suggested that in regions of intermediate rainfall (from 1,000 to 2,500 mm) and mild seasonality (dry-season length less than 7 months), forest and savanna are bistable. The mechanism proposed to explain this bistability is the positive feedback between grasses and fire: low tree cover promotes fire spread and fire suppresses tree cover [Staver et al., 2011]. The studies of Staver et al. [2011] and Hirota et al. [2011] suggest that the risk of critical transition between forest and savanna increases with altered rainfall regime. The theory of fire-mediated critical transition between alternative stable states in the vegetation is controversial. Hanan et al. [2014] showed that discontinuities in remotely sensed tree cover might be attributed to the statistical procedure of data calibration rather than a real-world property. In addition, a less abrupt transition between forest and savanna was found when considering shorter woody vegetation types (trees with <0.1m diameter and height below 5m) [Veenendaal et al., 2015]. It has been also argued that other factors also

control the forest-savanna boundary, such as grazing by herbivores [Bond and Keeley, 2005], water resource constraints [Bertram and Dewar, 2013] and soil chemical properties [Veenendaal et al., 2015]. Regardless of the processes controlling the natural forest-savanna boundary, land use in interaction with climate change might trigger critical transition in some Amazon forests.

### **1.3.3.2 Critical transition in the vegetation triggered by interactions between fire, inter-annual drought and land use**

Interactions between drought, fire and land use amplify forest vulnerability to environmental changes [Cochrane and Laurance, 2008]. The susceptibility of forests to fire with increasing drought is further altered by land-use change through thinning, provision of ignition sources and fragmentation [Aragão et al., 2008, Asner and Alencar, 2010]. During the drought of 2005, the number of “hot pixels” where an active fire was detected was 43% higher in deforested area compared to the expected value under normal rainfall conditions [Aragão et al., 2008].

The potential of drought interacting with fire to lead to a local tipping point has been recently shown using ground-based measurements in a southern Amazon forest. Abrupt increase in fire-induced tree mortality (up to 462%) has been measured in a burn experiment during an extreme drought event; the results was an opening of the canopy (up to 31% decline in canopy cover), favoring invasion of grasses (up to 80%) and increasing fire intensity [Brando et al., 2014]. In another fire manipulation experiment, 8 years of increasing fire frequency (no fire, annual fire and 3-year intervals) increased the rate of grass invasion into the forest to up to 200 m from the edge, which resulted in a more than threefold increase in fine fuel loads [Silvério et al., 2013]. Thus, the synergistic effect of fire, inter-annual drought and land use might activate grass-fire feedbacks. This could lead to a transition of the forest to a grass-dominated ecosystem in the near-term future [Nepstad et al., 2008].

### **1.3.3.3 Critical transitions in the vegetation as simulated by conceptual models**

To evaluate the sensitivity of the vegetation-savanna boundary to environmental changes and search for tipping points beyond which critical transitions would occur, several conceptual models have been developed on the basis of a fire-mediated bistability [Hirota et al., 2010, Staal et al., 2015, van Nes et al., 2014]. These conceptual models rely on principal equations linking the tree-cover dynamic with annual rainfall and seasonality and fire occurrence interacting back with tree cover and rainfall. Using such a simple

model, Hirota et al. [2010] showed that a warming of up to 6% and a rainfall reduction of up to 20% might lead to a transition of 6% of the current forest area to savanna in eastern Amazonia. Although these conceptual models do not explicitly represent mechanisms of plant physiology and competition for resources, they capture complex interactions among seasonal rainfall, grasses and natural fires that control the natural dynamics of forest-savanna boundaries [Hirota et al., 2010]. Nevertheless, the effect of land-use interacting with inter-annual drought and fire are not considered in these modeling studies although they represent key processes for reaching potential tipping points in the Amazon forest (see previous section).

Some conceptual models have also represented vegetation-rainfall feedbacks in a very simple way [Da Silveira Lobo Sternberg, 2001, van Nes et al., 2014]. For example, recycled rainfall was assumed to linearly depend on forest cover and critical transition in the vegetation was assumed to occur beyond a certain rainfall threshold [Da Silveira Lobo Sternberg, 2001]. Using such assumptions, Da Silveira Lobo Sternberg [2001] simulated a stable vegetation despite a reduction in dry-season oceanic moisture inflow and concluded a weak vegetation-rainfall feedback effect on the system stability. However in this study, the approach was not based on observational data. Using another conceptual model calibrated to remotely sensed tree-cover data, van Nes et al. [2014] showed the potential of local vegetation-rainfall feedbacks to enhance hysteresis in the vegetation compared to a case where only grass-fire feedbacks are considered. In this study, however, moisture transport between different locations in the Amazon forest was not considered as it is done in this thesis.

## **1.4 Assessing potential cascade dynamics in the Amazon vegetation-rainfall system**

### **1.4.1 Combining the concepts of forest resilience and cascading moisture recycling**

As shown in previous sections, several processes may cause an abrupt response of the forest to changing environmental conditions at various levels in the spatial scale. The abrupt mortality of trees to pronounced drought is controlled by soil properties and tree characteristics that vary at the level of a few meters<sup>2</sup> [Phillips et al., 2010]; grass-fire feedbacks leading to critical transition from a forest to a grass-dominated ecosystem are observed at the hectare level [Brando et al., 2014]; land-use and fire disturbances interacting with extreme drought events affect the forest over thousands of kilometers<sup>2</sup> [Aragão et al., 2007, Nepstad et al., 2014]; moisture transport and recycling occur at the

continental scale [van der Ent et al., 2010], yet all these processes interact in a complex way [Reyer et al., 2015, Rietkerk et al., 2011, Scheffer et al., 2005]. So far, most previous modeling studies assessing potential critical transitions in the vegetation focused on one of these effects without considering the interactions between them. Moreover, few existing modeling studies combining these effects consider the transport and recycling of moisture in the Amazon forest based on observational data.

In this thesis, the concepts of forest resilience and cascading moisture recycling are combined in an integrated modeling framework based on observational data (see chapter 4). More specifically, critical transitions in the vegetation at the grid cell level ( $1.5^\circ$  longitude and latitude, i.e., around 170 km width at the equator) affect rainfall in other grid cells due to a reduction of evapotranspiration and the resultant downwind transport of moisture. As a result, the resilience of the remaining forest is eroded, potentially leading to further forest loss. Hence, a coupling of these concepts allows one to account for interacting effects between local critical transition in the vegetation and large-scale moisture transport and recycling. The proposed empirical model is used to analyze the sensitivity of the Amazon vegetation-rainfall system to environmental perturbations (dry-season intensification and deforestation).

#### **1.4.2 A complex network approach to investigate the stability of the system**

In this thesis, the sensitivity of the vegetation-rainfall system to environmental perturbations is analyzed using a complex network approach. A widely used method in complex network analysis to test the fragility of a system to perturbations aims at removing a fraction of the nodes or edges from the network and measuring its ability to maintain its connectivity (usually measured by the size of the so-called giant component). The deletion of nodes can be either random (random failure) or targeted to a particular class of nodes, usually the highly connected ones (attacks). Depending on their topology, the response of the networks to attacks or random failures differs. For example the World Wide Web network stays connected despite a large fraction of nodes being removed during random failure experiments, but collapses rapidly as a response to an attack. Interestingly, particular types of networks (the so-called scale-free networks) fall apart if the fraction of nodes removal exceeds a certain critical value (Boccaletti et al. [2006] and references therein). In chapter 4, a similar experiment is applied to identify hot spots where deforestation would greatly destabilize the Amazon vegetation-rainfall system.

The complex network approach has also been applied to study cascade dynamics in various systems such as innovation propagation in society, catastrophic regime shifts in



ecosystems or power-grid blackouts (Scheffer et al. [2012], Watts [2002] and references therein). In this approach, the systems of interest are typically modeled as networks whose nodes can flip between alternative stable states. The probability of a node being in one state is favored by having neighbors in that state [Scheffer et al., 2005, Watts, 2002]. In chapter 4, a similar cascade model is developed in which the forest grid cells covering the Amazon basin can shift between alternative stable states and are linked to each other by moisture recycling. By this approach, spatial propagation of forest loss resulting from vegetation-rainfall feedbacks can be simulated. To assess the properties affecting the stability of the Amazon vegetation-rainfall system, the effects of the heterogeneity and connectivity of the nodes are analyzed, which are usually mentioned as key factors controlling the response of a complex system to perturbations [Boccaletti et al., 2006, Scheffer et al., 2005, Watts, 2002].

### **1.4.3 The benefits and shortcomings of an empirical approach**

This thesis is mainly based on the analysis of observational data. This section illustrates the benefits and shortcomings of such an empirical approach compared to a process-based modeling approach using two examples.

#### **1.4.3.1 Access to subsurface water during seasonal drought**

The capacity of the vegetation to access subsurface water during seasonal drought is a key factor controlling evapotranspiration in the tropics [Da Rocha et al., 2009, Fisher et al., 2009]. A reduction of this capacity after forest loss might greatly enhance seasonal drought with important consequences for the stability of the vegetation-rainfall system as explained previously. However, most hydrological models perform badly in representing groundwater and rooting depth in the Amazon basin, leading to an under-estimation of dry-season evapotranspiration by up to 1mm/day in tropical forests [Miguez-Macho and Fan, 2012]. In chapter 4, evapotranspiration is calculated using a simple function calibrated to observation-based gridded data of evapotranspiration, rainfall and tree cover. The capacity of the vegetation to access subsurface water during seasonal drought is estimated as a function of tree cover and cumulative water deficit [Aragão et al., 2007] calibrated to satellite data. By this approach, important and complex ecohydrological processes are accounted for, without an explicit representation of the ground water dynamic and rooting depth, which are still poorly understood.

It is clear that such an empirical approach is limited by the quality and availability of the data. This limitation is particularly critical for evapotranspiration estimates in the Amazon basin where difficult access to the dense forest is a clear obstacle to extensive

measurements of latent heat from flux towers. Hence, the quality of gridded evapotranspiration data relies on the accuracy of algorithms and on the forcing data of climatic and biotic variables. In this thesis, this issue was partly addressed using evapotranspiration data derived from merging forty different products from various categories (vegetation model output, reanalysis and remotely sensed data) (Landflux-EVAL, Mueller et al. [2013]).

### **1.4.3.2 Critical transition in the vegetation with altered rainfall regime**

This section describes the advantages and limitations of applying an empirical approach to represent critical transition in the vegetation. Following Hirota et al. [2011], the probability to find forest in a given rainfall regime can be quantified using the empirical density function of tree cover for different rainfall regimes based on remotely sensed data. This probability is assumed to be an indicator of forest resilience and decreases non-linearly with decreasing rainfall, which is interpreted as an indication of an approaching bifurcation point (where forest is no longer stable) [Hirota et al., 2011]. However, critical transitions are typically triggered by stochastic perturbations on the forest (e.g., fire and extreme drought events) before the bifurcation point is reached [Scheffer et al., 2012]. Hence, in chapter 4, critical transitions in the vegetation are represented as a stochastic process depending on the empirical indicator of forest resilience. In other words, a forest grid cell shifts when its resilience exceeds a randomly sampled threshold. Although this approach does not represent any ecological processes, it implicitly makes it possible to account for the synergistic effect of inter-annual drought, fire and land-use change that is usually not considered in modeling studies [Nepstad et al., 2008]. As a counterpart, the dynamic of the vegetation is not represented as it is in DGVMs. However, as discussed in Sect. 1.1.2.3, the expected response of the vegetation to changing climate is still poorly understood and represented in process-based modeling studies. Hence, the model presented in chapter 4 is deliberately kept very simple in order to avoid uncertainties associated with increasing model complexity. The aim of the model is not to make future projections or a thorough assessment of the Amazon rainforest stability under environmental change, but rather to analyze the sensitivity of the Amazon vegetation-rainfall system to particular environmental perturbations.

## **1.5 Research questions and structure of the thesis**

The overall structure of the thesis is illustrated in Fig. 1.2.

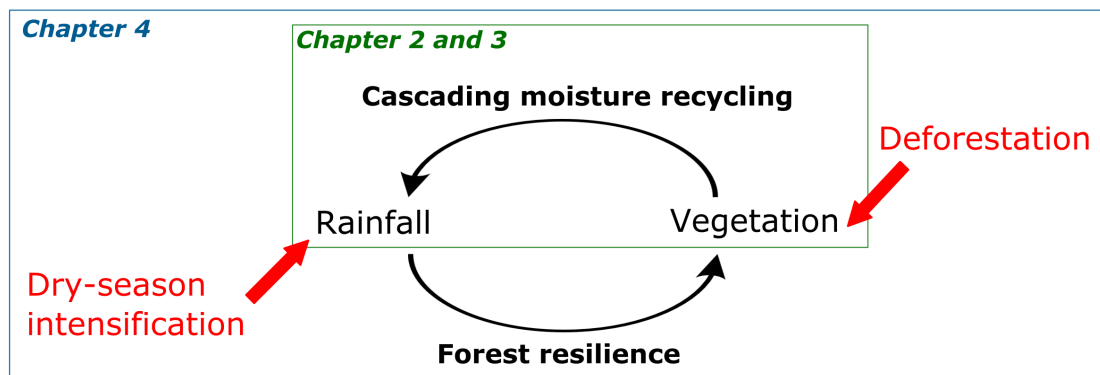


FIGURE 1.2 **Scheme of structure of the thesis.** In chapters 2 and 3 (green box), a complex network approach is applied to analyze cascading moisture recycling. In chapter 4 (blue box), the stability of the vegetation-rainfall system to environmental perturbations (dry-season intensification and deforestation) is assessed. The concepts of cascading moisture recycling and forest resilience are combined in an empirical modeling framework.

### 1.5.1 Chapter 2 and 3: Analysis of cascading moisture recycling in South America

The first part of this thesis (Chapter 2 and 3) aims to improve our understanding of the complex interactions between the terrestrial and atmospheric components of the hydrological cycle. For this purpose, the concept of cascading moisture recycling has been introduced in Sect. 1.2.2 as moisture transport from the source to the sink of rainfall on the continent that involves re-evaporation cycles along the way. This raises following research questions:

Q1: Where are key regions that sustain cascading moisture recycling in South America?

Q2: What is the importance of cascading moisture recycling in South America?

These questions are addressed from a complex network perspective. However, tools to study the particular type of complex networks describing water fluxes (directed and weighted networks) were missing. Therefore, extended measures from complex network analysis are introduced and evaluated in **Chapter 2**. The presented results partially answer **Q1**. The answer to **Q1** is deepened in **Chapter 3**, where further results from complex network analysis are presented. To confirm findings and to answer **Q2**, a new methodology is developed to systematically quantify the contribution of cascading moisture recycling to rainfall over the continent. The robustness and flexibility of the methodological approach is shown by using two different combinations of datasets and comparing results with previous studies using traditional metrics (e.g., regional recycling ratio). These two chapters have been published in peer-reviewed journals. Even though

these two chapters focus on South America and in particular on the transport of moisture from the Amazon basin to the La Plata basin, they lay the foundation for the fourth chapter.

### 1.5.2 Chapter 4: Analysis of self-amplified Amazon forest

The second part of this thesis (**Chapter 4**) aims to analyze the vulnerability of the Amazon forest to environmental perturbations. In particular, the following questions are addressed:

- Q3: Where are the “hot spot” regions where deforestation would greatly destabilize the Amazon ecosystem?
- Q4: What is the potential of vegetation-rainfall feedbacks to lead to self-amplifying Amazon forest loss?
- Q5: Can we identify tipping points in deforestation and rainfall change beyond which large-scale Amazon forest loss (dieback) would occur?
- Q6: Which properties affect the stability of the Amazon vegetation-rainfall system?

To address these questions, an empirical and stochastic modeling framework is developed, inspired by existing cascade models for complex networks. The proposed model is used to assess cascade dynamics in the Amazon vegetation-rainfall system under deforestation and/or reduced oceanic moisture inflow. This model is a combination of (1) an empirical indicator of forest resilience to describe critical transitions in the vegetation at grid-cell level, (2) a moisture recycling network to account for changes in moisture transport and recycling and (3) a simple evapotranspiration model to estimate changes in evapotranspiration after vegetation shifts and/or rainfall changes.

To answer **Q3**, the reduction of the overall forest resilience after deforestation of each individual grid cells is quantified. To answer **Q4** and **Q5**, experiments of gradual decrease of oceanic moisture inflow in combination with deforestation are performed and the corresponding cascading forest loss is evaluated. These scenarios are compared with recent statistical projections of dry-season intensification in the Amazon basin for the end of the twenty-first century. To answer **Q6**, the effect of spatial heterogeneity in the resilience thresholds for critical transition in the vegetation is evaluated, as well as the moisture recycling connectivity. The results are presented and discussed in a letter format submitted to the journal *Nature*.

## Chapter 2

# Node-weighted measures for complex networks with directed and weighted edges for studying continental moisture recycling

An edited version of this chapter has been published in the journal *Europhysics Letter*:

Zemp, D. C., Wiedermann, M., Kurths, J., Rammig, A. and Donges, J. F.: Node-weighted measures for complex networks with directed and weighted edges for studying continental moisture recycling, *Europhysics Letters*, 107, 58005, doi:10.1209/0295-5075/107/58005, 2014.

This article was selected as one of the highlighted article of the year by the editorial board (Editor's Choice Articles 2014)<sup>1</sup>.

---

<sup>1</sup>“[...] letters covering important new research, in topical areas, that the [Editorial] Board found particularly insightful and useful.” (EPL website)

## Abstract

In many real-world networks nodes represent agents or objects of different sizes or importance. However, the size of nodes are rarely taken into account in network analysis, possibly inducing bias in network measures and confusion in their interpretation. Recently, a new axiomatic scheme of node-weighted network measures has been suggested for networks with undirected and unweighted edges. However, many real-world systems are best represented by complex networks which have directed and/or weighted edges. Here, we extend this approach and suggest new versions of the degree and the clustering coefficient associated to network motifs for networks with directed and/or weighted edges and weighted nodes. We apply these measures to a spatially embedded network model and a real-world moisture recycling network. We show that these measures improve the representation of the underlying systems' structure and are of general use for studying any type of complex network.

## 2.1 Introduction

In the course of the last decade complex network theory has become of great interest and has been widely applied in different domains including biology [Zhou et al., 2006], communication [Capocci et al., 2006], social science [Newman and Park, 2003], economy [Baskaran et al., 2011] and climatology [Donges et al., 2011, 2009b, Tsonis et al., 2006, Yamasaki et al., 2008]. The systems of interest are modeled as networks with nodes representing agents (e.g., cortical areas, topics in wikipedia, locations on the Earth) and edges standing for interactions between them (e.g., transmission of signals, hyperlinks, trades and statistical correlations). Several statistical measures have been developed to investigate the architecture of complex networks, e.g., by counting neighbors or measuring the tendency to form triangles [Boccaletti et al., 2006, Newman and Park, 2003].

In most of the studies, nodes represent agents or objects of different sizes or importance (for example heterogeneity in demography among countries, in surface area among gridded data points and in capacity among airports). However, the size of the nodes is rarely taken into account in the network properties, which can induce bias and ambiguity in the network measures [Heitzig et al., 2012]. In climate networks [Donges et al., 2009b, Gozolchiani et al., 2008, Tsonis et al., 2006], certain network measures tend to artificially increase towards the poles due to a decrease in surface area represented by the nodes and thus an increase in node density [Wiedermann et al., 2013]. Similarly, a region in the brain which is central in respect to its number of connections is not necessarily central when considering the volume of the brain it is connected to [Heitzig et al., 2012].

Recently, a novel framework for node-weighted network measures has been suggested based on the concept of “node-splitting invariance (n.s.i.)”, i.e., network measures unaffected by local aggregation or splitting of nodes [Heitzig et al., 2012]. Using node weights like volumes of the regions in brain networks, surface areas in climate networks, market values in world trade networks, sizes of the IP address space in the world-wide-web networks and article sizes in Wikipedia, the n.s.i. network measures improve the representation of the systems compared to their standard counterparts [Heitzig et al., 2012, Wiedermann et al., 2013]. However, n.s.i. network measures have been suggested only for networks with undirected and unweighted edges so far. This means that connections are considered to be symmetric and edges are usually established between nodes if the strength of the connection between them (for example statistical correlation in the case of climate networks) exceeds a certain threshold.

However, many real-world systems are best represented by networks with directed and/or weighted edges. Examples include world trade networks (with edge weights proportional to the amount traded with distinction between import and export), social networks (with edge weights proportional to the intensity of connection between people), air transport networks (with edge weights proportional to the number of available seats in flights between two airports) [Fagiolo, 2007] and moisture recycling networks (with edge weight proportional to the amount of moisture transported between grid cells) [Zemp et al., 2014b].

In this work we use the n.s.i framework to suggest measures (degree, strength and clustering coefficient possibly associated with motifs) for networks with directed and/or weighted edges by assigning weights to all nodes in the network as well. We apply our novel measures to two spatially embedded networks in which node weights are proportional to surface areas that are represented by them: (1) a benchmark network model in which edge weights depend on the geographical distance between nodes (in consistency with a previous study on the length scales of moisture feedback) [van der Ent and Savenije, 2011] and (2) a real-world network in which the edges represent direction and amount of moisture traveling from its source (evapotranspiration) to its final destination (precipitation) in South America. We show that the proposed n.s.i. measures improve the representation of the system compared to standard measures.

## 2.2 Preliminaries

Consider a graph  $G = (V, E)$  with a given set of nodes  $V$ , edges  $E$  and the number of nodes  $|V| = N$ . Each node in the network is identified by a natural number  $i = 1, \dots, N$ .  $A = \{a_{ij}\}_{i,j \in V}$  is the adjacency matrix of size  $N \times N$  with  $a_{ij} = 1$  iff there is an edge

connecting node  $i \in V$  and  $j \in V$  ( $i \neq j$ ) and  $a_{ij} = 0$  otherwise. If the network is directed (i.e., the edges have a direction associated to them),  $A$  is in general not symmetric ( $a_{ij} \neq a_{ji}$ ) and  $a_{ij} = 1$  iff there is a directed edge originating from node  $i \in V$  and pointing towards node  $j \in V$  and zero otherwise. We can assign to each edge  $E_{ij}$  an intensive weight  $m_{ij} \in [0, 1]$  representing the strength of the dependency between nodes  $i$  and  $j$  and define an edge weight matrix  $M = \{m_{ij}\}_{i,j \in V}$ . In this work we will present measures for different types of networks: binary undirected networks (BUN), edge-weighted undirected networks (WUN), binary directed networks (BDN) and edge-weighted directed networks (WDN).

In addition, we assign to each node  $i$  a positive and extensive weight  $w_i$  representing the size or importance of the node (sizes, surfaces, volumes, masses etc.) [Heitzig et al., 2012]. We define the total weight  $W = \sum_{i \in V} w_i$  as the node-weighted counterpart of the number of nodes  $N$ . A framework has been introduced that allows for the definition of node splitting invariant (n.s.i.) network measures which takes into account the weight of the nodes. For transferring standard network measures to their n.s.i counterparts we follow a four step construction mechanism as described in [Heitzig et al., 2012]: (a) sum up weights  $w_i$  whenever the original measure counts nodes or strengths, (b) treat every node  $i \in V$  as if it were connected with itself, (c) allow equality for  $i$  and  $j$  wherever the original measure involves a sum over distinct nodes  $i$  and  $j$  and (d) 'plug in' n.s.i. versions of measures wherever they are used in the definition of other measures. Step (b) is needed because the twin nodes that result from a splitting of one given node are linked due to their similarity. As a result, the node resulting from the merging of the twin nodes is connected to itself [Heitzig et al., 2012]. To achieve this step, we connect each node to itself using the extended adjacency matrix  $A^+ = \{a_{ij}^+\}_{i,j \in V}$  with  $a_{ij}^+ = a_{ij}$  and  $a_{ii}^+ = 1$ . An equivalent extended edge weight matrix is not needed as it is common to assign a weight to the self-loops already which can be equal to zero if the node is not connected to itself.

## 2.3 Definition of measures

In this section we will present some of the common local network measures  $f(G)$ , in particular the degree and clustering coefficient for networks with directed and/or weighted edges, and their n.s.i counterparts  $f^*(G)$ . Other global or local measures (e.g., the betweenness centrality) can also be corrected using the n.s.i. framework [Heitzig et al., 2012] but will not be developed in this paper.



### 2.3.1 Degree and strength

The degree and its n.s.i counterpart called “area-weighted connectivity” in the context of spatially embedded networks has been described for BUN [Heitzig et al., 2012, Tsonis et al., 2006]. We generalize to the case of a directed network (BDN and WDN). For a node  $i$ , the in-degree  $k_i^{in} = \sum_{j \neq i} a_{ji}$  is the number of edges pointing towards  $i$  and the out-degree  $k_i^{out} = \sum_{j \neq i} a_{ij}$  is the number of edges originating from  $i$ . As these measures only count nodes, making them n.s.i. can be achieved by considering steps (a), (b) and (c) in the construction mechanism. Hence,  $k_i^{in*} = \sum_{j \in V} w_j a_{ji}^+$  and  $k_i^{out*} = \sum_{j \in V} w_j a_{ij}^+$ . In the case of an undirected network (BUN and WUN), it is easy to see that the n.s.i degree is  $k_i^* = k_i^{in*} = k_i^{out*}$ .

For edge-weighted networks the concept of degree is extended to the one of strength. In a WDN, the in-strength  $s_i^{in} = \sum_{j \neq i} m_{ji}$  measures the total strength of edges pointing towards  $i$  and the out-strength  $s_i^{out} = \sum_{j \neq i} m_{ij}$  measures the total strength of edges originating from  $i$ . Using steps (a), (b) and (c), the n.s.i. versions of these measures are  $s_i^{in*} = \sum_{j \in V} w_j m_{ji}$  and  $s_i^{out*} = \sum_{j \in V} w_j m_{ij}$ . If the network is not directed (WUN), we have  $s_i^* = s_i^{in*} = s_i^{out*}$ .

While the standard version of the in- and out- degree and the in- and out-strength can take integer values between 0 and  $N - 1$ , the n.s.i version of these measures can take real numbers between 0 and  $W$ .

### 2.3.2 Clustering coefficient and motifs

In simple networks (BUN), the clustering coefficient measures the tendency to form clusters or triangles formed by three connected nodes. It is defined as the ratio between the number of triangles which involve the node  $i$  and the total number of triangles that  $i$  could have formed [Fagiolo, 2007]:

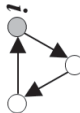
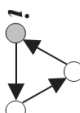
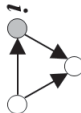
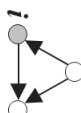
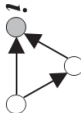
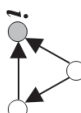
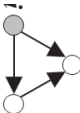
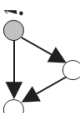
$$C_i = \frac{\sum_{j \neq i} \sum_{h \neq (i,j)} a_{ij} a_{ih} a_{jh}}{k_i(k_i - 1)} = \frac{(A^3)_{ii}}{k_i(k_i - 1)}. \quad (2.1)$$

The n.s.i version of this measure obtained by using all four steps has already been suggested for BUN [Heitzig et al., 2012]:

$$C_i^* = \frac{\sum_{j \in V} \sum_{h \in V} w_j w_h a_{ij}^+ a_{ih}^+ a_{jh}^+}{(k_i^*)^2} = \frac{((A')^3)_{ii}}{w_i (k_i^*)^2}, \quad (2.2)$$

with  $A' = \{a_{ij}^+ w_j\}$ .

TABLE 2.1 Network motifs taxonomy (Mid. stands for Middleman), patterns and the associated quantities used in the calculation of the directed clustering coefficients. On the left side, quantities used in the standard version:  $t_i$  is the number of triangles formed by  $i$ ,  $\tilde{t}_i$  is its edge-weighted counterpart of  $t_i$  and  $T_i$  is the maximum number of such triangles that  $i$  can form [Fagiolo, 2007]. On the right side, the n.s.i versions of these quantities are given.

Tax.	Patterns	$t_i$	$\tilde{t}_i$	$T_i$	$t_i^*$	$\tilde{t}_i^*$	$T_i^*$
Cycle	 	$(A)_{ii}^3$	$(\hat{M})_{ii}^3$	$k_i^{in} k_i^{out} - k_i^{bil}$	$(A')_{ii}^3$	$(\hat{M}')_{ii}^3$	$k_i^{*in} k_i^{*out}$
Mid.	 	$(AA^T A)_{ii}$	$(\hat{M}\hat{M}^T \hat{M})_{ii}$	$k_i^{in} k_i^{out} - k_i^{bil}$	$(A'A^T A)_{ii}$	$(\hat{M}'\hat{M}'^T \hat{M}')_{ii}$	$k_i^{*in} k_i^{*out}$
In	 	$(A^T A^2)_{ii}$	$(\hat{M}^T \hat{M}^2)_{ii}$	$k_i^{in} (k_i^{in} - 1)$	$(A'^T (A')^2)_{ii}$	$(\hat{M}'^T (\hat{M}')^2)_{ii}$	$(k_i^{*in})^2$
Out	 	$(A^2 A^T)_{ii}$	$(\hat{M}^2 \hat{M}^T)_{ii}$	$k_i^{out} (k_i^{out} - 1)$	$((A')^2 A'^T)_{ii}$	$((\hat{M}')^2 \hat{M}'^T)_{ii}$	$(k_i^{*out})^2$

In the case of a WUN, one has to take into account the edge weights involved in the triangles. There are several ways to define the contribution of the triangle depending on the application of the network analysis. Here, in agreement with [Fagiolo, 2007], we decide to take the geometric mean of the weights of the three involved edges. The clustering coefficient for edge-weighted networks is then:

$$\tilde{C}_i = \frac{\sum_{j \neq i} \sum_{h \neq (i,j)} m_{ij}^{1/3} m_{ih}^{1/3} m_{jh}^{1/3}}{k_i(k_i - 1)} = \frac{(\hat{M}^3)_{ii}}{k_i(k_i - 1)}, \quad (2.3)$$

with  $\hat{M} = M^{[1/3]} = \{m_{ij}^{1/3}\}$ .

The n.s.i version of this measures then reads as:

$$\tilde{C}_i^{r*} = \frac{\sum_{j \in V} \sum_{h \in V} w_j w_h m_{ij}^{1/3} m_{ih}^{1/3} m_{jh}^{1/3}}{(k_i^*)^2} = \frac{((\hat{M}')^3)_{ii}}{w_i (k_i^*)^2}, \quad (2.4)$$

with  $\hat{M}' = \{(m_{ij})^{1/3} w_j\}$ .

In directed networks, the notion of cluster or triangle is replaced by the notion of network motifs [Milo et al., 2002]. Four types of network motifs have been emphasized depending on the direction of the edges involved in the triangle [Fagiolo, 2007] (see Table 2.1 for illustration). In the case of a BDN, the clustering coefficient of nodes  $i$  associated to a motif is defined as  $C_i = t_i/T_i$ , the fraction between the number of triangles  $t_i$  that belong to the particular motif actually formed by  $i$  and the total number of triangles  $T_i$  of that motif that  $i$  could have formed [Fagiolo, 2007]. The numerator  $t_i$  can be calculated by simple operations on the adjacency matrix  $A$  and the denominator  $T_i$  can be calculated by using the in-degree, out-degree and the bilateral degree ( $k_i^{bil} = \sum_{j \neq i} a_{ji} a_{ij}$  is the number of bilateral edges between  $i$  and its neighbors) (see Table 2.1). This measure has been generalized for the case of WDN by taking into account the edge-weighted contribution of the triangles [Fagiolo, 2007] and becomes  $\tilde{C}_i = \tilde{t}_i/T_i$  where  $\tilde{t}$  is the edge-weighted counterpart of  $t$  and can be calculated by substituting the matrix  $A$  with the matrix  $\hat{M} = M^{[1/3]} = \{m_{ij}^{1/3}\}$ .

The n.s.i version of these measures becomes:

$$C_i^* = \frac{t_i^*}{w_i T_i^*} \quad (2.5a)$$

$$\tilde{C}_i^{r*} = \frac{\tilde{t}_i^*}{w_i T_i^*}, \quad (2.5b)$$

where  $t_i^*$  is calculated by substituting  $A$  with  $A' = \{a_{ij}^+ w_j\}$  and  $A^T$  with  $A^{T'} = \{a_{ji}^+ w_j\}$ ,  $\tilde{t}^*$  by substituting  $\hat{M}$  with  $\hat{M}' = \{(m_{ij})^{1/3} w_j\}$  and  $\hat{M}^T$  with  $\hat{M}^{T'} = \{(m_{ji})^{1/3} w_j\}$  and  $T^*$  is obtained by substituting the in- and out- degree with their n.s.i counterparts as

described above. The bilateral degree is no longer needed in the n.s.i version of the measure. In fact, it was subtracted in the denominator of the clustering coefficient for the motifs Cycle and Middleman in order to exclude the false triangles formed by a node and a pair of directed edges pointing to and originating from the same node [Fagiolo, 2007]. In the n.s.i version of the clustering coefficient, a node connected to itself and bilaterally connected with another one forms a triangle and is accounted for in the clustering coefficient. All standard and n.s.i versions of the clustering coefficient can take values between 0 and 1.

## 2.4 Application 1: Benchmark network

In order to investigate the impact of the n.s.i correction on the network measures, we first construct an ensemble of 100 realizations of an undirected and edge-weighted (WUN) benchmark network model. Nodes represent grid cells which cover the global Earth surface (excluding the poles) with a spatial resolution of  $\Delta = 5^\circ$  in longitude and latitude resulting in a total number of  $N=2,592$ . This is a typical representative of grids found in many datasets used in climate and environmental sciences. The probability  $p_{ij}$  that node  $i$  and node  $j$  are linked is a function of the geodesic distance between them<sup>2</sup>. We assign to each edge a weight which is equal to the probability ( $m_{ij} = p_{ij}$ ). This relationship between the distance and the weights of the edges has been used in other benchmark networks [Heitzig et al., 2012] and is consistent with a previous study on the length scales of moisture feedback [van der Ent and Savenije, 2011]. In this model which is perfectly homogeneous and isotropic, we expect the same network properties for all latitudes. To account for the irregular sampling, we assign to each node  $i \in V$  a weight which represents the size of the portion of the Earth's surface it covers:  $w_i = \cos(\text{latitude}_i)$  [Tsonis et al., 2006]. In addition, we construct another ensemble of this benchmark network model in which we pick randomly  $n_\lambda = \cos(\text{latitude}_\lambda) \cdot N$  nodes for each latitude  $\lambda$  (1654 nodes in total) such that the globe is covered approximately homogeneously as achieved in a previous study [Gozolchiani et al., 2011, Wang et al., 2013].

Figure 2.1 shows the zonal average of the standard and the n.s.i. version of strength and edge-weighted clustering coefficient applied to these benchmark networks averaged over all ensembles. The standard deviations of the clustering coefficient are larger than those of the strength due to finite size effect (i.e., there are more neighbors than triangles). The standard strength and edge-weighted clustering coefficient  $\tilde{C}$  increase towards the poles. Regarding the strength, it is due to (1) a higher number of neighbors in this area and (2)

<sup>2</sup> $p_{ij} = \exp(-g_{ij}/\lambda)$  with  $\lambda$  representing the typical length scale and  $g_{ij}$  the geodesic distance between  $i$  and  $j$ . In this case we chose  $\lambda = 1,110$  km to ensure an edge density of about 0.02.

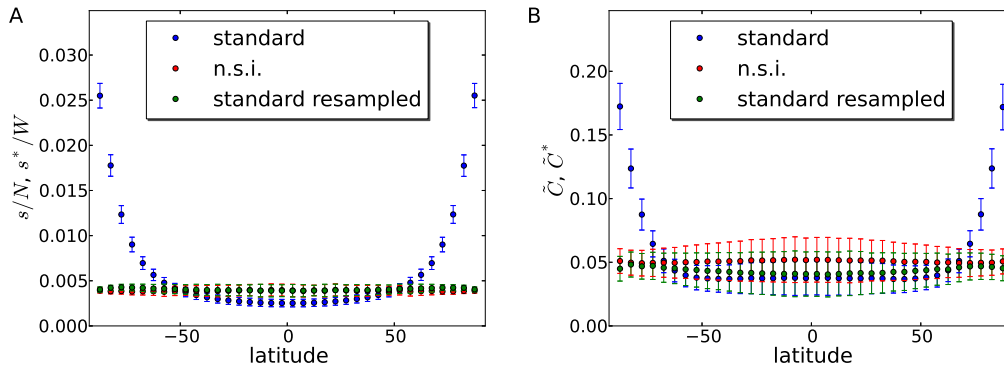


FIGURE 2.1 Zonal averages (symbols) and standard deviations (error-bars) of the standard and n.s.i. versions of (A) the normalized strength and (B) the edge-weighted clustering coefficient applied to the benchmark edge-weighted and undirected network (WUN) model.

higher weights of the edges connecting nodes at the poles. Regarding  $\tilde{C}$ , it is explained by (1) an increase in the probability that two neighbors of a node are also neighbors and (2) an increase in the weights of the edges involved in the triangles. This effect disappears after taking into account the surface covered by grid cells in different latitudes using the n.s.i. correction, as well as after sampling the nodes homogeneously on the globe. We note that for both measures, the first effect has been observed in the binary versions of the measures (degree and clustering coefficient) in a previous study [Heitzig et al., 2012]. However, the second factor is specific to edge-weighted networks as it is due to increasing weights of the edges due to a decreasing geodesic distance between nodes with increasing latitude. Thus, edge-weighted network measures experience systematic biases at latitudes higher than about  $50^\circ$  N or lower than  $50^\circ$  S due to increased node density which can be corrected using the n.s.i. versions of the measures. Sampling networks homogeneously would also enable to fix these biases, but generally introduces an additional uncertainty. The n.s.i. correction has the advantage of directly avoiding such undesired operations.

## 2.5 Application 2: Moisture recycling network

Next, we consider the output of the Water Accounting Model-2 layers (WAM-2layers) [van der Ent et al., 2014] as a directed and edge-weighted complex network with self-interactions (WDN). WAM-2layers is forced by satellite data of hydrological cycle components and wind speed and diagnose the spatial distribution of atmospheric moisture from a certain location. Nodes in the network represent grid cells and edges the direction and amount of water traveling from its source (evapotranspiration) to its final destination (precipitation). Grid cells are regularly distributed over the South American

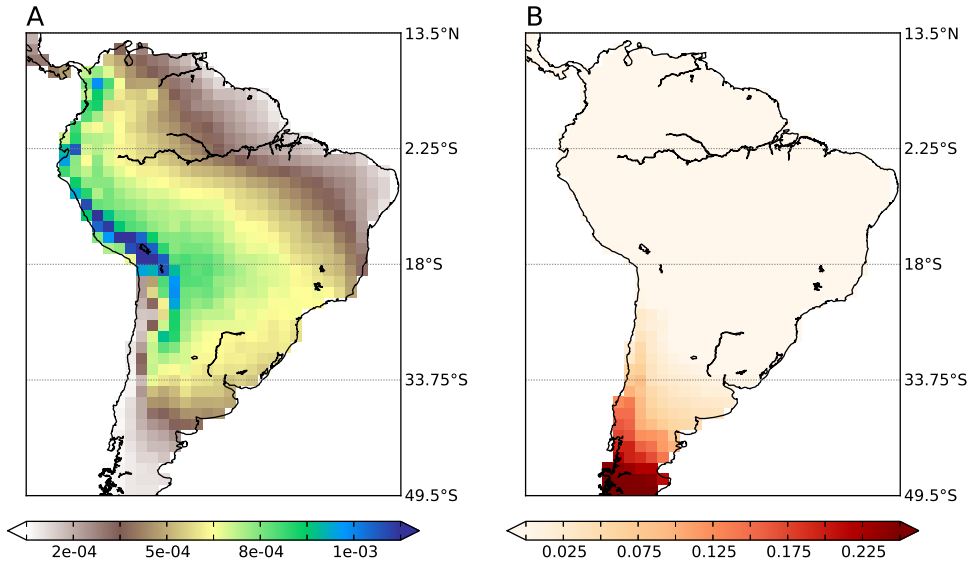


FIGURE 2.2 (A) Normalized n.s.i. in-strength ( $s^{in*}/W$ ) (B) relative decrease of this measure compared to the standard version ( $(s^{in}W - s^{in*}N)/s^{in}W$ ).

continent with a spatial resolution of 1.5 degree longitude and latitude, which leads to a total number of  $N=681$  nodes. The weight  $m_{ij}$  of an edge pointing from node  $i$  to node  $j$  is the amount of moisture recycled from  $i$  to  $j$  (i.e., evapotranspiration in  $i$  which precipitates in  $j$ ) and  $m_{ii}$  is the amount of locally recycled moisture. All the weights are normalized by the maximum amount of moisture recycled in the network such that  $0 < m_{ij} < 1 \forall i, j = 1, \dots, N$ . We note that the weights of the edges follow a similar relationship to the geodesic distances between nodes as modeled in the benchmark network. Again, to account for the irregular sampling, we assign to each node  $i$  a weight as in the benchmark network:  $w_i = \cos(\text{latitude}_i)$ .

The in- and out-strength have been rescaled to quantify respectively the fraction of precipitation that has been last evaporated from continental grid cells (Fig. 2.2A) and the fraction of the evapotranspiration which precipitates in continental grid cells (Fig. 2.3A). These measures highlight sources and sinks of continental moisture and are in agreement with a previous study on continental moisture recycling on the global scale [van der Ent et al., 2010]. Due to the increasing node density towards the South pole, there is an overestimation of up to 30% of these quantities (Fig. 2.2B and 2.3B) in the southern part of South America which is corrected by the n.s.i. versions of these measures. Note that for out-strength the bias due to increasing node density towards the south pole extends significantly further northwards than for in-strength.

The n.s.i. edge-weighted clustering coefficient ( $\tilde{C}^*$ ) associated to the different motifs enables us a direct interpretation in terms of moisture flux. i)  $\tilde{C}^*$  associated with the motif “In” and “out” show regions which have the tendency to integrate and distribute

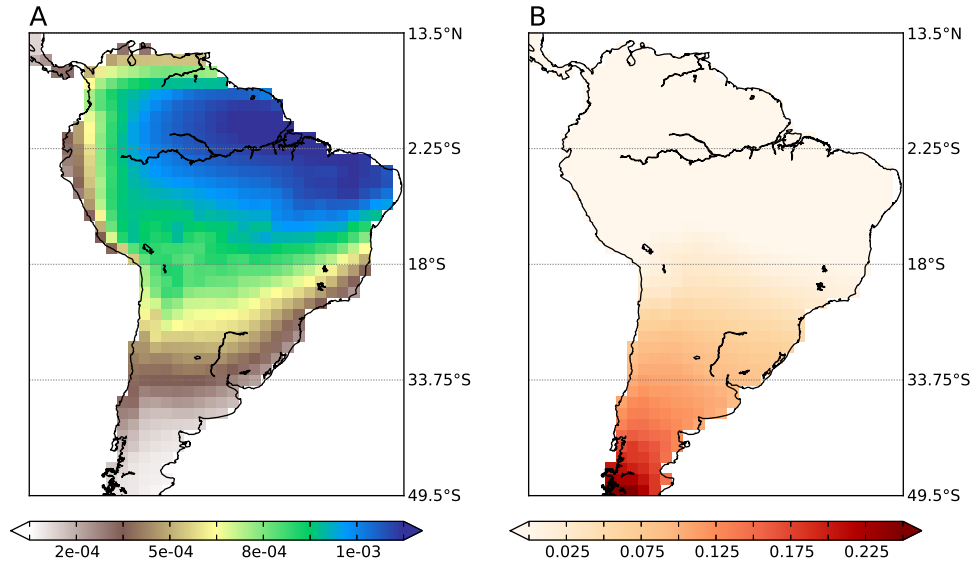


FIGURE 2.3 (A) Normalized n.s.i. out-strength ( $s^{out*}/W$ ) and (B) relative decrease of this measure compared to the standard version ( $(s^{out*}W - s^{out*N})/s^{out*}W$ ).

moisture (Figs. 2.4A and 2.4B). ii)  $\tilde{C}^*$  associated with the motif “Middleman” highlights intermediary regions involved in alternative pathways to the direct transport of moisture (Fig.2.4C). iii) If  $\tilde{C}^*$  is associated with the motif “Cycle”, high values indicate regions where moisture transport forms a closed loop, i.e., where evapotranspiration returns as precipitation in the same grid cell after one precipitation-evaporation event (Fig. 2.4D). Considered together, these results highlight the architecture of moisture recycling in South America. The eastern side of the Amazon basin is a source of moisture for the south-western part of the basin and the subtropical South America and moisture precipitates and evaporates on the way in the central-western part of the Amazon basin. However, the standard versions of the measure are overestimated in the southern part of South America where the node density increases. The n.s.i. versions are slightly decreasing compared to the standard versions of the measures when approaching the Pole, indicating that the n.s.i. correction allows to get rid of this overestimation (Fig. 2.5). We note that the use of the n.s.i. version has shifted the scale of the clustering coefficient.

In South America, the n.s.i. corrections do not lead to strong qualitative changes in the results of the presented measures because the southern part is dry and therefore there is little moisture transport south of  $35^\circ$  S. However on a global scale, moisture is transported from and into regions located close to the North pole [van der Ent et al., 2010]. Therefore, the use of n.s.i. versions of network measures provides significant qualitative and quantitative improvement of the representation of moisture recycling.

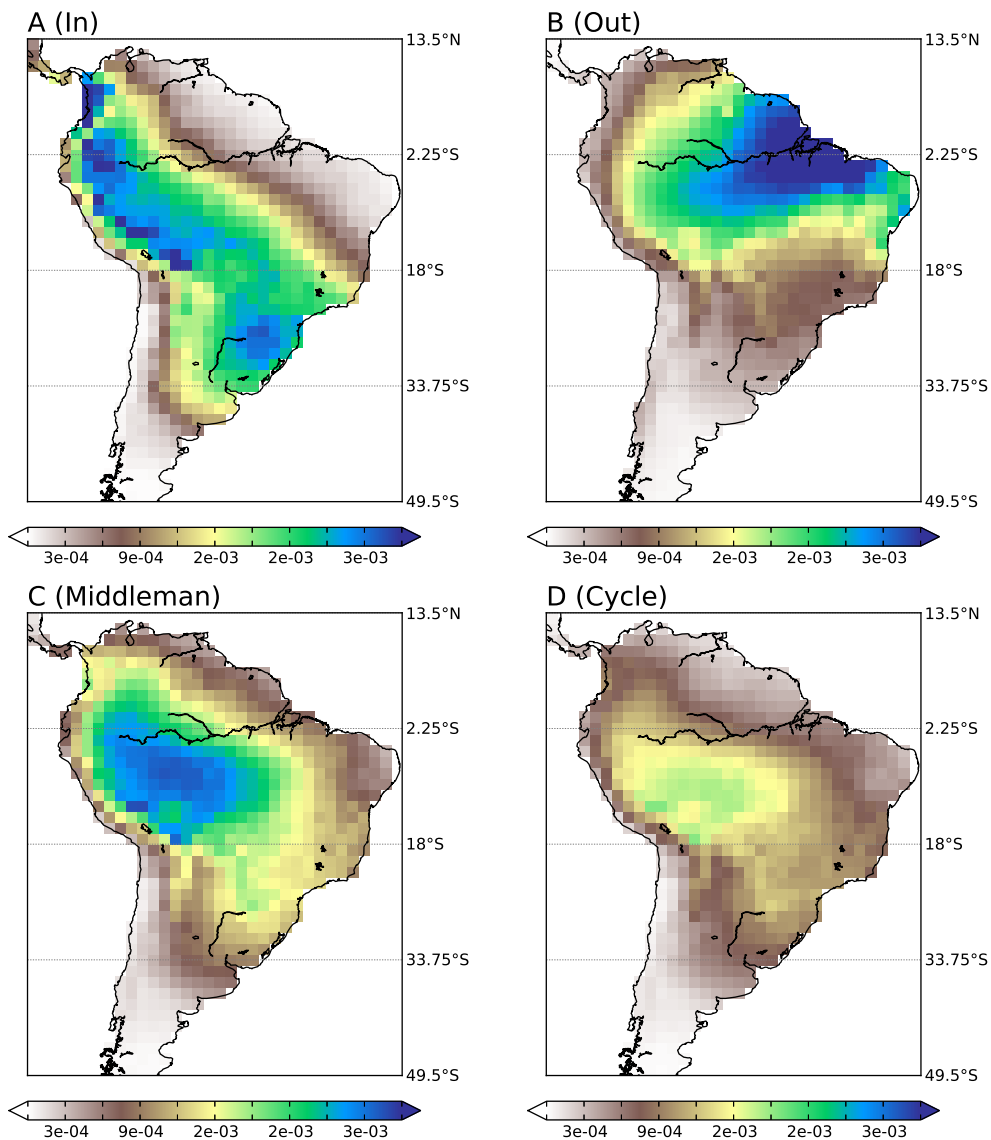


FIGURE 2.4 N.s.i. edge-weighted and direct clustering coefficients  $\tilde{C}^*$  associated with the different network motifs.

## 2.6 Conclusion

In this work, we have developed new versions of some measures for directed and/or edge-weighted networks in order to take into account the weights of nodes. These measures respect the well-established criterion of node-splitting invariance (n.s.i.), which means that they are invariant with respect to local splitting or aggregation of nodes. These measures include the usual edge-weighted and/or directed degree but also clustering coefficient associated to different network motifs. In a first part we have given the standard and the n.s.i. versions of these measures and in a second part we have applied them to two different spatially embedded networks: (1) a benchmark network model which is undirected and edge-weighted on a global scale and (2) a real-world directed



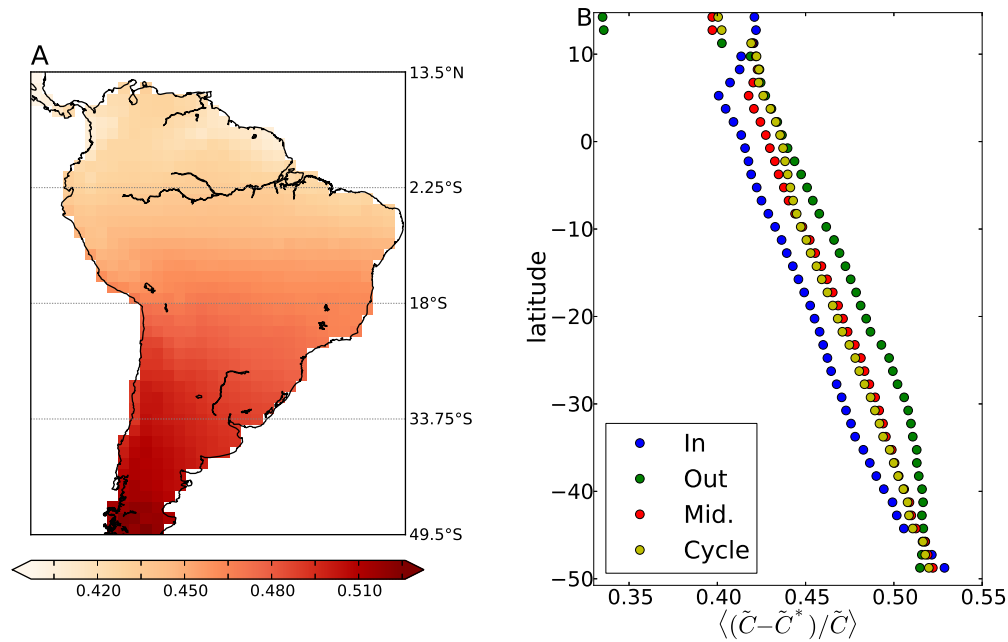


FIGURE 2.5 Relative decrease in the edge-weighted clustering coefficient after n.s.i. correction  $(\tilde{C} - \tilde{C}^*)/\tilde{C}$  as observed in (A) a map for the motif Middleman and (B) zonal averages for all motifs.

and edge-weighted moisture recycling network constructed using an atmospheric water tracking model over South America. In both networks we have assigned to each node a weight representing the surface area represented by it. We have shown that the use of our measures avoids systematic biases created by a higher node density and larger weights of the edges towards the poles. In the moisture recycling network there is little moisture transport from and to the southern part of South America. We argue that on global scale it should lead to a more accurate estimation of the contribution of export and import of continental moisture and to a better identification of key regions for the indirect transport of moisture. These improvements are possible because the heterogeneity of the size or the importance of nodes can be taken into account in the network analysis, which is not the case in most complex network studies. Therefore, we expect that the proposed measures might lead to important improvements in the analysis of many real-world complex systems such as chemical, neuronal, social, trade, climate, traffic or ecological networks.

## 2.7 Acknowledgments

This paper was developed within the scope of the IRTG 1740 / TRP 2011/50151-0, funded by the DFG / FAPESP and the IRTG 9751. J.F. Donges acknowledges funding from the Stordalen Foundation and BMBF (project GLUES). We thank R. J. Vand der

Ent for providing us with the model output, C.-F. Schleussner for discussions and K. Thonicke for comments on the manuscript.

## Chapter 3

# On the importance of cascading moisture recycling in South America

An edited version of this chapter (together with appendix A and B) has been published in the journal *Atmospheric Chemistry and Physics*:

Zemp, D. C., Schleussner, C.-F., Barbosa, H. M. J., van der Ent, R. J., Donges, J. F., Heinke, J., Sampaio, G., and Rammig, A.: On the importance of cascading moisture recycling in South America, *Atmos. Chem. Phys.*, 14, 13337-13359, doi:10.5194/acp-14-13337-2014, 2014.

## Abstract

Continental moisture recycling is a crucial process of the South American climate system. In particular, evapotranspiration from the Amazon basin contributes substantially to precipitation regionally as well as over other remote regions such as the La Plata basin. Here we present an in-depth analysis of South American moisture recycling mechanisms. In particular, we quantify the importance of cascading moisture recycling (CMR), which describes moisture transport between two locations on the continent that involves re-evaporation cycles along the way. Using an Eulerian atmospheric moisture tracking model forced by a combination of several historical climate data sets, we were able to construct a complex network of moisture recycling for South America. Our results show that CMR contributes about 9–10% to the total precipitation over South America and 17–18% over the La Plata basin. CMR increases the fraction of total precipitation over the La Plata basin that originates from the Amazon basin from 18–23 to 24–29% during the wet season. We also show that the south-western part of the Amazon basin is not only a direct source of rainfall over the La Plata basin, but also a key intermediary region that distributes moisture originating from the entire Amazon basin towards the La Plata basin during the wet season. Our results suggest that land use change in this region might have a stronger impact on downwind rainfall than previously thought. Using complex network analysis techniques, we find the eastern side of the sub-tropical Andes to be a key region where CMR pathways are channeled. This study offers a better understanding of the interactions between the vegetation and the atmosphere on the water cycle, which is needed in a context of land use and climate change in South America.

### 3.1 Introduction

Continental moisture recycling, the process by which evapotranspiration from the continent returns as precipitation to the continent [Brubaker et al., 1993, Eltahir and Bras, 1994, van der Ent et al., 2010], is particularly important for the South American hydrological cycle. In the Amazon basin, between 25 and 35% of the moisture is regionally recycled [Bosilovich and Chern, 2006, Burde et al., 2006, Dirmeyer et al., 2009, Eltahir and Bras, 1994, Trenberth, 1999]. Particularly during the wet season, the moisture from the Amazon basin is exported out of the basin, transported via the South American low-level jet (SALLJ) along the Andes and contributes to precipitation over the La Plata basin [Arraut et al., 2012, Arraut and Satyamurty, 2009, Dirmeyer et al., 2009, Drumond et al., 2014, 2008, Marengo, 2005, Martinez and Dominguez, 2014, van der Ent et al., 2010].

Land use change – in particular deforestation in the Amazon basin – alters the evapotranspiration rate and affects the water cycle (see review in Marengo, 2006). A resulting reduction in regional moisture supply may have important consequences for the stability of Amazon rainforests [Betts et al., 2004, Cox et al., 2004, Hirota et al., 2011, Knox et al., 2011, Oyama and Nobre, 2003, Spracklen et al., 2012]. In addition, downwind rainfall reduction may have negative effects on rainfed agriculture in the La Plata basin [Keys et al., 2012, Rockström et al., 2009]. Even if the regional impact of changes in precipitation patterns from deforestation has been intensively studied using simulations from atmospheric general circulation models with deforestation scenarios [Bagley et al., 2014, Da Silva et al., 2008, Hasler et al., 2009, Lean and Warrilow, 1989, Medvigy et al., 2011, Nobre et al., 1991, 2009, Sampaio et al., 2007, Shukla et al., 1990, Walker et al., 2009, Werth and Avissar, 2002], the magnitude of rainfall reduction and the location of the most affected regions are still uncertain. In order to improve predictability of rainfall changes with future land use and climate change, further advancement in our understanding of continental moisture recycling in South America is needed.

To identify the sources and sinks of continental moisture and to quantify regional and continental moisture recycling rates in South America, several methods have been used including isotopes [Gat and Matsui, 1991, Salati et al., 1979, Victoria et al., 1991], atmospheric bulk models [Brubaker et al., 1993, Burde et al., 2006, Eltahir and Bras, 1994, Trenberth, 1999] and quasi-isentropic back-trajectory method [Bagley et al., 2014, Dirmeyer et al., 2009, Spracklen et al., 2012]. In addition, an Eulerian numerical atmospheric moisture tracking experiment allows one to identify the spatial distribution of evapotranspiration from a specific region. It has been performed online with a general circulation model [Bosilovich and Chern, 2006] or a posteriori (offline) with reanalysis data (Keys et al., 2012, Sudradjat et al., 2002, van der Ent et al., 2010; see a review of the methods in van der Ent et al., 2013 and Burde and Zangvil, 2001).

In most of the previous atmospheric moisture tracking studies, moisture from a group of grid cells covering a region of interest (typically the continent) is tracked simultaneously until it returns to the land surface as precipitation or leaves the domain. This approach is useful for investigating how evapotranspiration from a specific location is transported in the atmosphere and precipitates at first in another location. However, precipitating moisture can be re-evapotranspired in the same location (re-evaporation cycle) and can be transported further downwind before it falls again as precipitation over land. In most of the previous studies, only moisture recycling with no intervening re-evaporation cycles (direct moisture recycling, DMR) is considered. Here, we track moisture evaporating from each grid cell within a larger domain (i.e., the South American continent) individually. By doing so, we are able to diagnose for each grid cell the amount of evaporating moisture that precipitates in any other cell, i.e., to build a moisture recycling

TABLE 3.1 Input data sets used for building moisture recycling networks. The first year of the period is omitted from the results because of model spin-up.

Input name	Evapotranspiration product	Precipitation product	Period
Input MOD	MODIS	TRMM	2000–2010
Input LFE	LandFlux-EVAL	Average of CRU, GPCC, GPCP and CPC	1989–1995

network. Such an approach enables us to study not only the DMR between important sub-regions of the South American continent (e.g., the Amazon and the La Plata basin), but also the moisture transport that involves at least one re-evaporation cycle (cascading moisture recycling, CMR).

While only a few previous studies deal with the importance of CMR [Goessling and Reick, 2013, Numaguti, 1999], these studies are based on general circulation models rather than on observation-based data. In the following, we quantify the importance of CMR for the regional climate in South America using numerical atmospheric moisture tracking a posteriori with historical climatological data sets. Our analysis is based on precipitation, evapotranspiration, wind and humidity data sets from a combination of observation-based, reanalysis and merged synthesis products (average of several existing products).

Our network-based approach allows us to apply analysis methods developed in complex network theory to improve our understanding of moisture recycling pathways in South America. The potential of complex network-based analysis of the climate system has been shown in a range of applications such as the detection of teleconnections [Donges et al., 2009a,b, Tsonis et al., 2008], the propagation of extreme events [Boers et al., 2013, Malik et al., 2012] and El Niño forecasting [Ludescher et al., 2013]. While previous network-based studies relied on statistical analysis of correlations between time series in the network construction, our approach is based on a flux-based network, which represents a substantial methodological advancement.

In this study we focus on three key questions:

1. What is the importance of CMR in South America and in particular for the moisture transport from the Amazon basin towards the La Plata basin?
2. What are the important intermediary regions for the transport of moisture from sources to sinks on the continent?

### 3. What are the key regions where the pathways of CMR are channeled?

In Sect. 2.1 we describe the tagged water experiment using the Eulerian atmospheric moisture tracking model WAM-2layers (Water Accounting Model- two layers) and we explain how we use it to build moisture recycling networks. We explain the assumptions made in the proposed analysis in Sect. 2.2. We develop new measures in Sects. 2.3 and 2.4 and we present the complex network analysis in Sect. 2.5. An explanation of the complementarity of the measures is presented in Sect. 2.6. After comparing the continental and regional recycling ratios with other existing studies in Sect. 3.1, we present and discuss new results on the importance of CMR in Sect. 3.2 and on complex network analysis in Sect. 3.3. We present an in-depth analysis of the moisture recycling between the Amazon basin and the La Plata basin in Sect. 3.4. Finally, we warn against possible effects of land use change in the intermediary regions in Sect. 3.5. As many terms have been introduced in this study, we refer the reader to the glossary in Appendix A.

## 3.2 Methods

### 3.2.1 Building moisture recycling networks

#### 3.2.1.1 Description of the moisture tagging experiment in WAM-2layers

In this study we make use of the offline Eulerian atmospheric moisture tracking model WAM-2layers (Water Accounting Model-two layers) version 2.3.01 [van der Ent et al., 2014]. It is an update of a previous version that has been used in a variety of publications focusing on moisture tracking and moisture recycling (e.g., Keys et al., 2012, van der Ent et al., 2010, van der Ent and Savenije, 2011). The actual tracking in WAM-2layers is performed a posteriori with two different data sets (see input data in Sect. 3.2.1.2). Evapotranspiration from each grid cell is tagged and subsequently tracked in the atmosphere by applying water balance principles to each grid cell, consisting of a well-mixed upper and lower part. The two-layer approach is simplified compared to full 3-D tracking, but was shown to perform comparably well [van der Ent et al., 2013].

The WAM-2layers runs on a  $1.5^\circ$  longitude–latitude grid. Because the local moisture recycling is scale dependent, the amount of locally recycled moisture within a grid cell depends on the spatial resolution of the model [van der Ent and Savenije, 2011, Fig. 4]. However, in our study, the re-evaporation cycles are occurring along the pathway of moisture recycling. Since we are integrating over all pathways contributing to the large-scale moisture transport, the spatial resolution has little influence on our results. The

typical length scale of direct links in moisture recycling is larger than 1000 km (ca.  $9^\circ$ ) in the region [van der Ent and Savenije, 2011, Fig. 5], which indicates that our resolution is sufficient to analyze the processes of interest.

We omitted the first year of the considered period from the results because of model spin-up. The outputs are aggregated first to monthly, then to seasonally average imports and exports between all land grid cells. This temporal resolution is reasonable for our purpose since the timescale of moisture recycling does not exceed 30 days in the studied region [van der Ent and Savenije, 2011, Fig. 5].

These seasonal averages are used to build two seasonal moisture recycling networks, which are assumed to be static for the whole season. This implies that in the proposed analysis, for each season moisture is tracked forward and backward in space but not in time.

### 3.2.1.2 Input of WAM-2layers

In order to reduce the uncertainty associated with the input data, we used two different data sets (that we call input MOD and input LFE; see Table 3.1) as input for WAM-2layers. The input MOD covers the period 2000–2010 and contains 3-hourly precipitation estimates from the Tropical Rainfall Measuring Mission (TRMM) based on the algorithm 3B-42 (version 7) [Huffman et al., 2007] and 8 days of evapotranspiration estimates from Moderate Resolution Imaging Spectroradiometer (MODIS) based on the MOD16 ET algorithm [Mu et al., 2011]. Precipitation data sets from TRMM are considered to be reliable over South America and in particular in the Amazon basin where others products perform poorly due to the lack of ground-based measurements [Franchito et al., 2009, Rozante et al., 2010]. TRMM precipitation data are shown to represent high-frequency variability sufficiently well [Kim and Alexander, 2013]. However, it is systematically biased during the dry season in the north-eastern coast of Brazil, where precipitation is underestimated [Franchito et al., 2009] and at the junction of Argentina, Paraguay and Brazil, where it is overestimated [Rozante and Cavalcanti, 2008]. Evapotranspiration from MODIS is estimated using the Penman–Monteith equation [Monteith, 1965] forced by satellite and meteorological reanalysis data. Like other observation-based evapotranspiration estimations, the quality of the MODIS data set depends on the quality of the forcing data and the parameterization of the algorithm. The MODIS evapotranspiration data set has been validated with 10 eddy flux towers located in the Amazonian region under various land-cover types [Loarie et al., 2011, Ruhoff, 2011].



The input LFE covers the period 1989–1995 and contains monthly evapotranspiration averaged from 40 different products (LandFlux-EVAL, Mueller et al., 2013), as well as monthly precipitation averaged from four different observation-based precipitation data sets: Climate Research Unit (CRU) [New et al., 2000], the Global Precipitation Climatology Centre (GPCC) [Adler et al., 2003, Huffman et al., 1995], the Global Precipitation Climatology Project (GPCP) [Adler et al., 2003] and the unified climate prediction center (CPC) from the National Oceanic and Atmospheric Administration (NOAA) [Chen et al., 2008]. The four precipitation data sets are interpolations from rain gauge data (in combination with satellite observation in the case of GPCC) and have been considered as the forcing data set for the observation-based evapotranspiration product in LandFlux-EVAL [Mueller et al., 2013]. Here, we include the evapotranspiration products in LandFlux-EVAL that are not only derived from observations but also calculated via land surface models and output from reanalysis.

Both data sets are complemented by 6-hourly specific humidity and wind speed in three dimensions from the ERA-Interim reanalysis product [Dee et al., 2011] for the corresponding periods. Because these two variables are used to get the horizontal moisture fluxes, the choice of the reanalysis product matters for the eventual results of the WAM-2layers [Keys et al., 2014]. Humidity estimation has been improved in the ERA-Interim product in comparison with other reanalysis products [Dee and Uppala, 2008].

The temporal resolution of the input data needed in WAM-2layers is 3 h. Therefore, we downscaled the input MOD and LFE based on the temporal dynamics found in the ERA-Interim evapotranspiration and precipitation products. In addition, all data are downscaled to 0.5 h as requested by the numerical scheme of WAM-2layers. All data are upscaled to a regular grid of  $1.5^\circ$  longitude–latitude and cover the South American continent to  $50^\circ$  S, which is the southernmost latitude covered by the TRMM product.

The long-term seasonal average of evapotranspiration and precipitation as well as moisture flux divergence (evapotranspiration–precipitation) are shown in Figs. 3.1 and 3.2. The high rainfall in the South Atlantic Convergence Zone (including the Amazon basin, central and south-eastern Brazil) during the wet season (December to March) compared to the dry season (June to September) characterizes the South American monsoon system (SAMS) [Arraut and Satyamurty, 2009, Grimm et al., 2004, Liebmann et al., 1999].

The evapotranspiration and precipitation in the input MOD have an overall positive bias compared to the input LFE. While the spatial patterns of evapotranspiration show good agreement on a continental scale, there are also several distinct differences. In particular the wet season evapotranspiration in sub-tropical South America is much weaker in the input MOD than LFE. Interpreting and explaining the differences between the data sets

is beyond the scope of this study. For an evaluation of the different types of products (model calculation, observation-based and reanalysis), we refer the reader to Mueller et al. [2011].

In both inputs, the evapotranspiration exceeds the total precipitation in the southern part of the Amazon basin during the dry season, indicating that this region is a net source of moisture for the atmosphere (Figs. 3.1c and 3.2c). This is in agreement with previous studies demonstrating a maintaining of the greenness of the Amazon forests [Morton et al., 2014] and the absence of water stress during the dry season due to the deep root system, which enables the pumping of the water from the deeper water table [Miguez-Macho and Fan, 2012, Nepstad et al., 1994].

We find that, averaged over the full time period, evapotranspiration exceeds precipitation in north-eastern Brazil and in the Atacama Desert in both data sets, as well as along the Andes in the input MOD. Possible explanations for the imbalance in these arid to semi-arid regions are irrigation or biases in the input data as mentioned above. As this might lead to a bias in moisture recycling ratios due to an overestimation of the contribution of evapotranspiration to local precipitation, we will exclude these grid cells from our analysis.

### 3.2.1.3 Construction of a complex network based on WAM-2layers

The output of WAM-2layers is a matrix  $\mathbf{M} = \{m_{ij}\}$  for all  $i, j \in N$  with  $N$  the number of grid cells in the continent ( $N = 681$ ). The non-diagonal element  $m_{ij}$  gives the amount of evapotranspiration in grid cell  $i$  that precipitates in grid cell  $j$ , and the diagonal element  $m_{ii}$  is the amount of evapotranspiration that precipitates in the same grid cell (locally recycled moisture). The output of WAM-2layers can be interpreted as the adjacency matrix of a directed and weighted complex network with self-interactions, where nodes of the network represent continental grid cells and links between nodes represent the direction and amount of moisture transported between them (Fig. 3.3).

### 3.2.2 Basic assumptions

In order to track moisture forward or backward from a given region ( $\Omega$ ) that can be of any shape and scale (grid cell, basin, continent), we assume that the moisture composition within the surface reservoir and the atmosphere for each grid cell remains the same. This implies that, in each grid cell, the tagged fraction of precipitation is linearly proportional to the tagged fraction of evapotranspiration and the tagged fraction of transported

moisture:

$$\frac{P_{\Omega}}{P} = \frac{E_{\Omega}}{E} = \frac{m_{\Omega}}{m}, \quad (3.1)$$

where  $E$  is the total evapotranspiration,  $P$  is the total precipitation,  $m$  is the transported moisture towards or from another grid cell,  $P_{\Omega}$  is the tagged fraction of precipitation,  $E_{\Omega}$  is the tagged fraction of evapotranspiration and  $m_{\Omega}$  is the tagged fraction of transported moisture towards or from another grid cell. We call tagged fraction the share of the moisture originating from  $\Omega$  in the case of a backward tracking and the share of moisture precipitating over  $\Omega$  in the case of a forward tracking.

This assumption is valid under two conditions: (1) evapotranspiration follows directly after the precipitation event or (2) the fraction of tagged moisture in the surface reservoir and the atmosphere can be assumed to be temporally constant (i.e., in steady state) [Goessling and Reick, 2013]. The first condition is usually fulfilled during interception and fast transpiration, which are important components of the total evapotranspiration, particularly in warm climates and for shallow rooted plants [Savenije, 2004]. However, in seasonal forests with deep rooted trees, the moisture that is evaporated during the dry season can be held back for several months [Savenije, 2004]. By analyzing a seasonally static moisture recycling network, we account for this limitation. The second condition is fulfilled if the soil water at the beginning has the same composition (in terms of tagged fraction) as the atmospheric moisture at the end of the season.

### 3.2.3 Moisture recycling ratio

Common measures to quantify the strength of the direct link between precipitation in a specific location and evapotranspiration from another location are the moisture recycling ratios (called hereafter DMR ratio) [Bagley et al., 2014, Bosilovich and Chern, 2006, Dirmeyer et al., 2009, Eltahir and Bras, 1994, Keys et al., 2012, Trenberth, 1999, van der Ent et al., 2010]. The DMR ratios are only used to investigate DMR. Here, we further develop these measures in order to take CMR into account.

#### 3.2.3.1 Direct moisture recycling ratios

Two kinds of DMR ratios have been developed in a previous study [van der Ent et al., 2010]: the direct precipitation recycling ratio and the direct evapotranspiration recycling ratio. The direct precipitation recycling ratio ( $\rho_{\Omega}$ ) has been defined as the fraction of precipitation that is originating from evapotranspiration from a defined region ( $\Omega$ ) with

no intervening re-evaporation cycle. The  $\rho_\Omega$  for grid cell  $j$  is calculated as

$$\rho_{\Omega,j} = \frac{\sum_{i \in \Omega} m_{ij}}{P_j}, \quad (3.2)$$

where  $m_{ij}$  is the amount of evapotranspiration in  $i$  that precipitates in  $j$  with no intervening re-evaporation cycle and  $P_j$  is the precipitation in  $j$ . We note that  $\rho_\Omega$  averaged over all grid cells in  $\Omega$  gives the regional recycling ratio, i.e., the fraction of precipitation that is regionally recycled [Burde et al., 2006, Eltahir and Bras, 1994, van der Ent and Savenije, 2011]. High values of  $\rho_\Omega$  indicate the direct sink regions of evapotranspiration from  $\Omega$ , i.e., the regions that are dependent on evapotranspiration coming directly (i.e., through DMR) from  $\Omega$  for local precipitation. A direct sink region receives moisture from  $\Omega$  at first and might distribute it further downwind (Fig. 3.4).

Similarly, the direct evapotranspiration recycling ratio ( $\varepsilon_\Omega$ ) has been defined as the fraction of evapotranspiration that falls as precipitation over a defined region ( $\Omega$ ) with no intervening re-evaporation cycle. The  $\varepsilon_\Omega$  for grid cell  $i$  is calculated as

$$\varepsilon_{\Omega,i} = \frac{\sum_{j \in \Omega} m_{ij}}{E_i}, \quad (3.3)$$

where  $E_i$  is the evapotranspiration in  $i$ . High values indicate the direct source regions of precipitation over  $\Omega$ , i.e., the regions that contribute directly (i.e., through DMR) to rainfall over  $\Omega$ . A direct source region distributes moisture towards  $\Omega$ , which might be originating from further up-wind regions (Fig. 3.4).

If  $\Omega$  is the entire South American continent,  $\varepsilon_\Omega$  becomes the continental evapotranspiration recycling ratio ( $\varepsilon_c$ ) and  $\rho_\Omega$  the continental precipitation recycling ratios ( $\rho_c$ ) as defined in van der Ent et al. [2010]. Considered together,  $\varepsilon_c$  and  $\rho_c$  indicate sources and sinks of continental moisture, respectively. In this study we neglect possible contributions of moisture in South America from and to other continents, since these contributions to the overall moisture budget are small (van der Ent et al., 2010, Table 2). However, below we omit the area-weighting from the formulae for clarity..

### 3.2.3.2 Cascading moisture recycling ratios

We define the cascading precipitation recycling ratio ( $\rho_\Omega^{\text{casc}}$ ) as the fraction of precipitation that is originating from evapotranspiration from  $\Omega$  and that has run through at least one re-evaporation cycle on the way. High values indicate the cascading sink regions of evapotranspiration from  $\Omega$ , i.e., the regions that are dependent on evapotranspiration coming indirectly (i.e., through CMR) from  $\Omega$  for local precipitation. A cascading sink

TABLE 3.2 Overview of regional precipitation recycling ratio in the Amazon basin ( $\overline{\rho_{Am}(Am)}$ ) as found in many studies. Abbreviations: the European Centre for Medium-Range Weather Forecasts (ECMWF); Geophysical Fluid Dynamics Laboratory (GFDL); Climate Prediction Center Merged Analysis of Precipitation (CMAP); initial conditions (IC); October–November–December (OND); Data Assimilation Office (DAO); integral moisture balance (IMB); National Centers for Environmental Prediction (NCEP) – Department of Energy (DOE); World Monthly Surface Station Climatology distributed by the National Center for Atmospheric Research (NCAR).

Study	Method	Data set	Period	$\overline{\rho_{Am}(Am)}$ (%)
Brubaker et al. [1993]	atmospheric bulk model	GFDL and NCAR	1963–1973	24
Eltahir and Bras [1994]	atmospheric bulk model	ECMWF reanalysis	1985–1990	25
		GFDL	1963–1973	35
Trenberth [1999]	atmospheric bulk model	CMAP and NCEP-NCAR reanalysis	1979–1995	34
Bosilovich and Cherrn [2006]	AGCM with water vapor tracers	IC from the model	1948–1997	27.2 during OND
Burde et al. [2006]	atmospheric bulk model (general), atmospheric bulk model (Budyko model), atmospheric bulk model (IMB)	DAO	1981–1993	31
				26
				41
Dirmeyer et al. [2009]	quasi-isentropic back-trajectory method	DOE reanalysis	1979–2003	10.8 for $10^6 km^2$ area
van der Ent et al. [2010]	Eulerian atm. moisture tracking model	ERA-Interim reanalysis	1999–2008	28
Zemp et al. (this study)	Eulerian atm. moisture tracking model	TRMM and MODIS	2001–2010	28
Zemp et al. (this study)	Eulerian atm. moisture tracking model	LandFlux-EVAL and average of CRU, GPCC, GPCC, CPC	1990–1995	24

region is the last destination of evapotranspiration from  $\Omega$  before it is advected over the ocean (Fig. 3.4).

We also define the cascading evapotranspiration recycling ratio ( $\varepsilon_{\Omega}^{\text{casc}}$ ) as the fraction of evapotranspiration that falls as precipitation over  $\Omega$  after at least one re-evaporation cycle on the way. High values indicate the cascading source regions of precipitation over  $\Omega$ , i.e., the regions that contribute indirectly (i.e., through CMR) to rainfall over  $\Omega$ . A cascading source region is the origin of moisture that is distributed from somewhere else towards  $\Omega$  (Fig. 3.4).

The moisture inflow (outflow) that crosses the border of  $\Omega$  may be counted several times as it is involved in several pathways of CMR. To avoid this, we only track moisture that crosses the border of  $\Omega$ . This implies that we consider re-evaporation cycles outside  $\Omega$  only (Fig. 3.4). For a complete description of the methodology, we refer the reader to Appendix B.1.

### 3.2.3.3 Application to the Amazon basin and the La Plata basin

To study the moisture recycling between the Amazon basin (defined by the red boundaries in Fig. 3.1e) and the La Plata basin (defined by the purple boundaries in Fig. 3.1d), we use  $\rho_{\Omega}$  and  $\rho_{\Omega}^{\text{casc}}$  with  $\Omega$  being all grid cells covering the Amazon basin ( $\rho_{\text{Am}}$  and  $\rho_{\text{Am}}^{\text{casc}}$ , respectively) and  $\varepsilon_{\Omega}$  and  $\varepsilon_{\Omega}^{\text{casc}}$  with  $\Omega$  being all grid cells covering the La Plata basin ( $\varepsilon_{\text{Pl}}$  and  $\varepsilon_{\text{Pl}}^{\text{casc}}$ , respectively). High values of  $\rho_{\text{Am}}$  and  $\rho_{\text{Am}}^{\text{casc}}$  indicate together the sink regions of evapotranspiration from the Amazon basin and high values of  $\varepsilon_{\text{Pl}}$  and  $\varepsilon_{\text{Pl}}^{\text{casc}}$  highlight source regions of precipitation over the La Plata basin (Fig. 3.4).

Considered together, the DMR ratios and the CMR ratios provide a full picture of the source–sink relationship between the Amazon basin and the La Plata basin that is needed to estimate the effects of land use change for downwind precipitation patterns.  $\rho_{\text{Am}}^{\text{casc}}$  and  $\rho_{\text{Am}}$  quantify the local dependency on incoming moisture from the Amazon basin (with and without re-evaporation cycles) and therefore the local vulnerability to deforestation in the Amazonian rainforests. Considering  $\rho_{\text{Am}}$  only would lead to underestimation of this dependency. On the other hand,  $\varepsilon_{\text{Pl}}$  and  $\varepsilon_{\text{Pl}}^{\text{casc}}$  provide information on the upwind regions that contribute to rainfall over the La Plata basin and, consequently, that should be preserved from intensive land use change in order to sustain water availability in the La Plata basin.

### 3.2.4 Quantifying cascading moisture recycling

To quantify the importance of CMR for the total moisture inflow (precipitation,  $P$ ) and outflow (evapotranspiration,  $E$ ), we cut off all re-evaporation of moisture originating from the continent and we estimate the resulting reduction in total moisture inflow ( $\Delta P_c$ ) and outflow ( $\Delta E_c$ ; see Appendix B.3 for further information on the methodology).  $\Delta P_c/P$  is the fraction of precipitation that comes from re-evaporation of moisture originating from the continent, i.e., that has been evaporated in at least two locations on the continent.  $\Delta P_c/P$  quantifies the importance of CMR for local rainfall.  $\Delta E_c/E$  is the fraction of total evapotranspiration that is a re-evaporation of moisture originating from the continent and that further precipitates over the continent, i.e., that lies within CMR pathways.  $\Delta E_c/E$  quantifies the local contribution to CMR. High values of  $\Delta E_c/E$  indicate intermediary regions. Regions that have a larger  $\Delta E_c/E$  than the 80th percentile (calculated for all continental values in each seasonal network) are called intermediary regions in the following.

In addition, we are interested in the importance of re-evaporation cycles that are occurring in the intermediary regions for the total moisture in- and outflow. We use the same approach as above. We cut off all re-evaporation in the intermediary region of moisture originating from the continent and we estimate the resulting reduction in total moisture inflow ( $\Delta P_m$ ) (see Appendix B.3).  $\Delta P_m/P$  is the fraction of total moisture inflow that comes from CMR in the intermediary region (i.e., that has run through at least one re-evaporation cycle in the intermediary region). It quantifies the dependency on CMR in the intermediary region for local rainfall.

### 3.2.5 Complex network analysis

We investigate important moisture recycling pathways using two measures from complex network analysis: clustering coefficient associated with Middleman motifs and betweenness centrality.

#### 3.2.5.1 Clustering coefficient associated with Middleman motifs ( $\tilde{C}$ )

In complex network theory, motifs are defined as significant and recurring patterns of interconnections that occur in the network [Milo et al., 2002]. Here, we are interested in a particular pattern of directed triangles: the Middleman motif [Fagiolo, 2007]. In our study, a grid cell forms a Middleman motif if it represents an intermediary on an alternative pathway to the direct transport of moisture between two other grid cells (Fig. 3.3).

The clustering coefficient is a measure from complex network analysis that measures the tendency to form a particular motif [Fagiolo, 2007]. Here, it reveals intermediary locations in CMR pathways, as the alternative to the DMR between sources and sinks. To account for moisture fluxes along the network links, we compute the weighted version of the clustering coefficient associated with Middleman motifs ( $\tilde{C}$ ) [Fagiolo, 2007, Zemp et al., 2014b] for each grid cell as described in the Appendix B.4.1.

A grid cell has a high  $\tilde{C}$  if it forms a lot of Middleman motifs and if these motifs contribute largely to relative moisture transport.  $\tilde{C}$  is equal to zero if the grid cell forms no Middleman motif at all.

It is worth to note that the Middleman motif considers three interconnected grid cells, which corresponds to CMR pathways involving only one re-evaporation cycle. These pathways usually contribute most to moisture transport between two locations. In fact, the amount of moisture transported in a pathway typically decreases with the number of re-evaporation cycles involved in the pathway. This is in agreement with a previous study counting the number of re-evaporation cycles using a different methodology [Goessling and Reick, 2013]. Other motifs formed by three grid cells linked by moisture recycling have been used to highlight different patterns in moisture transport (e.g., cycle, integration and distribution) [Zemp et al., 2014b], but are not analyzed here.

### 3.2.5.2 Betweenness centrality ( $B$ )

$B$  aims to highlight nodes in the network with central position “to the degree that they stand between others and can therefore facilitate, impede or bias the transmission of messages” in the network [Freeman, 1977, p. 36]. Here, we use it to reveal intermediary grid cells where CMR pathways are channeled.

To compute it, we first identify for each pair of grid cells the moisture recycling pathways with the greatest throughput, called optimal pathways (see methodology in Appendix B.4.2). These pathways can include any number of re-evaporation cycles. As the optimal pathway is usually the direct one (without any re-evaporation cycle), we first had to modify the network such that the optimal pathways involve re-evaporation cycles. To do so, we removed from the network all long-range moisture transport, i.e., occurring over distances larger than 15 geographical degrees. The choice of this threshold does not influence the results qualitatively on a yearly basis (Fig. B.3). During the dry season, removing long-range moisture transport affects moisture inflow over the La Plata basin; therefore, the results of the  $B$  will be interpreted with caution during this season.

Once optimal pathways are identified, we find intermediary grid cells that they have in common (see Appendix B.4.3). A grid cell has a high  $B$  if many optimal pathways pass



through it: moisture runs often through re-evaporation cycles in the grid cell. It has a  $B$  equal to 0 if none of these pathways pass through it: i.e., moisture never runs through re-evaporation cycles in the grid cell.

### 3.2.6 Similarities and differences between the presented measures

We expect similar spatial patterns in the results of  $\Delta E_c/E$  (fraction of evapotranspiration that lies within CMR pathways; see Sect. 3.2.4), the  $B$  (betweenness centrality; see Sect. 3.2.5.2) and the  $\tilde{C}$  (clustering coefficient, Sect. 3.2.5.1). In fact, all three measures reveal important intermediary grid cells in CMR pathways. However, the three measures are based on different concepts and methods.

1. While  $\Delta E_c/E$  is calculated by inhibiting re-evaporation of moisture from continental origin,  $B$  is based on the notion of optimal pathways and  $\tilde{C}$  relies on particular motifs formed by three connected grid cells.
2. An implication of (1) is that  $\Delta E_c/E$  quantifies the local contribution to CMR,  $\tilde{C}$  refers to CMR pathways as alternative to the direct transport of moisture between two locations and  $B$  shows locations where CMR pathways are channeled.
3. In the  $\tilde{C}$ , only CMR pathways with one re-evaporation cycle are considered. Using  $\Delta E_c/E$  and  $B$ , all number of cycles are possible in the pathways.
4. Moisture recycling pathways involving long-range transport are not considered in the calculation of the  $B$ .

For these reasons,  $\Delta E_c/E$ ,  $B$  and  $\tilde{C}$  are complementary measures. There are also some similarities between the calculation of the cascading precipitation recycling ratio ( $\rho_\Omega^{\text{casc}}$ ) and  $\Delta P_c/P$ , which are described in the Appendix B.2.

## 3.3 Results and discussion

### 3.3.1 Comparison of continental and regional moisture recycling ratios with other existing studies

The main continental source of precipitation over South America is the Amazon basin, with large heterogeneity in time and space (Figs. 3.1e, 3.1j, 3.2e and 3.2j and Table 3.3). Around 70 to 80 % of the evapotranspiration in the southern part of the Amazon basin falls as precipitation over the continent during the wet season but only 30 to 40 % during

the dry season. As the evapotranspiration in the Amazon basin is high and varies little in space and time (Figs. 3.1b, 3.1g, 3.2b and 3.2g), this observation indicates that during the dry season, a high amount of moisture from the southern part of the Amazon basin is advected out of the continent. Using a Lagrangian particle dispersion model, Drumond et al. [2014] also found a maximum contribution of moisture from the Amazon basin to the ocean during this period.

The main sink regions of moisture originating from the continent are the western part of the Amazon basin during the dry season, the south-western part of the basin during the wet season and the La Plata basin especially during the wet season (Figs. 3.1d, 3.1i, 3.2d and 3.2d and Table 3.3). In fact, in the La Plata basin, 42 to 45 % of the precipitation during the wet season and 35 % during the dry season evaporated from the continent. This difference between seasons is explained by a weaker transport of oceanic moisture associated with the sub-tropical Atlantic high and by an intensification of the SALLJ that transports moisture in the meridional direction during this season [Marengo et al., 2004]. The importance of continental moisture recycling in the La Plata basin during the wet season has been emphasized in previous studies [Drumond et al., 2008, Martinez and Dominguez, 2014]. Despite this importance, we find that the ocean remains the main source of moisture over the La Plata basin in agreement with previous studies [Arraut and Satyamurty, 2009, Drumond et al., 2014, 2008]. However, some other studies estimated a higher contribution of moisture from the continent to precipitation over the La Plata basin [Keys et al., 2012, Martinez and Dominguez, 2014, van der Ent et al., 2010].

There are uncertainties in the moisture recycling ratios depending on the quality of the data sets used, the assumptions made in the methods and the boundaries used to define the domain [for example in Brubaker et al., 1993, the Amazon region is represented by a rectangle]. Considering these uncertainties, the regional precipitation recycling ratio in the Amazon basin compares well with previous studies using other data sets and methodologies (Table 3.2). The spatial patterns of continental moisture recycling ratios (Figs. 3.1d, 3.1i, 3.1e, 3.1j, 3.2d, 3.2i, 3.2e and 3.2j) are slightly different from those found by van der Ent et al. [2010]— see their Figs. 3 and 4, due to the differences in the versions of the model (here we use WAM-2layers) and the data sets used. The continental precipitation recycling ratio in the Amazon basin reaching 27 to 30 % during the Southern Hemisphere summer is slightly below estimates of 36.4 % found by Bosilovich and Chern [2006]. The maps of DMR ratios (Fig. 3.8a, and c, e and g) are in good agreement with the regional recycling ratio reported in previous studies (Eltahir and Bras, 1994, Figs. 4 and 6; Burde et al., 2006, Figs. 2 and 8; Dirmeyer et al., 2009; see <http://www.iges.org/wcr/>, Moisture Sources by Basin).

We note that our analysis period from 2001 to 2010 (for the input MOD) includes two major droughts in the Amazon basin [Lewis et al., 2011, Marengo et al., 2008]. Because the land–atmosphere coupling on the hydrological cycle increases during drought years [Bagley et al., 2014], this might influence the output of the atmospheric moisture tracking model used in this study. Analyzing these periods separately is ongoing research.

### 3.3.2 Importance of cascading moisture recycling

Continental moisture recycling is of crucial importance for South American precipitation patterns (Figs. 3.1 and 3.2). We now quantify this importance (Fig. 3.5).

The share of cascading moisture on total moisture inflow is on average 9–10 % in the South American continent (Table 3.3). Regions that are dependent on CMR for local rainfall (Fig. 3.5a, c, e and g) are also dominant sinks of moisture from the continent (Fig. 3.1d, 3.1i, 3.2d and 3.2i).

We note that CMR contributes more to the precipitation over the Amazon basin during the dry season (8–11 % on average, up to 25 % in the western part) compared to the wet season (6–8 % on average). This is explained by the fact that during the dry season, moisture is mainly transported from the eastern to the western part of the Amazon basin (Figs. 3.1 and 3.2). Our results show that during the dry season, this moisture transport involves re-evaporation cycles in the central part of the basin (blue boundaries in Fig. 3.5b and f). In fact, 15–23 % of the total evapotranspiration from the Amazon basin is involved in CMR during the dry season.

During the wet season, CMR plays also an important role as 17–18 % of the total precipitation over the La Plata basin comes from CMR. The intermediary region where re-evaporation cycles are taking place is mainly the south-western part of the Amazon basin (blue boundaries in Fig. 3.5d and h). In this intermediary region, up to 35 % of the total evapotranspiration is involved in CMR during the wet season. We note that the shape of the intermediary regions varies slightly among the two data sets during the wet season, probably explained by the differences in evapotranspiration patterns (Figs. 3.1g and 3.2g).

In order to evaluate the importance of the intermediary region for rainfall over the La Plata basin, we quantify the share of the moisture inflow in the La Plata basin that has run through re-evaporation cycles in the intermediary regions. This share is 9 % during the wet season and 5 % during the dry season. These estimations represent about half of the share of total moisture inflow over the La Plata basin that comes from CMR during the wet season (Table 3.3). These results mean that the intermediary regions

are important for cascading moisture transported towards the La Plata basin during the wet season. In Sect. 3.3.4, we reveal the direct and cascading sources of precipitation over the La Plata basin and we understand the seasonal variability.

The share of cascading moisture on the total moisture inflow reaches up to 35–50% on the eastern side of the central Andes, one of the most vulnerable biodiversity hotspots on Earth [Myers et al., 2000]. However, this latter observation should be considered with caution due to the imbalance of the water cycle in this area, which might lead to an overestimation of the regional recycling process and an overestimation of the importance of cascading moisture recycling.

### 3.3.3 Complex network analysis

We have shown the importance of CMR for South American moisture transport (Fig. 3.5). Using the clustering coefficient associated with the Middleman motif ( $\tilde{C}$ ), we are able to identify intermediary locations involved in cascading pathways as alternatives to the direct transport of moisture (Fig. 3.6a, c, e and g). These regions coincide with the intermediary regions identified with a different method (blue boundaries in Fig. 3.5). These results mean that the CMR pathways involving the intermediary regions are not the only pathways of moisture recycled from sources to sinks on the continent, but are complementing the direct transport of moisture over long distances.

The betweenness centrality ( $B$ ) reveals intermediary regions where CMR pathways are channeled. We note that regions with high  $B$  coincide with regions with high  $\tilde{C}$  during the wet season, but not as much during the dry season (Fig. 3.6). This might be a result of the cutting of long-range links from the network in the calculation of  $B$ , which affects moisture transport towards the sub-tropical South America during the dry season.

High values of  $B$  are found along a narrow band east of the sub-tropical Andes (Fig. 3.6d and h), indicating that CMR pathways are channeled in this region. This observation may be explained by the combined effect of the acceleration of the SALLJ [Vera et al., 2006a] and the high precipitation and evapotranspiration during the wet season (Figs. 3.1 and 3.2) allowing for an intensive local exchange of moisture between the vegetation and the atmosphere.

### 3.3.4 Moisture recycling from the Amazon basin to the La Plata basin

We have shown the importance of the Amazon basin as the dominant source of continental moisture and the La Plata basin as a central sink region (see Figs. 3.1 and 3.2). In

the following, we further investigate the importance of DMR and CMR for the transport of moisture between the two basins (Figs. 3.7 and 3.8).

In the La Plata basin, 18–23 % of the precipitation during the wet season and 21–25 % during the dry season originated from the Amazon basin with no intervening re-evaporation cycles (Table 3.3). This is in good agreement with the yearly average estimates of 23 % found in Dirmeyer et al. [2009, see <http://www.iges.org/wcr/>] and 23.9 % found in Martinez and Dominguez [2014]. However, these estimations take only DMR into account. Here, considering, considering CMR increases the fraction of precipitation over the La Plata basin that comes from the Amazon basin by 6 % during the wet season (Table 3.3). As mentioned above, this might be explained by the high evapotranspiration and precipitation allowing for an exchange of moisture on the way and by the intensification of the SALLJ during this time of the year [Marengo et al., 2004]. This result suggests that the impact of deforestation in the Amazonian forest on rainfall over the La Plata basin might be larger than expected if only direct transport of moisture between the two basins is considered.

The southern part of the Amazon basin is a direct source of precipitation over the La Plata basin (Fig. 3.7a, c, e and g). This finding is in agreement with Martinez and Dominguez [2014] and Keys et al. [2014]. However, if CMR is considered, the entire Amazon basin becomes an evaporative source of moisture for the La Plata basin during the wet season (Fig. 3.7d and h). On average, 16–23 % of the total evapotranspiration from the Amazon basin during the wet season ends as rainfall over the La Plata basin after at least one re-evaporation cycle (Table 3.3). This result means that during the wet season, the southern part of the Amazon basin is not only a direct source of moisture for the La Plata basin but also an intermediary region that distributes moisture originating from the entire basin. This finding is in agreement with other measures showing intermediary regions (Sects. 3.3.2 and 3.3.3).

### 3.3.5 Possible impact of land-cover change in the intermediary regions

The southern part of the Amazon basin is a key region for moisture transport towards the La Plata basin. It is a source of moisture for precipitation over the La Plata basin all year round. In addition, it is an intermediary region for the indirect transport of moisture (through CMR) originating from the entire Amazon basin during the wet season (Sect. 3.3.4).

Land-cover change in the southern part of the Amazon basin might weaken continental moisture recycling and might lead to a substantial decrease in the total precipitation locally and downwind. Among the affected regions, important impacts would be observed

in particular in the south-western part of the Amazon basin that has already a high probability to experience a critical transition from forest to savanna [Hirota et al., 2011] and in the La Plata basin that is dependent on incoming rainfall for agriculture [Keys et al., 2012, Rockström et al., 2009]. At the eastern side of the central Andes, the impact of an upwind weakening of CMR might be reduced since precipitation in this region is ensured by orographic lifting [Figueroa and Nobre, 1990].

### 3.4 Conclusions

In this work, we investigated the exchange of moisture between the vegetation and the atmosphere on the way between sources and sinks of continental moisture in South America. We have introduced the concept of cascading moisture recycling (CMR) to refer to moisture recycling between two locations on the continent that involve one or more re-evaporation cycles along the way. We have proposed measures to quantify the importance of CMR, to track moisture from a given region further backward or forward in space and to identify intermediary regions where re-evaporation cycles are taking place. We have used for the first time a complex network approach to study moisture recycling pathways.

We have tracked moisture evaporating from each grid cell covering the South American continent until it precipitates or leaves the continent using the Eulerian atmospheric moisture tracking model WAM-2layers (Water Accounting Model- two layers). In order to reduce the uncertainty associated with the input data, we have used two different sets of precipitation and evapotranspiration data from (1) observation-based and (2) merged synthesis products, together with reanalysis wind speeds and humidity data. We have shown that even if the amount of water transported through CMR pathways is typically smaller than the one transported directly in the atmosphere, the contribution by the ensemble of cascading pathways cannot be neglected. In fact, 9–10 % of the total precipitation over South America, as well as 17–18 % of the precipitation over the La Plata basin, comes from CMR. The La Plata basin is highly dependent on moisture from the Amazon basin during both seasons, as 18–23 % of the total precipitation over the La Plata basin during the wet season, as well as 21–25 % during the dry season, comes directly from the Amazon basin. To these direct dependencies, 6 % of the precipitation during the wet season can be added if CMR is considered.

During the dry season, CMR plays an important role for the moisture transport from the eastern to the western part of the Amazon basin. Indeed, 15–23 % of the total evapotranspiration in the Amazon basin is involved in CMR during the dry season.

The south-western part of the Amazon basin is an important direct source of incoming moisture over the La Plata basin all year round. However, during the wet season, it is not only a direct source but also an intermediary region that distributes moisture from the entire Amazon basin into the La Plata basin. Land use change in these regions may weaken moisture recycling processes and may have stronger consequences for rainfed agriculture and natural ecosystems regionally and downwind as previously thought.

In addition, we showed that the eastern flank of the sub-tropical Andes – located in the pathway of the South American low-level jet – plays an important role in the continental moisture recycling as it channels many cascading pathways. This study offers new methods to improve our understanding of vegetation and atmosphere interactions on the water cycle needed in a context of land use and climate change.

### **3.5 Acknowledgements**

This paper was developed within the scope of the IRTG 1740/TRP 2011/50151-0, funded by the DFG/FAPESP. J. Donges acknowledges funding from the Stordalen Foundation and BMBF (project GLUES), R. J. van der Ent from NWO/ALW and A. Rammig from the EU-FP7 AMAZALERT (raising the alert about critical feedbacks between climate and long-term land use change in the Amazon) project, grant agreement no. 282664. We thank K. Thonicke and P. Keys for comments on the manuscript, P. Manceaux for his help on designing the network schemes and B. Mueller for her contribution on the data pre-processing.

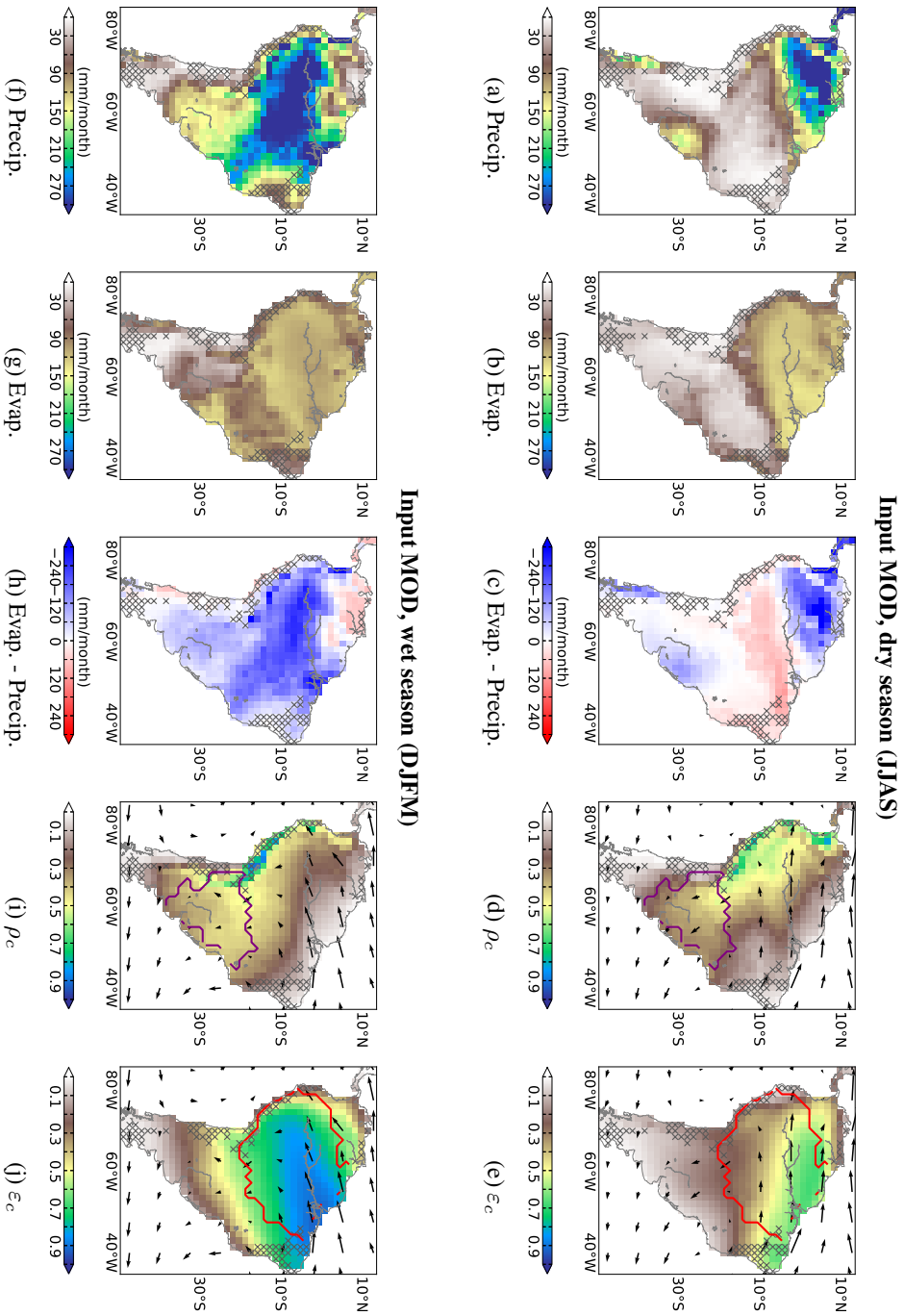


FIGURE 3.1 WAM-2layers input and output as calculated for the period 2001–2010 for MODIS and TRMM (input MOD; see Table 3.1): long-term seasonal mean of precipitation (**a**, **f**), evapotranspiration (**b**, **g**), precipitation–evapotranspiration (**c**, **h**), continental precipitation recycling ratio  $\rho_c$  (**d**, **i**) and continental evapotranspiration recycling ratio  $\epsilon_c$  (**e**, **j**) indicating respective sinks and sources of continental moisture. Here and in the following figures, the vectors indicate the horizontal moisture flux field (in  $\text{m}^3$  of moisture  $\times \text{m}^{-2} \times \text{month}^{-1}$ ) and the hatches represent grid cells where mean annual evapotranspiration exceeds mean annual precipitation. The red lines delimit the Amazon basin and the purple lines delimit the La Plata basin. Results are given for the dry season (upper row) and the wet season (lower row).



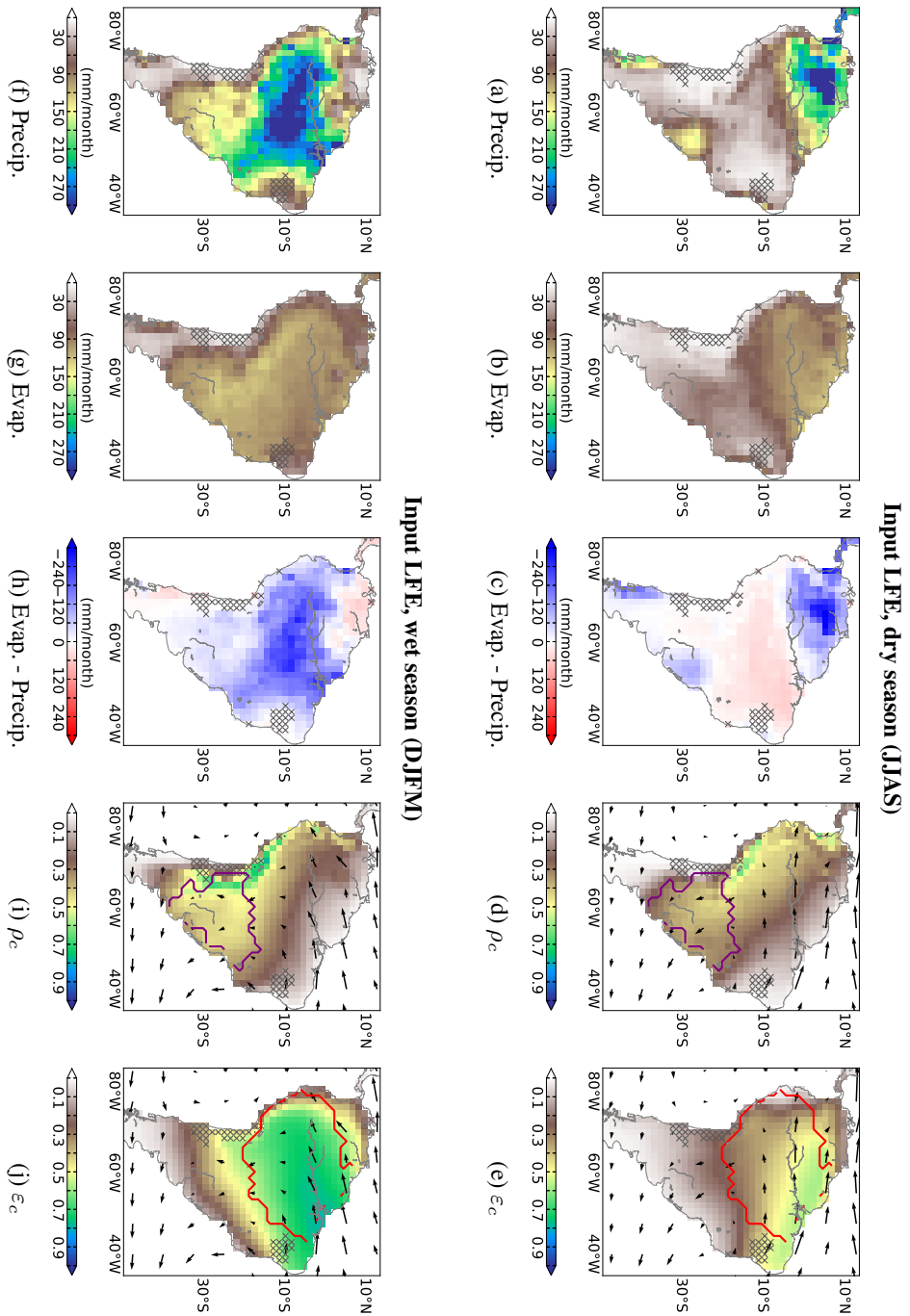


FIGURE 3.2 Same as Fig. 3.1 for the period 1990–1995 as calculated from LandFlux-EVAL and an average of four observation-based precipitation products (input LFE; see Table 3.1).

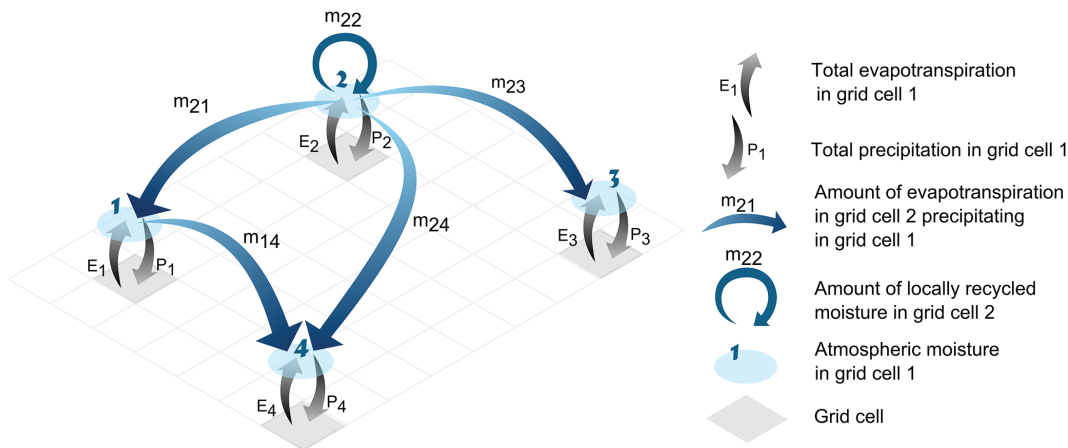


FIGURE 3.3 Schematic representation of the moisture recycling network. The exchange of moisture from 2 to 4 uses two alternative pathways: the direct one ( $m_{24}$ ) and the cascading pathway ( $m_{21}m_{14}$ ). The grid cell 1 is an intermediary on an alternative pathway to the direct transport of moisture between 2 and 4. Thus, grid cell 1 forms a Middleman motif with grid cells 2 and 4.

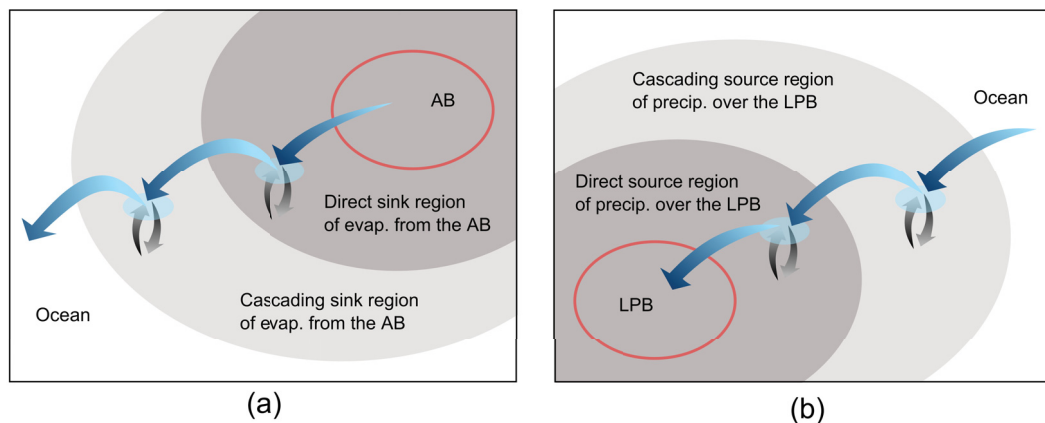


FIGURE 3.4 Schematic representation of the sink and source regions as quantified by the moisture recycling ratios. In addition to the direct source and sink regions identified using DMR ratios (dark gray), the cascading source and sink regions identified using CMR ratios (light gray) are highlighted. Of specific interest for this study are: direct and cascading sink regions of evapotranspiration (evap.) from the Amazon basin (AB) (a) and direct and cascading source regions of precipitation (precip.) over the La Plata basin (LPB) (b).

TABLE 3.3 Importance of direct moisture recycling (DMR) and cascading moisture recycling (CMR) for the total precipitation (precip.) and evapotranspiration (evap.) averaged for the La Plata basin (LPB), the Amazon basin (AB) and for the South American continent during the wet season (DJFM), the dry season (JJAS) and all year round calculated for the input MOD/LFE (in %).

Notation	Description	La Plata basin				Amazon basin				South America				
		wet	dry	year	year	wet	dry	year	year	wet	dry	year	year	
$\rho_c$	fraction of precip. originating from the continent	42/45	35/35	41/43	30/27	35/30	32/29	30/29	29/26	31/29				
$\rho_{Am}$	fraction of precip. originating from the AB through DMR	23/18	25/21	24/20	26/22	30/25	28/24	18/15	21/18	20/17				
$\rho_{Am}^{casc}$	fraction of precip. originating from the AB through CMR	6/6	2/3	4/6	-/-	-/-	-/-	11/9	6/6	8/8				
$\epsilon_c$	fraction of evap. that falls as precip. over the continent	43/40	16/16	35/32	77/68	45/41	65/57	56/29	31/28	47/42				
$\epsilon_{Pl}$	fraction of evap. that falls as precip. over the LPB through DMR	32/28	12/11	26/22	16/11	7/6	11/10	15/13	7/6	12/11				
$\epsilon_{Pl}^{casc}$	fraction of evap. that falls as precip. over the LPB through CMR	-/-	-/-	-/-	23/16	1/2	10/7	13/8	1/1	6/4				
$\Delta P_c/P$	fraction of precip. that comes from CMR in the continent	17/18	14/12	17/17	8/6	11/8	10/7	10/9	9/7	10/9				
$\Delta P_m/P$	fraction of precip. that comes from CMR in the intermediary region	9/9	5/5	8/9	4/3	6/4	4/4	4/4	5/3	4/4				
$\Delta E_c/E$	fraction of evap. that lies within CMR pathways	11/13	9/8	9/11	11/8	23/15	12/10	13/9	15/10	10/8				

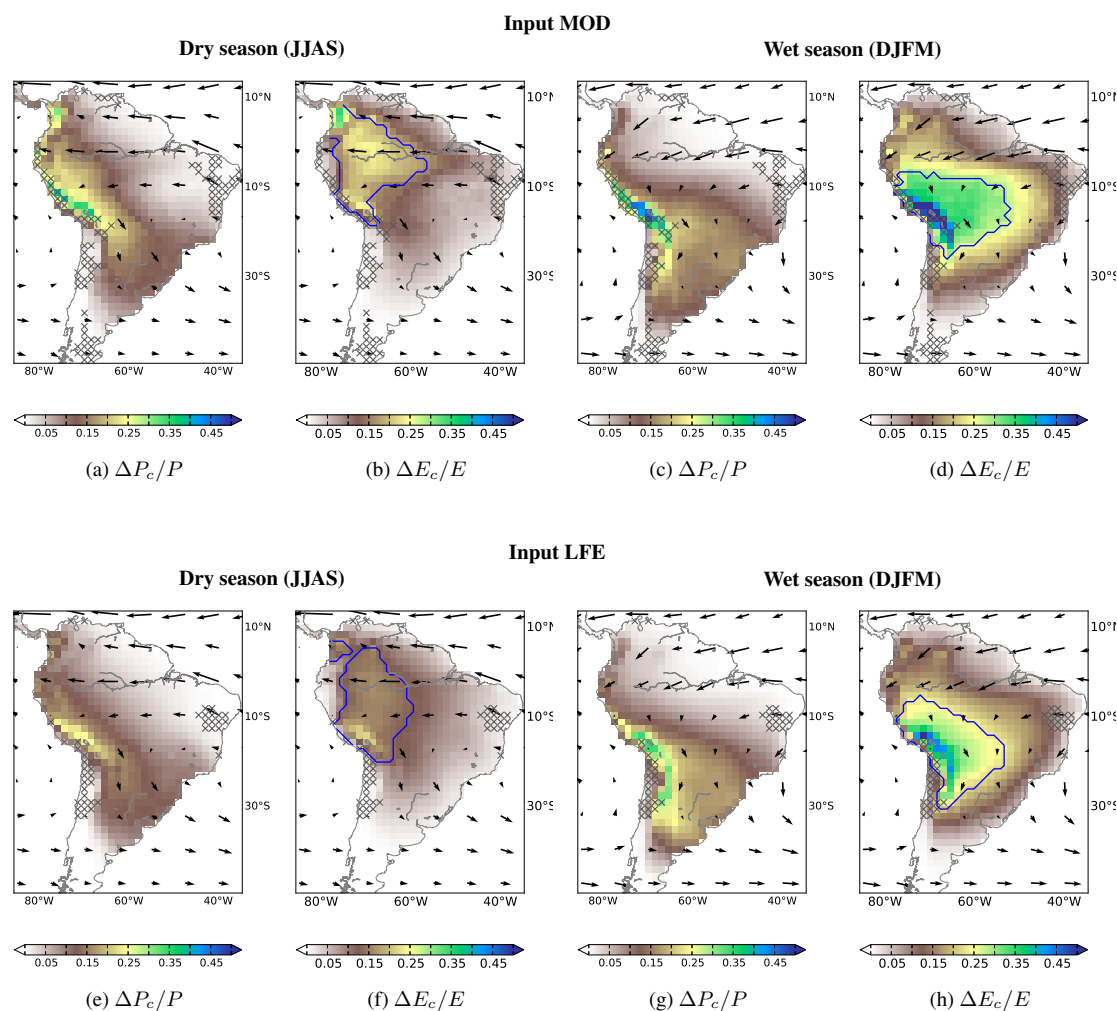


FIGURE 3.5 Fraction of total precipitation originating from CMR ( $\Delta P_c/P$ ) (a, c, e, g) and fraction of total evapotranspiration that lies within CMR pathways ( $\Delta E_c/E$ ) (b, d, f, h). While high values of  $\Delta P_c/P$  indicate regions that are dependent on CMR for local rainfall, high values of  $\Delta E_c/E$  indicate regions that contribute to CMR. The blue boundaries define the regions that have  $\Delta E_c/E > 80$  percentile (calculated for all continental values in each seasonal moisture recycling network) and that are called intermediary regions. Results are obtained using the input MOD (upper row) and input LFE (lower row) (see Table 3.1) and are given for the dry season (left) and the wet season (right).

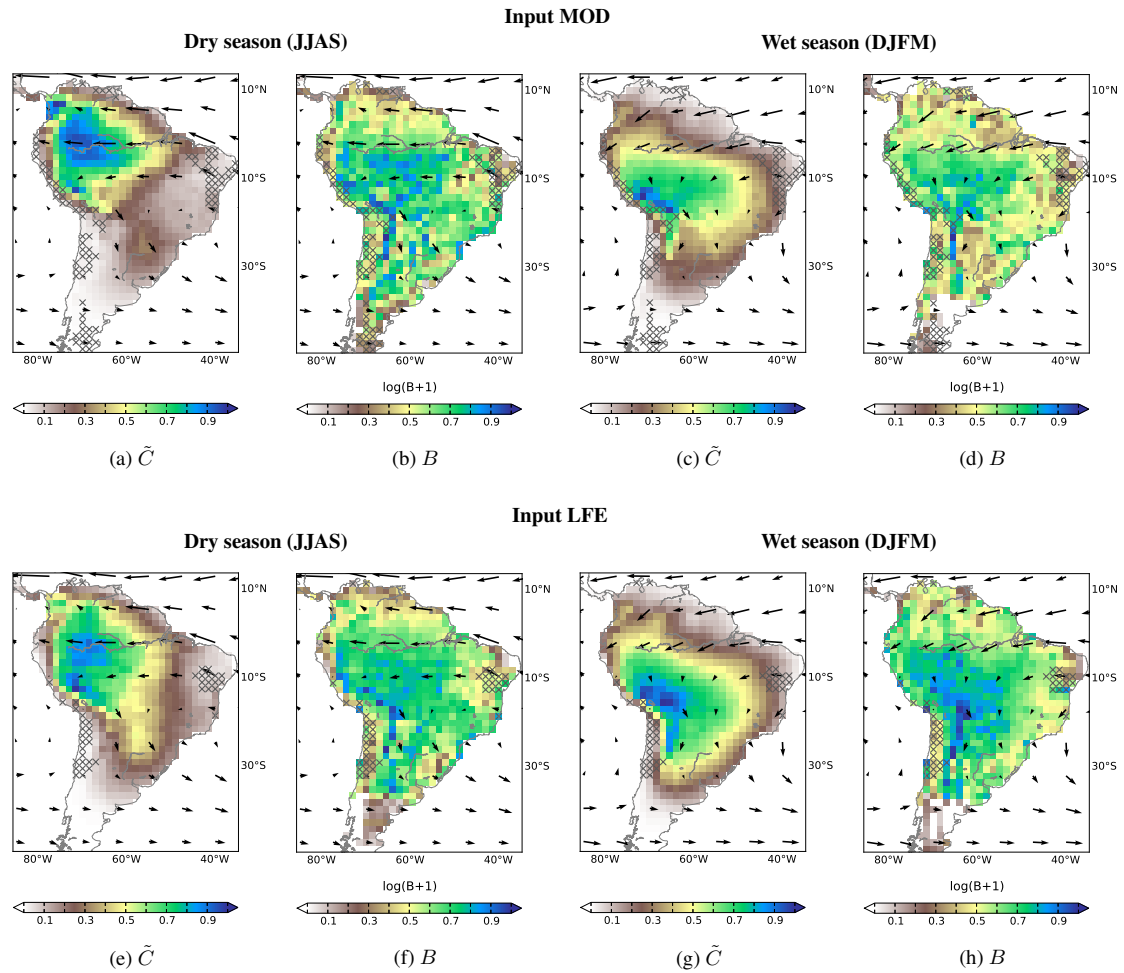


FIGURE 3.6 Results of complex network analysis. Clustering coefficient  $\tilde{C}$  associated with the motif Middleman (a, c, e, g) and betweenness centrality  $B$  (b, d, f, h). While high values of  $\tilde{C}$  indicate intermediary locations where CMR allows for alternative pathways to the direct transport of moisture, high values of  $B$  indicate regions where pathways of CMR are channeled. Results are obtained using the input MOD (upper row) and input LFE (lower row) (see Table 3.1) and are given for the dry season (left) and the wet season (right).

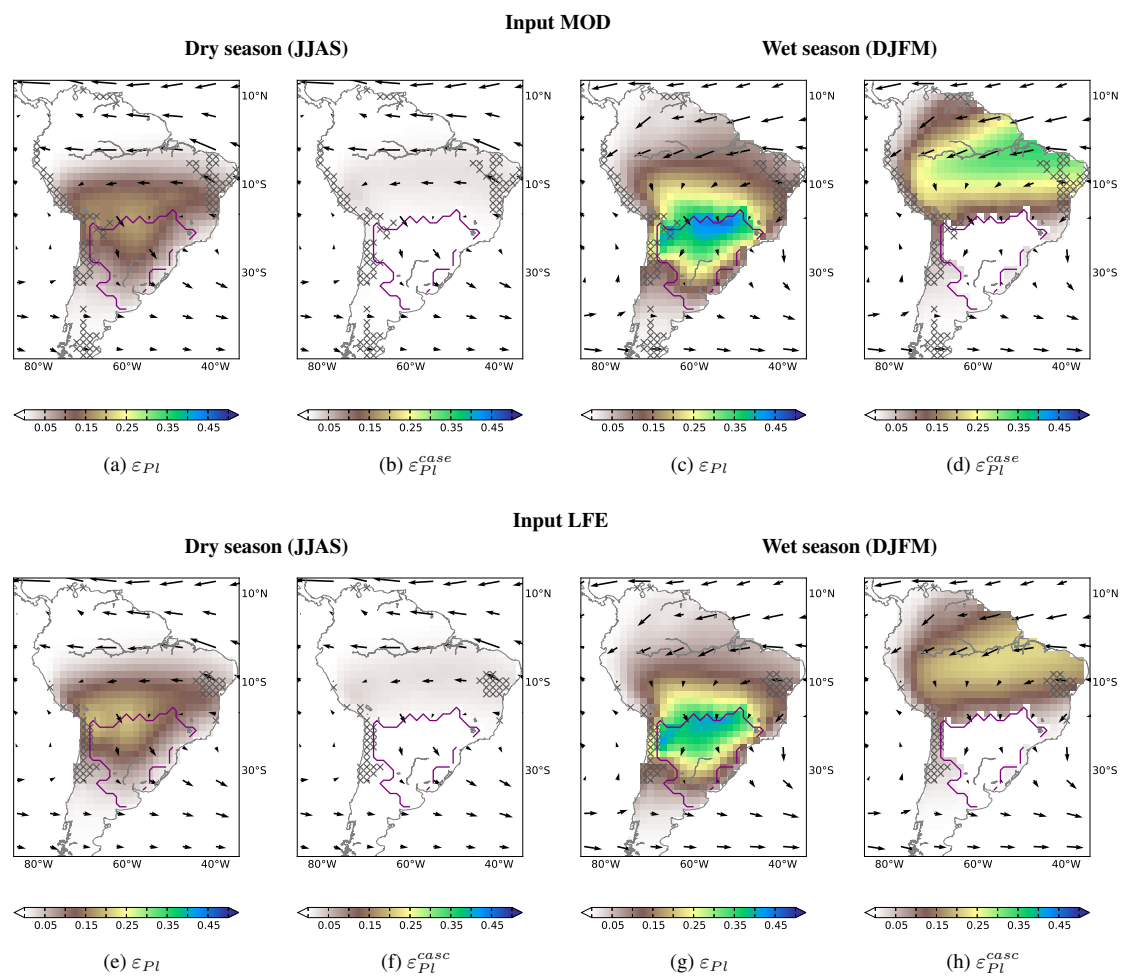


FIGURE 3.7 Fraction of evapotranspiration that precipitates over the La Plata basin (defined by the purple boundaries) through DMR ( $\varepsilon_{Pl}$ , **a**, **c**, **e** and **g**) and CMR ( $\varepsilon_{Pl}^{casc}$ , **b**, **d**, **f** and **h**). Considered together,  $\varepsilon_{Pl}$  and  $\varepsilon_{Pl}^{casc}$  show source regions of precipitation over the La Plata basin. Results are obtained using the input MOD (upper row) and input LFE (lower row) (see Table 3.1) and are given for the dry season (left) and the wet season (right).

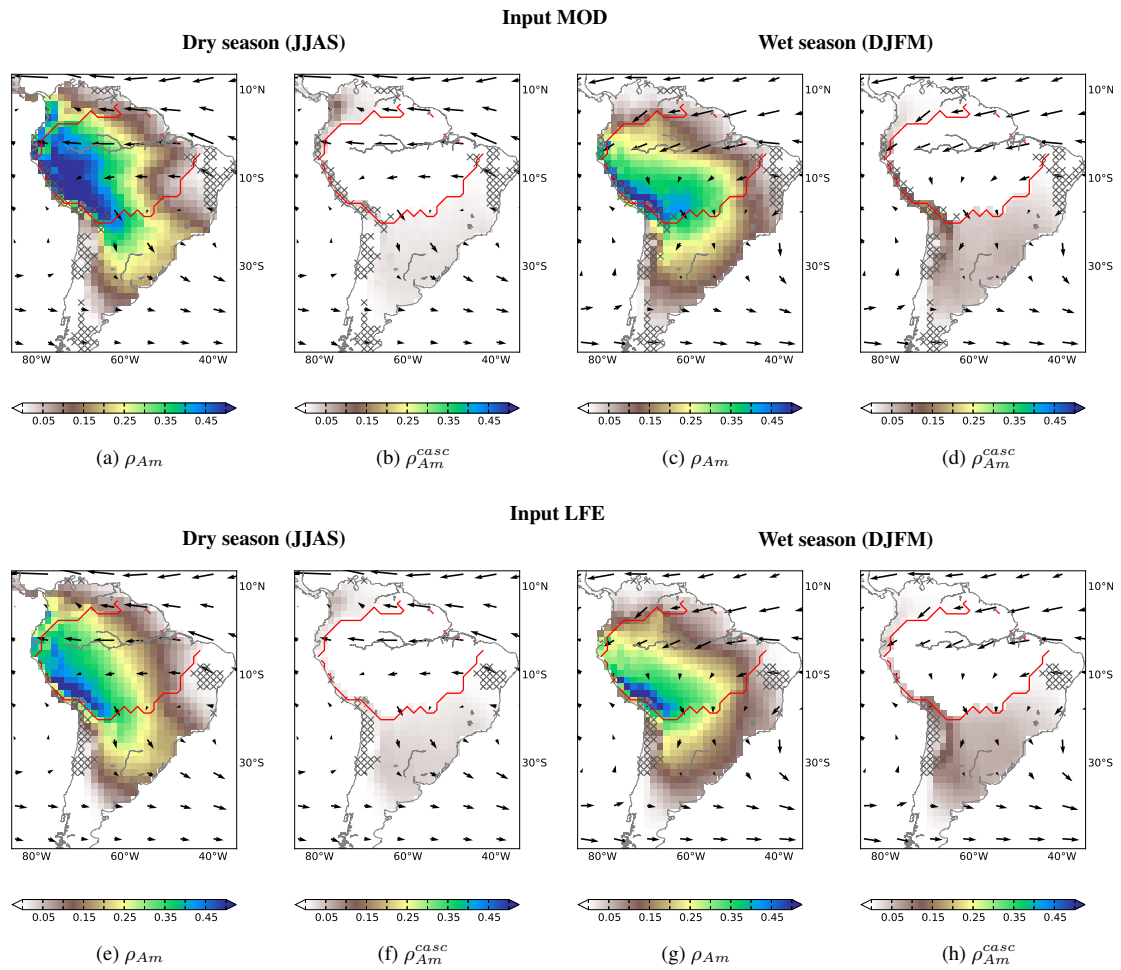


FIGURE 3.8 Fraction of precipitation that originates from the Amazon basin (defined by the red boundaries) through DMR ( $\rho_{Am}$ , **a**, **c**, **e** and **g**) and CMR ( $\rho_{Am}^{casc}$ , **b**, **d**, **f** and **h**). Considered together,  $\rho_{Am}$  and  $\rho_{Am}^{casc}$  show sink regions of evapotranspiration from the La Plata basin. Results are obtained using the input MOD (upper row) and input LFE (lower row) (see Table 3.1) and are given for the dry season (left) and the wet season (right).





## Chapter 4

# Self-amplified Amazon forest loss with dry-season intensification

This chapter (together with appendix C) has been submitted to the Journal *Nature*.  
The list of the co-author is the following:

Delphine C. Zemp<sup>1,2</sup> Carl-Friedrich Schleussner<sup>2,3</sup> Henrique M. J. Barbosa<sup>4</sup> Marina Hirota<sup>5,6</sup>, Gilvain Sampaio<sup>7</sup>, Arie Staal<sup>8</sup>, Lan Wang-Erlandsson<sup>9,10</sup> and Anja Rammig<sup>2,11</sup>

1, Department of Geography, Humboldt Universität zu Berlin, Berlin, Germany

2, Potsdam Institute for Climate Impact Research (PIK), Potsdam, Germany

3, Climate Analytics, Berlin, Germany

4, Instituto de Física, Universidade de São Paulo, São Paulo, S.P., Brazil

5, Department of Physics, Federal University of Santa Catarina, Florianópolis, SC, Brazil

6, Functional Ecology Lab, Institute of Biology, University of Campinas, Campinas, Brazil

7, Center for Earth System Science (CCST), National Institute For Space Research (INPE), São José dos Campos, S.P., Brazil

8, Aquatic Ecology and Water Quality Management Group, Wageningen University, Wageningen, The Netherlands

9, Department of Water Management, Delft University of Technology, Delft, The Netherlands

10, Stockholm Resilience Centre, Stockholm University, Stockholm, Sweden

11, Technische Universität München, Munich, Germany

## Abstract

Vegetation-atmosphere interactions are of key importance to sustain precipitation and forest resilience across the Amazon basin. Interacting effects of land-use change and rainfall variability may trigger local critical transitions from tropical forest to grass-dominated ecosystems [Brando et al., 2014]. As dry-season evapotranspiration rates for forest are higher than for savanna or treeless vegetation [Da Rocha et al., 2009, Von Randow et al., 2004], forest loss could weaken large-scale continental moisture recycling that currently amounts to 25-50% of total Amazonian rainfall [Eltahir and Bras, 1994, Zemp et al., 2014a]. While regionally-driven feedbacks between forest loss and rainfall reduction may threaten the ecological integrity of the Amazon forest [Coe et al., 2013, Nepstad et al., 2008, Oyama and Nobre, 2003], the severity and extent of this threat is yet unknown in relation to projected prolonged dry seasons [Boisier et al., 2015] and rising deforestation rates [Fearnside, 2015] in the future. To tackle this uncertainty we used empirical estimates of moisture recycling [van der Ent and Savenije, 2011] and local forest resilience [Hirota et al., 2011] to model the coupled Amazon vegetation-rainfall system as a heterogeneous and interconnected dynamic complex network. We found an exponential increase of self-amplified Amazon forest loss with dry-season intensification. While it is expected that this process affects up to 10% of the current forest, particularly in central and western Amazonia, a complete Amazon dieback cannot be ruled out [Good et al., 2013]. Our results suggest that self-amplified forest loss is diminished by the variability in the forest's sensitivity to altered rainfall regime, highlighting the importance of plant diversity [Claussen et al., 2013] and landscape heterogeneity [van Nes and Scheffer, 2005] for the stability of the forest. Considering the strong internal connectivity of the Amazon forest in establishing conservation management strategies is essential to maintain the forest ecosystem integrity. Our results pave the way for accounting for the non-linear and complex vegetation-atmosphere interactions in estimating impacts of global environmental changes in the Amazon basin and beyond.

## Main text

Non-linear relations between rainfall and tree-cover distribution suggest that abrupt shifts from forest to an alternative stable vegetation state (savanna-type of ecosystem) [Hirota et al., 2011] may result from feedbacks between fire and forest cover [Brando et al., 2014, Staver et al., 2011]. The complex interplay between logging, clearing and inter-annual drought might push the south-southeastern (SSE) Amazon forest towards such critical transition [Coe et al., 2013, Nepstad et al., 2008]. The risk of reaching a

so-called tipping point in SSE Amazonia is increased by a projected dry-season intensification under climate change [Boisier et al., 2015] and further deforestation [Fearnside, 2015]. Forest loss could amplify drought by weakening the evaporative source of atmospheric moisture that recycles back to precipitation [Bagley et al., 2014]. As locations where deforestation would lead to a maximal increase of the ecological vulnerability of the remaining forest (Fig. 4.1c) coincide with regions likely to be deforested or degraded in the near future [Nepstad et al., 2008], it is crucial to evaluate the risk of spatial propagation of forest loss (“cascading forest loss”). Because substantial uncertainties exist regarding the effects of changing climate on vegetation-climate feedback mechanisms and their consequences for the Amazon forest [Good et al., 2013], there is a need to identify processes, extent and key regions of potential cascading forest loss.

Here we assess the potential of cascading forest loss in the Amazon region using a complex network approach that has been widely applied to study cascading effects, such as fluctuations in stock markets, propagation of social movements or ecosystem regime shifts [Watts, 2002]. We built an empirical cascade model (see Fig.C1) based on a vegetation-rainfall network where the nodes that represent individual forest grid cells within the Amazon basin can flip to an alternative stable state (savanna or treeless). The nodes are linked by water fluxes from source to sink of rainfall [van der Ent et al., 2010] (Fig. 4.2) and flip according to simple threshold rules in the probability to find forest for a given rainfall regime (forest resilience [Hirota et al., 2011]) (see Methods).

Feedbacks between vegetation and rainfall increase forest vulnerability under severe dry-season intensification as projected for the end of the 21st century [Boisier et al., 2015] (see Methods) (Fig. 4.3c and d). Beyond 2 mm/day of oceanic moisture inflow reduction during the extended dry season (June-November), cascading forest loss increases exponentially with decreasing oceanic moisture inflow (Fig. 4.3g). This results from (1) a non-linear decrease of forest resilience (see Fig. C3) and (2) a stronger reduction of evapotranspiration after forest loss (see Fig. C10), with increasing water deficit, as well as (3) an increased contribution of moisture recycling to total rainfall under reduced oceanic moisture inflow (see Fig. C4). For a reduction of 6 mm/day, which corresponds to a complete breakdown of oceanic moisture inflow in almost three quarters of the Amazon forest during the extended dry season, forest loss attributed to cascading effects in the vegetation-rainfall system exceeds 10% of the current forest area. Under such a drastic scenario, SSE Amazon forests with the lowest resilience are lost as a direct response to oceanic moisture inflow reduction (blue regions in Fig. 4.3f), triggering cascading forest loss in remote regions such as central and western Amazonia (green regions in Fig. 4.3f). Cascading effects in the vegetation-rainfall system may be even stronger than expected as the reduction of dry-season evapotranspiration after deforestation measured from flux

towers [Von Randow et al., 2004] is greater than our predictions based on gridded multi-data sets (see Fig. C10). Considering uncertainties associated with evapotranspiration changes, up to 40% of the current forest might be lost through cascading effects and an Amazon dieback (almost 95% forest loss) is found for 6 mm/day oceanic moisture inflow reduction (dashed red line in Fig. 4.3g).

Given the prominence of cascading effects in the coupled Amazon vegetation-rainfall system, understanding the specific network properties defining its dynamics is of key interest. Previous studies on cascade dynamics in complex networks suggested that the systems' responses to perturbations are controlled by two main properties, heterogeneity and connectivity of the nodes in the network [Scheffer et al., 2012, Watts, 2002]. Heterogeneity in forest resilience thresholds may arise, for instance, from spatial variability in forest adaptability to drought, in land surface properties controlling water availability for trees and in human-induced or natural disturbances to the forest. To evaluate the importance of this heterogeneity, we investigate the effect of the width of the bell-shaped resilience threshold distribution on cascade size (see Methods). Our results (Fig. 4.4a) show that heterogeneity in forest resilience thresholds weakens the tendency of high-order cascades. In other words, if individual forest patches shift at different critical rainfall regimes, propagation of forest loss is usually stopped in the early stage of the cascade. Hence, variability in the Amazon forest's sensitivity to altered rainfall regime alleviates the risk of long-term cascading forest loss. This finding stresses the importance of plant diversity [Claussen et al., 2013] and heterogeneity of the landscape [Claussen et al., 2013] for the vegetation stability.

We evaluate the effect of connectivity by gradually removing moisture recycling links that contribute to rainfall over the Amazon basin according to their geographical distance (Fig. 4.4b). Beyond 6 mm/day oceanic moisture inflow reduction during the extended dry season, removing all links from the network leads to a complete Amazon dieback (black line in Fig. 4.3g). We note that without moisture recycling, more than 30% of current forest would not be displayed already today (see Fig. C5a). The amount of moisture transported through a link decreases exponentially with its geographical distance [van der Ent and Savenije, 2011]. Hence, gradually removing short-range links rapidly leads to a sharp decline in rainfall from continental origin and thus to an Amazon dieback (Fig. C5). On the contrary, removal of the 20% longest-range links (link distance up to  $23^\circ$ , i.e. 2500 km) increases the cascading forest loss by around 50% (black dots and circles in Fig. 4.4b) although less than 4% of the total amount of moisture recycled is affected (blue line in Fig. 4.4b). Thus, even if long-range links do not contribute largely to the total amount of moisture recycling, they play a crucial role for the Amazon forest stability by providing remote moisture input. If removal of links continues beyond this point (link distance less than  $23^\circ$ ), the share of the cascading effect declines. The most

probable cause of this decline is an overall reduction in the moisture being recycled, which reduces the strength of interactions among nodes.

To sum up, our sensitivity analysis of the Amazon vegetation-rainfall system stability shows the potential of forest loss in SSE Amazonia, most likely directly affected by land-use and rainfall variability [Coe et al., 2013], to erode the resilience of the remaining forest. Combined with a drastic dry-season intensification driven by decreases in oceanic moisture inflow, this could lead to large-scale self-amplifying forest loss.

In the last decade, two “once-in-a-century” droughts [Marengo et al., 2011] substantially reduced carbon storage in Amazonian forests [Lewis et al., 2011] and affected the canopy structure and water content with low recovery in the following years [Saatchi et al., 2013], showing the vulnerability of the Amazonian forests to such extreme events. Deforestation has the potential to enhance such droughts [Bagley et al., 2014]. Hence, if such events occur more frequently, as suggested by current trends [Marengo et al., 2011] and climate projections [Cox et al., 2008], they may gradually destabilize different regions of the forest. This could push the system towards large-scale self-amplified forest loss in a step-wise process without similarly drastic changes in the climatology.

Vegetation and rainfall are part of an interconnected complex system that requires a holistic approach when considering the stability of the Amazon forest to environmental changes such as increasing drought projected with global warming [Dai, 2013]. Our results emphasize the importance of maintaining the structural and functional diversity of Amazonian forests and their connectivity (short-range and long-range) to reduce the risk of long-term self-amplified forest loss. Disturbances to the forest should be avoided particularly in the hot spot regions (Fig.4.1c) that play a crucial role for the resilience of the remaining forest.

## 4.1 Methods

### 4.1.1 Modeling cascading forest loss

Our approach is based on a well-established simple cascade model for complex networks [Watts, 2002]. We initialize 1000 ensemble simulations in which each grid cell has a resilience threshold randomly sampled from a normal distribution with mean  $\Phi$  and standard deviation  $\sigma$ .

The thresholds are fixed for the duration of the simulation. A simulation run comprises the following steps (Fig. C1): (1) moisture from oceanic origin propagates through the network on a monthly time scale by moisture transport involving re-evaporation

cycles [Zemp et al., 2014a] (Fig. 4.2). Moisture propagation is determined using the output of a Eulerian model of atmospheric moisture tracking [van der Ent et al., 2010] and a simple evapotranspiration model (see Methods Sect. 4.1.3), both calibrated to merged climate data (Landflux-EVAL and average of CRU, GPCC, GPCP and CPC; see Supplementary Information (SI) Sect. 1.2.1). (2) Rainfall regime characterized by the annual precipitation and Maximum Cumulative Water Deficit (MCWD) [Aragão et al., 2007] is calculated on a grid-cell basis. (3) The probability to find forest (tree cover  $\geq 55\%$ ) for a given rainfall regime (forest resilience) is calculated for each grid-cell using the output of a logistic regression [Hirota et al., 2011] on remotely sensed data (MOD44B v5 and TRMM3B-42 v7, see SI Sect. 1.3.1). (4) A critical transition occurs in all grid cells for which the forest resilience crosses the individual threshold. Shifts between savanna ( $5\% \geq \text{tree cover (TC)} > 55\%$ ) and a treeless state ( $\text{TC} < 5\%$ ) are not considered (see explanation in Fig. C7). After a shift, forest is converted to a treeless state to represent the combined effect of deforestation and drought-induced forest degradation unless stated otherwise. (5) Local evapotranspiration is updated in grid cells where shifts occurred. To evaluate the confidence interval of the cascading forest loss, evapotranspiration from forest and non-forest (savanna and treeless) grid cells represent the 95% upper bound and 5% lower bound of the estimations, respectively. The model runs with grid cells updating their status until equilibrium in vegetation cover is reached.

The results shown in the main text assume  $\phi = 0.3$  and  $\sigma = 0.05$ , limiting the occurrence of shifts under the historical rainfall regime (Fig. 4.3a) to the zone where forest and savanna are currently bistable (See Fig. C6). Results for different parameter settings are shown in Fig. C2.

#### 4.1.2 Quantifying cascading effects

The model setup allows us to discern the importance of the cascading effect of regional vegetation-rainfall feedbacks and the direct effect of the initial rainfall regime on forest loss. This is done by comparing the fully coupled vegetation-rainfall system (“cascade-mode on”) with a one-way coupled system in which changes in vegetation states do not alter evapotranspiration rates (“cascade-mode off”). Three metrics are of interest: the difference between forest loss in the cascade-mode “off” and “on” versions, which quantifies the area of cascading forest loss; the relative difference between the shifting frequency in these two versions, which quantifies the share of cascading effect in forest loss (“share of cascading effect”); the number of model iterations until equilibrium indicating the presence of higher-order cascades, which can be interpreted as a time span of the cascade (“cascade size”).

### 4.1.3 Simple evapotranspiration model on a monthly time scale

To estimate changes in local evapotranspiration with changing rainfall or vegetation state, we use a function adapted from a simple evapotranspiration model on a monthly scale (see [Gerrits et al., 2009] and see SI Sect. 1.2). It accounts for the most important factors controlling monthly evapotranspiration ( $E$ ) in the Amazon basin as identified by flux tower measurements [Da Rocha et al., 2009]: atmospheric demand (monthly potential evapotranspiration  $E_{pot}$ ) and access of sub-surface water during seasonal drought (carry-over factor  $F_{CO}$ ).  $F_{CO}$  depends on the capacity of the vegetation to access sub-surface water and on the soil water storage from the preceding wet season. Here, we assume that  $F_{CO}$  is a linear function of cumulative water deficit ( $C_{WD}$ , [Aragão et al., 2007]):

$$E = \min\left(F_{CO} + \frac{P}{p_1} * (1 - \exp(-\frac{p_2}{P})), E_{pot}\right) \quad (4.1)$$

$$F_{CO} = -p_3 * C_{WD} + p_4 \quad (4.2)$$

While the parameters  $p_1, p_2, p_3, p_4$  depend on land-surface properties (soil and vegetation) and daily rainfall characteristics [Gerrits et al., 2009], for simplicity we consider here only the vegetation control. For each vegetation state we fit the previous equation to historical merged data (see SI Sect. 1.2.5 and Fig. C8).

### 4.1.4 Dry-season intensification scenarios

We present two different setups to study the effects of decreasing monthly oceanic moisture inflow during the extended dry season (June-November) with the period 1989-1995 as baseline. In a first setup, oceanic moisture inflow is homogeneously decreased with 2 mm/day increments until a complete failure of this inflow in most of the Amazon basin (8 mm/day reduction). In a second setup, two stylized scenarios (“moderate” and “severe”) are generated based on long-term precipitation change projections for the extended dry season in the Amazon basin from a previous study [Boisier et al., 2015]. This combines observation-based data and the ensemble mean of CMIP5 climate models for the highest greenhouse gas emission scenario (RCP 8.5) for the end of the twenty-first century. In the moderate dry-season intensification scenario, monthly oceanic moisture inflow is reduced homogeneously by [0.32, 0.48, 0.64, 0.8, 0.53, 0.27] mm/day (June - November). In the severe dry-season intensification scenario, 0.5 mm/day moisture inflow reduction is added to the moderate scenario to account for the upper boundary defined by the standard deviation of the statistical projections [Boisier et al., 2015].

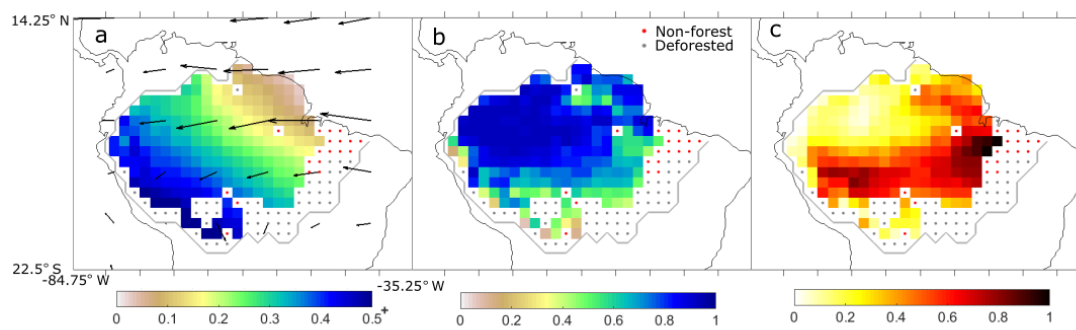


FIGURE 4.1 **Continental precipitation recycling ratio, forest resilience and hot spots where deforestation would lead to a maximal impact on the resilience of the remaining forest.** a) Fraction of annual rainfall originating from continental evapotranspiration as computed by an atmospheric moisture tracking algorithm [van der Ent et al., 2010] on merged climate data. Arrows represent vertically integrated moisture fluxes. b) Probability to find forest in the current rainfall regime inferred from analysis of remotely sensed tree cover and rainfall data. c) Normalized relative mean reduction of the overall resilience of the remaining forest after deforestation of each grid cell individually. Results are shown for grid cells currently covered by forest (tree cover  $\geq 55\%$ ) within the Amazon basin (gray boundary).

## Acknowledgements

We thank Ruud van der Ent for developing the atmospheric moisture tracking model used in this study, Jonathan F. Donges for discussion and Brigitte Mueller for providing the precipitation multi-data set. This paper was developed within the scope of the IRTG 1740/TRP 2011/50151-0, funded by the DFG/FAPESP. Financial supported was also provided by EU-FP7 ROBIN project under grant agreement 283093, by CNPq - Conselho Nacional de Desenvolvimento Científico e Tecnológico, project number 478314/2012-4, by project Microsoft/FAPESP 2013/50169-1, by SENSE Research School, by EU-FP7 project "AMAZALERT" (Grant agreement no. 282664) and by the Helmholtz Alliance "Remote Sensing and Earth System Dynamics".

## Author contributions

D.Z., C.S and A.R conceived the study, D.Z. conducted the analysis and wrote the paper with the support of all co-authors.



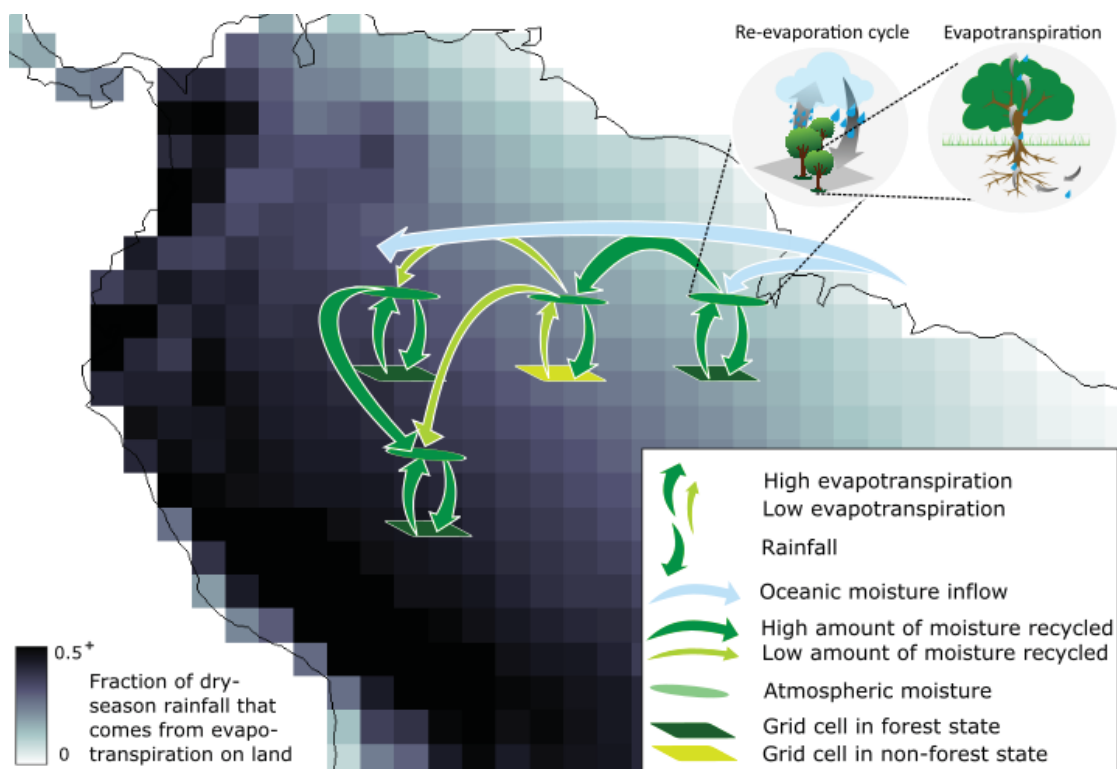


FIGURE 4.2 **Schematic representation of feedbacks between vegetation and rainfall, which may cause cascading forest loss.** After a shift of forest to a grass-dominated ecosystem, local evapotranspiration is reduced, which affects rainfall in other locations due to weakening of atmospheric moisture transport. This in turn reduces the resilience of the remaining forest and increases the risk of further vegetation shifts.

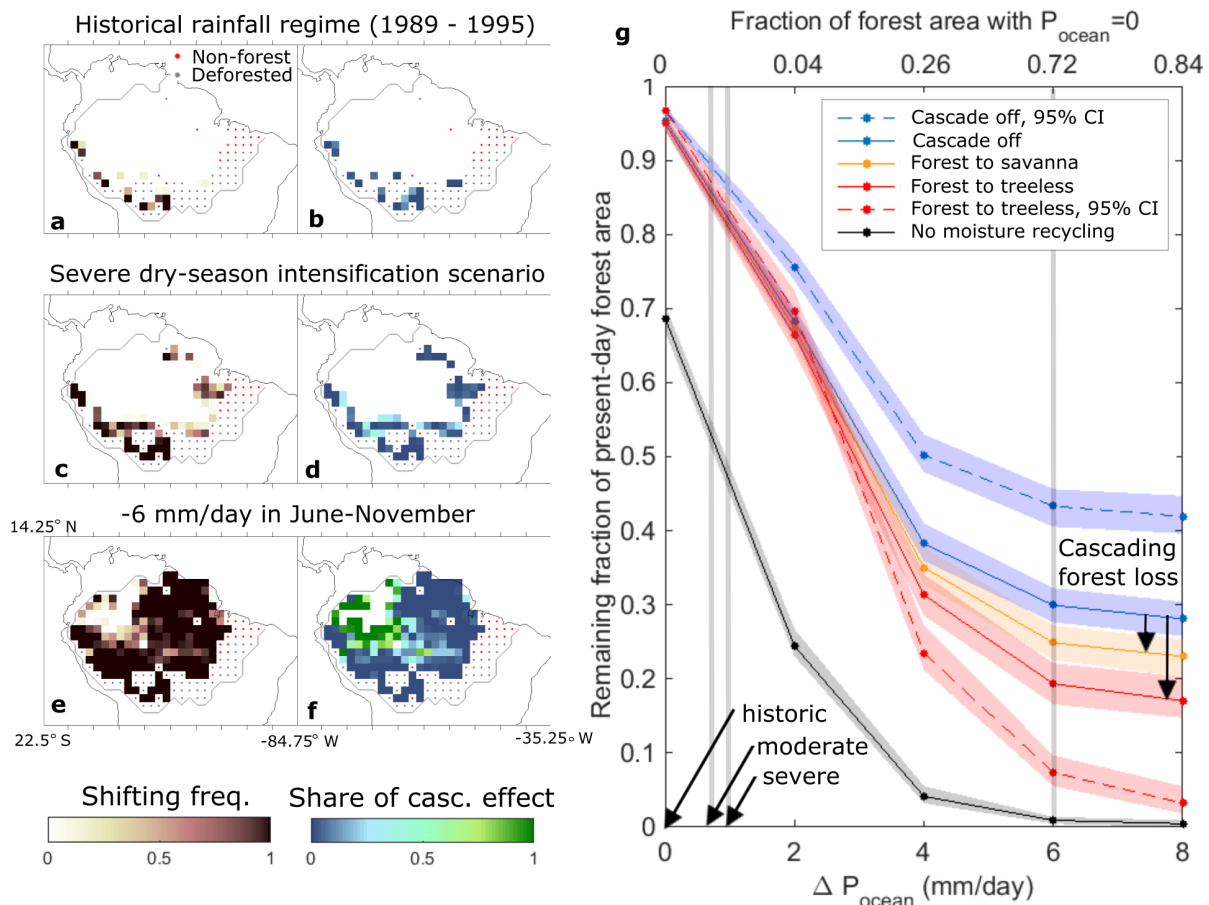


FIGURE 4.3

**Cascading forest loss for the historical rainfall regime and dry-season intensification experiments.** (a,c,e) Shifting frequency of tropical forests. (b,d,f) Share of the cascading effect in explaining shifting frequency. Only grid cells with a shifting frequency above 3% are shown. While low values indicate forest loss already for the initial rainfall regime, high values show forest loss due to cascading effects (see Methods). Note that forest and savanna are currently bistable, implying that forest could already have shifted due to a stochastic event even though it is found today. (g) Fraction of remaining Amazon forest area (median of all ensemble members as lines, 95% bound as shadings) as a function of monthly oceanic moisture inflow reduction during the extended dry season ( $\Delta P_{ocean}$ ). Results are shown with cascade-mode "off" (blue line) and "on" for conversion of forest to savanna (orange line) or treeless (red line). Results obtained using the 95% confidence interval (CI) of predicted evapotranspiration is also shown (dashed lines). For comparison, the maximum possible forest loss in the scenario of a complete failure of moisture recycling is also shown (black line). The dry-season intensification scenarios are indicated by gray vertical lines.

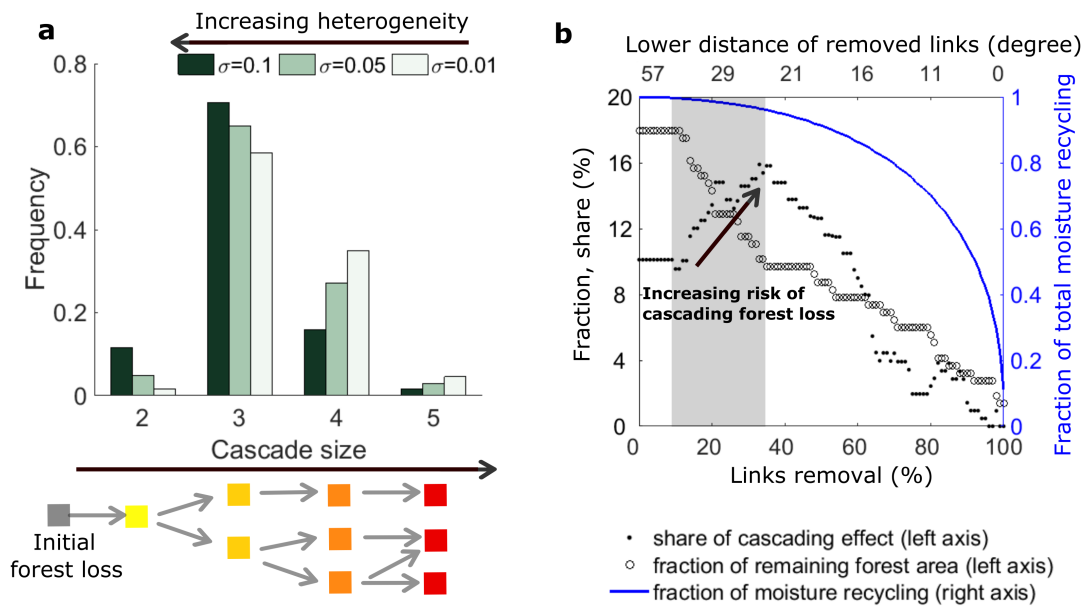


FIGURE 4.4 **Effect of heterogeneity and connectivity.** The results are obtained under an experiment of 6 mm/day reduction of oceanic moisture inflow during the extended dry-season (June–November). **a**, Distribution of cascade sizes with increasing heterogeneity ( $\sigma$ , see Methods). **b**, Share of cascading effect (black dots) and fraction of remaining forest area (black circles) when gradually removing moisture recycling links that contributes to rainfall over the Amazon basin according to their geographic distance in descending order (long links removed first) with an increment of 1% link density and with  $\sigma = 0$ . The corresponding relative decrease of the total rainfall recycling over the Amazon is also shown (blue lines, right axis).



## Chapter 5

# General conclusion

### 5.1 Achievements

This dissertation has laid down the foundation of vegetation-rainfall feedbacks analysis using a complex network approach. Although the work presented in this thesis does not exploit the full potential offered by the combination of forest resilience, moisture recycling and complex network concepts, it is a significant step towards a more detailed understanding of the non-linearities and complex interactions in the Amazon vegetation-rainfall system.

#### 5.1.1 Complex network analysis for weighted and directed networks

Complex network analysis is a powerful tool to better understand the architecture and functioning of a complex system with interacting elements. However, existing measures were not suited to study networks with directed and weighted edges and weighted nodes such as moisture recycling networks. Chapter 2 extends common measures such as the degree and the clustering coefficient in agreement with the node-splitting invariance principle. Applied to our purpose, these measures revealed key regions for cascading moisture recycling pathways in South America. They can be applied to any complex network sharing similar properties.

### **5.1.2 The new concept of cascading moisture recycling and associated methodological framework**

The concept of “cascading moisture recycling” has been introduced to describe moisture transport from the source to the sink of rainfall on the continent that involves re-evaporation cycles on the way. A new vocabulary has been suggested (Appendix A) to systematically describe this process on the continent. Based on the output of an Eulerian atmospheric-moisture tracking model, a methodological framework has been developed (Sect. 3.2.3 - 3.2.6) to quantify the importance of cascading moisture recycling and to highlight key regions where re-evaporation cycles are taking place. This framework has been applied to different combinations of climate datasets in South America. Its robustness and flexibility have been demonstrated. The suggested methodological framework could be adopted to study cascading moisture recycling in other regions of the world.

### **5.1.3 Cascade dynamics in the complex Amazon vegetation-rainfall system**

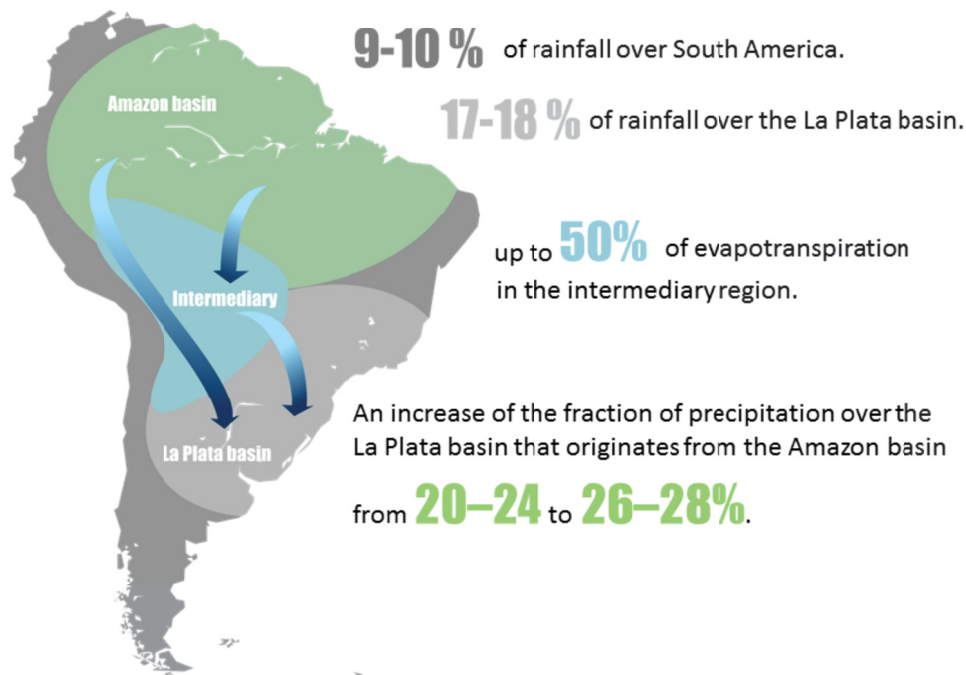
Based on the complex network theory, a methodology has been developed in Chapter 4 to 1) detect regions where deforestation would greatly affect the vegetation-rainfall system stability, 2) evaluate the risk of self-amplifying forest loss under dry-season intensification and deforestation and 3) assess important properties stabilizing the vegetation-rainfall system. The proposed model simulates cascading effects of reduced rainfall and forest loss. It emerges from the coupling of forest resilience calculations, moisture recycling networks and a simple evapotranspiration model, all calibrated to gridded observational-based data of tree cover and climate.

## **5.2 Answers to the research questions**

Q1: What is the importance of cascading moisture recycling in South America?

Key results from Chapter 3 are summarized in Fig. 5.1. Cascading moisture recycling is important as 9-10% of the total rainfall over South America is re-evaporated several times on land. This fraction reaches 7-10% over the Amazon basin and 17-18% over the La Plata basin. Considering cascading moisture recycling increases the fraction of rainfall over the La Plata basin that originates from the Amazon basin by 4-6% (from 20-24% to 26-28%). This means that the role of the Amazon forest for continental rainfall regulation has been under-estimated in previous studies that did not account for cascading moisture recycling.

Cascading moisture recycling represents ....



1

FIGURE 5.1 Key results showing the importance of cascading moisture recycling.

The southern part of the Amazon basin was identified by previous studies as a direct source of moisture for the La Plata basin. Results presented in Chapter 3 show that it is also an intermediary region that redistributes moisture evaporating from the entire Amazon forests towards the subtropics. Therefore, the entire Amazon basin (and not only the southern part as previously thought) plays a crucial role for the South American rainfall.

Q2: Where are key regions that sustain cascading moisture recycling in South America?

Key intermediary regions for the overall cascading moisture recycling in South America have been identified in Chapter 3. These regions cover not only the southern Amazon basin but also parts of Bolivia, Paraguay and northern Argentina where up to 50% of the evapotranspiration is involved in cascading moisture recycling, i.e. comes from the land and returns to the land as rainfall. Results also indicate that the eastern flank of the subtropical Andes is a key region where cascading moisture recycling pathways are channeled. Previously identified as a location where the South American Low Level Jet is accelerated, we now know that re-evaporation cycles are taking place along the way.

Q3: Where are the “hot spot” regions where deforestation would greatly destabilize the Amazonian ecosystem?

The regions where deforestation would greatly reduce the resilience of the remaining forest are shown in Chapter 4, Fig. 1c. Two reasons explain the location of these hot spots. Firstly, forest loss in the hot spots leads to strong evapotranspiration decrease, which is typically the case in southern and eastern Amazonia due to the pronounced dry seasons. Secondly, the hot spots are located up-wind of forests with low resilience where a small decrease in rainfall drastically reduces the resilience. Deforestation in these regions should be avoided to prevent damage to the remaining forest.

Q4: What is the potential of vegetation-rainfall feedbacks to lead to self-amplifying Amazon forests loss?

Fig. 3 in Chapter 4 suggests that vegetation-rainfall feedbacks have the potential to lead to self-amplifying forest loss in the Amazon basin if the dry season intensifies drastically. Three reasons explain this finding: (1) a non-linear decrease of forest resilience and (2) a stronger reduction of evapotranspiration after forest loss, with increasing water deficit, as well as (3) an increased contribution of moisture recycling to total rainfall under reduced oceanic moisture inflow.

Q5: Can we identify tipping points in deforestation and rainfall change beyond which large-scale Amazon forest loss (dieback) would occur?

At above 2 mm/day oceanic moisture inflow reduction during the extended dry season (June-November), cascading forest loss increases exponentially with further oceanic moisture inflow reduction. Beyond a 6 mm/day oceanic moisture inflow reduction in synergistic effect with deforestation, more than 10% of the present-day forest would be lost due to regional vegetation-rainfall feedbacks, in particular in central and western Amazonia (Chapter 4, Fig. 3). This area increases up to 40%, leading to a complete Amazon dieback, when uncertainties associated with the estimated evapotranspiration reduction after forest loss are taken into account. The imposed dry-season intensification in this scenario would correspond to a complete failure of oceanic moisture inflow in most of the Amazon forest during the extended dry season, which is far from recent statistical predictions of rainfall change for the end of the twenty-first century (0.75-1 mm/day reduction in June-November). Nevertheless, if extreme drought events become more frequent (as observed during the last decade and projected by a climate model), cascading forest loss could occur in a step-wise process without changes in the long-term mean dry-season rainfall.



Q6: Which properties affect the stability of the Amazonian vegetation-rainfall system under environmental changes?

Two properties stabilize the Amazonian vegetation-rainfall system (Chapter 4, Fig. 4): (1) spatial variability in forest resilience thresholds that may arise in the real world, for example, from variability in land-surface properties (e.g., soil texture and soil depth), forest characteristics (e.g., presence of drought-adapted taxa) and disturbance regimes on the forest (e.g., fire and extreme drought); (2) long-range moisture recycling links.

### 5.3 Potential further developments

On the basis of the methodological framework presented in Chapter 4, three further developments appear necessary and straightforward.

(1) The capacity of the vegetation to access sub-surface water during drought (i.e., carry-over factor) is represented as a linear function of the cumulative water deficit. As there is no reason to believe that this relationship is linear, an analysis of the sensitivity of the results to other assumptions is needed. More generally, to improve the estimation of the carry-over factor, an analysis of groundwater data in combination with evapotranspiration estimates and tree cover is required. Such analysis is possible thanks to recent improvements in soil moisture estimates from satellites observations [Dolman and De Jeu, 2010].

(2) Rainfall is assumed to decrease linearly with changes in atmospheric moisture storage. This assumption could be verified or adapted based on a simple correlation of these two variables found in remotely sensed data.

(3) The analysis presented in this thesis is based on a  $1.5^\circ$  longitude and latitude grid, which corresponds to almost  $30,000 \text{ km}^2$  at the equator. It would be desirable to down-scale the presented framework to a finer spatial resolution to better account for variabilities in land-surface properties. However, it should be kept in mind that the effect of increasing rainfall over the deforested area due to the “vegetation breeze” [Medvigy et al., 2011] becomes important at finer spatial scales. In addition, a coarse resolution is required for the numerical stability of the atmospheric moisture tracking experiment [van der Ent et al., 2014]. Hence, down-scaling to a finer resolution than  $1^\circ$  longitude and latitude grid is not recommended.

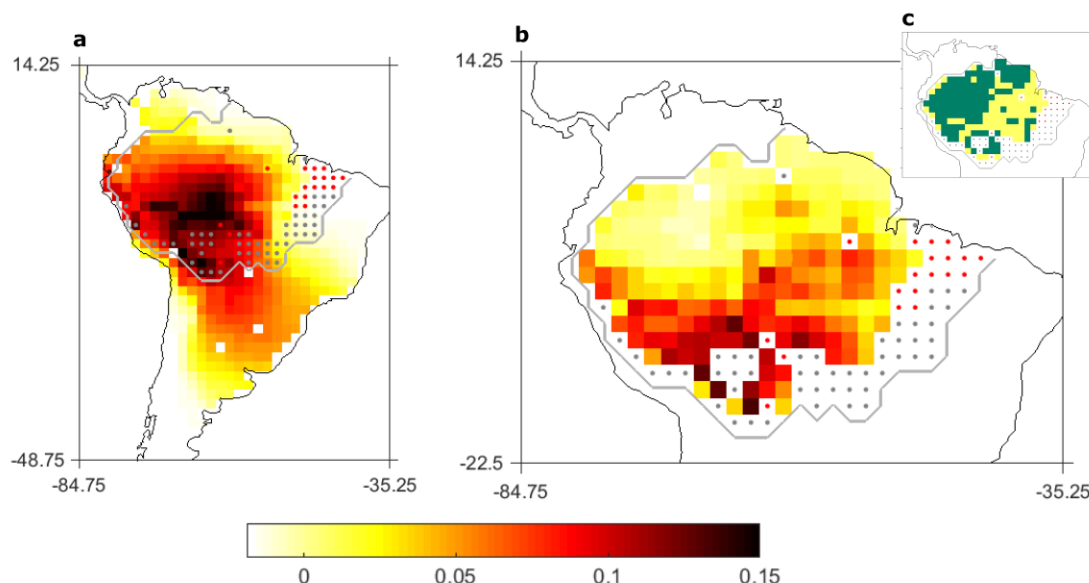


FIGURE 5.2 Effect of a business-as-usual deforestation scenario in 2050 on **a)** continental rainfall during the dry season (June-September) and **b)** the Amazon forest resilience. The color code indicates the fraction of simulated changes compared to historical conditions (1989-1995) when full uncertainties in evapotranspiration estimates are considered, as found using the modeling framework developed in Chapter 4. **c)** Deforestation scenario showing the remaining forest (green) and deforested areas in 2050 (yellow). The historical deforested area (red dots) and savanna (gray dots) are also shown. The vegetation cover data is based on Soares-Filho et al. [2006] and has been up-dated at  $1.5^\circ$  longitude and latitude grid using the most frequent value in the original dataset.

## 5.4 Potential further applications

### 5.4.1 Effect of inter-annual variability

A straightforward application of the cascade model presented in Chapter 4 is to analyze the potential effect of inter-annual rainfall variability on the stability of the Amazonian vegetation-rainfall system. It is expected that more frequent drought events lead to large-scale self-amplified forest loss without changes in the long-term mean dry-season rainfall. This expectation is supported by recent studies showing that current rates of deforestation already have the potential to increase inter-annual drought events [Bagley et al., 2014] and that inter-annual rainfall variability affects the probability that forest is able to survive in the tropics [Holmgren et al., 2013].

### 5.4.2 Effect of land-use change in tropical South America on continental rainfall

The modeling framework developed in Chapter 4 can also be applied to study the effect of specific land-use change scenarios in tropical South America on regional rainfall and Amazon forest resilience. An indication of the possible outcomes of such applications is given using a “business-as-usual” deforestation scenario for the middle of the twenty-first century [Soares-Filho et al., 2006] (Fig. 5.2). Results show that dry-season rainfall is reduced by 8% basin-wide, which leads to a reduction of the resilience of the remaining forest by 3% on average and up to 16% in southwestern Amazonia. It would be interesting to evaluate in greater detail the erosion of the forest resilience in different key regions in relation to gradual land-use change in the Amazon forest and/or the Brazilian savanna (cerrado). This would enable potential tipping points of land-use change in South America affecting the Amazon forest’s integrity to be identified and would complement previous modeling studies (e.g., Pires and Costa [2013], Sampaio et al. [2007]).

Finally, it would be interesting to analyze the effect of Amazon deforestation on rainfall reduction in subtropical South America in relation to extreme drought events. Such information could, for example, support or contradict the assertion found in the media that the extreme drought that affected Sao Paulo in 2014 is related to a weakening of moisture transport due to past deforestation in Amazonia.

### 5.4.3 Continental feedback on oceanic moisture inflow

The “biotic pump theory” [Makarieva et al., 2013] suggests that the effect of latent heat release overwhelms the well-documented temperature gradient as a driving force of wind speed. Although this theory is controversial (see editorial notes on the article), it would be interesting to investigate the possible acceleration of cascading forest loss by such feedback processes. Linking forest loss to reduced oceanic moisture inflow could be easily implemented in the cascade model presented in Chapter 4.

### 5.4.4 Cascading moisture recycling in Eurasia and Africa

The methodological framework to analyze cascading moisture recycling framework (Chapter 3) may be applied to other regions of the world such as Eurasia or tropical Africa, where continental moisture recycling provides a significant contribution to rainfall [Keys et al., 2012, van der Ent et al., 2010]. A previous study based on a GCM simulation [Numaguti, 1999] counted several re-evaporation cycles during summer in northwestern Asia. The framework presented in this thesis could be used in a straightforward manner

to complement this finding using observation-based data. Furthermore, one could identify key regions where re-evaporation cycles are taking place along the way from Europe to Asia and Africa. Such information is missing but valuable as fresh water in Asia and Africa is becoming a limited resource with changing climate and increasing global population density [Rockström et al., 2009].

In addition, the Congo rainforest is already affected by drying trends [Zhou et al., 2014]. Hence, this forest might be vulnerable to further rainfall changes triggered by intensive land-use change in the up-wind regions. This question can be addressed by applying the modeling framework presented in Chapter 4 to Africa.

#### **5.4.5 Critical transition in the vegetation-rainfall equilibrium in the Sahara/Sahel**

Similarly to the situation of the Amazon basin, the potential of vegetation-rainfall feedbacks to lead to shifts in bioclimatic equilibria in the western Sahara/Sahel region is an open question. Using conceptual models representing the interactions between vegetation and rainfall, Brovkin et al. [1998] simulated both a desert and a vegetated equilibrium. The green state dominates for the mid-Holocene climate, while the desert state is more probable for the current climate. This is in agreement with paleo-reconstruction of vegetation and climate that indicates abrupt changes in the vegetation cover during the past 6,000 years [Ortiz et al., 2000]. Brovkin et al. [1998] suggested that non-linear interactions between vegetation and climate caused this abrupt shift but this assertion was hotly debated [Brovkin and Claussen, 2008, Kröpelin et al., 2008]. Combining the concepts of vegetation resilience and moisture recycling networks in the Sahara/Sahel region, as done for the Amazon basin in this thesis, could provide valuable insights to the debate, although changes in land-surface properties (albedo and surface roughness) and heat fluxes were also considered as important drivers of the simulated changes [Brovkin et al., 1998].

#### **5.4.6 Effect of temperature and atmospheric CO<sub>2</sub> concentration**

Global warming will increase the atmospheric demand for evaporation (potential evapotranspiration). Whether this will lead to an increase in actual evapotranspiration in the Amazon forest is unclear, as the availability of sub-surface water for plants might be limited in some regions [Pokhrel et al., 2014]. Assessing this question is important to improve our understanding of the effect of climate change on the interactions between vegetation and rainfall. So far, the model presented in Chapter 4 only accounts for access to subsurface water by the vegetation during seasonal drought for current temperature.

A straightforward improvement would be to implement the potential evapotranspiration as a function of temperature.

In addition, one could think about the effect of temperature and atmospheric CO<sub>2</sub> concentration on forest resilience that is projected to play an important role for the distribution of the Amazon forest by the end of the twenty-first century [Huntingford et al., 2013]. However, this effect cannot be assessed using the approach adopted in this thesis (i.e., analysis of observation-based gridded data) due to a lack of environmental gradient. Nevertheless, recent ground-based measurements [Doughty, 2011, van der Sleen et al., 2014] and forthcoming results from a free-air CO<sub>2</sub> enrichment experiment in the Amazon forest (Amazon-FACE) provide valuable information that could be combined with the modeling framework presented in Chapter 4. This would allow one to fully account for the effect of climate change on the stability of the vegetation-rainfall system.

## 5.5 Perspectives and recommendations

The findings presented in this thesis highlight the importance of considering the Amazon forest as a connected entity. As a consequence of this connectivity, forest loss in a given location increases the ecological sensitivity of forest to land-use and climate change in remote areas. Amazon forest degradation from extreme drought events, intensive deforestation and logging, as experienced during the last decades, push the forest towards a savanna-type of ecosystem, in particular in southern and eastern Amazonia. As shown in this thesis, critical forest loss in these regions will affect the resilience of the remaining forest, thereby threatening the integrity of the entire Amazon forest.

As discussed in Chapter 1, climate change induced by increasing anthropogenic greenhouse gas emissions is likely to decrease precipitation over the Amazon basin, in particular during the dry season. The results presented in Chapter 4 show that drastic intensification of seasonal drought might lead to large-scale self-amplified forest loss. This would have direct consequences in terms of carbon release to the atmosphere, habitat destruction for biodiversity and changing climate in remote regions through atmospheric teleconnections. Results presented in Chapter 3 suggest that such a large-scale forest loss would weaken water supply for rainfall over the La Plata basin in a more drastic way than previously thought. The La Plata basin includes five countries (Brazil, Argentina, Uruguay, Paraguay and Bolivia), represents 70% of the total Gross National Product of the countries and is inhabited by 50% of their combined populations ([Vera et al., 2006a] and references herein). Therefore, strategies to preserve the integrity of the Amazon forest should be established at the international level.

Findings from Chapter 4 highlight the need to maintain a diverse and connected forest to reduce the risk of self-amplified forest loss. Several forest management and conservation strategies can be considered to mitigate this risk:

- maintain connectivity by expanding the network of protected areas and reinforcing the battle against illegal logging and deforestation in the existing protected areas,
- prioritize prevention of forest degradation in regions identified as hot spots of deforestation with a strict control of fire spread and logging,
- maintain the structural and functional diversity of the forests by avoiding selective logging in mature forests and promoting diversity of species and tree characteristics in managed forests.

# Appendix A

## Glossary

- Moisture recycling: the process by which evapotranspiration in a specific location on the continent contributes to precipitation in another location on the continent.
- Re-evaporation cycle: evapotranspiration of precipitating moisture in the same location.
- Cascading moisture recycling (CMR): moisture recycling that involves at least one re-evaporation cycle on the way.
- Direct moisture recycling (DMR): moisture recycling with no intervening re-evaporation cycle on the way.
- Intermediary: location where moisture runs through the re-evaporation cycle on its way between two locations on the continent (only in the case of CMR).
- Pathway of moisture recycling: set of locations on land involved in moisture recycling. A DMR pathway includes only the starting (evapotranspiration) and the destination (precipitation) locations, while a CMR pathway includes the starting, the destination and the intermediary locations.
- Optimal pathway: the pathway of moisture recycling that contributes most to moisture transport between two locations. It can be a direct or a cascading pathway.
- Direct source: land surface that contributes directly (i.e., through DMR) to rainfall over a given region.
- Cascading source: land surface that contributes indirectly (i.e., through CMR) to rainfall over a given region.

- 
- Source: land surface that contributes directly or indirectly to rainfall over a given region.
  - Direct sink: land surface that is dependent on evapotranspiration coming directly (i.e., through DMR) from a given region for local precipitation.
  - Cascading sink: land surface that is dependent on evapotranspiration coming indirectly (i.e., through CMR) from a given region for local precipitation.
  - Sink: land surface that is dependent on evapotranspiration coming directly or indirectly from a given region for local precipitation.



## Appendix B

# Supplementary information to the method in chapter 3

All grid cell measures are area-weighted as described in chapter 2.

### B.1 Cascading moisture recycling ratios

To calculate the CMR ratios as defined in Sect. 2.3.2, we calculate the individual contributions of CMR pathways consisting of  $k$  re-evaporation cycles ( $k \in \{1, \dots, n\}$ ), which add up to the total CMR contribution. We chose a maximum number of cycles  $n = 100$ , while the contribution of pathways with a number of cycles larger than three is close to zero.

The fraction of precipitation in grid cell  $j$  that comes from  $\Omega$  through CMR involving only one re-evaporation cycle is

$$\rho_{\Omega,j}^{(1)} = \frac{\sum_{i \notin \Omega} m_{ij} \cdot \rho_{\Omega,i}}{P_j}, \quad (\text{B.1})$$

where  $\rho_{\Omega,i}$  is the direct precipitation recycling ratio for grid cell  $i$  (Sect. 3.2.3.1). Following the same principle as in Eq. (B.1), the fraction of precipitation in  $j$  that comes from  $\Omega$  through CMR involving  $n$  re-evaporation cycles is

$$\rho_{\Omega,j}^{(n)} = \frac{\sum_{i \notin \Omega} m_{ij} \cdot \rho_{\Omega,i}^{(n-1)}}{P_j}, \quad (\text{B.2})$$

where  $\rho_{\Omega,i}^{(n-1)}$  is the fraction of precipitation in  $i$  that comes from  $\Omega$  through CMR involving  $n - 1$  re-evaporation cycles.  $\rho_{\Omega}^{\text{casc}}$  is the sum of all individual contributions of

the CMR pathways:

$$\rho_{\Omega,j}^{\text{casc}} = \rho_{\Omega,j}^{(1)} + \dots + \rho_{\Omega,j}^{(n)}. \quad (\text{B.3})$$

The fraction of evapotranspiration in grid cell  $i$  that falls as precipitation over  $\Omega$  after only one re-evaporation cycle is

$$\varepsilon_{\Omega,i}^{(1)} = \frac{\sum_{j \notin \Omega} m_{ij} \cdot \varepsilon_{\Omega,j}}{E_i}, \quad (\text{B.4})$$

where  $\varepsilon_{\Omega,j}$  is the direct evapotranspiration recycling ratio for grid cell  $j$  (Sect. 3.2.3.1). Similarly, the fraction of evapotranspiration in  $i$  that falls as precipitation over  $\Omega$  after  $n$  re-evaporation cycles is

$$\varepsilon_{\Omega,i}^{(n)} = \frac{\sum_{j \notin \Omega} m_{ij} \cdot \varepsilon_{\Omega,j}^{(n-1)}}{E_i}, \quad (\text{B.5})$$

where  $\varepsilon_{\Omega,j}^{(n-1)}$  is the fraction of evapotranspiration in  $j$  that precipitates over  $\Omega$  after  $n-1$  re-evaporation cycles.  $\varepsilon_{\Omega}^{\text{casc}}$  is the sum of the individual contribution of CMR pathways:

$$\varepsilon_{\Omega,i}^{\text{casc}} = \varepsilon_{\Omega,i}^{(1)} + \dots + \varepsilon_{\Omega,i}^{(n)}. \quad (\text{B.6})$$

## B.2 Robustness of the cascading moisture recycling ratios

In order to test the robustness of the cascading precipitation recycling ratios, we have computed the steps explained in B.1 with  $\Omega$  being the ocean. Thus,  $\rho_o$  is the fraction of precipitation that comes from the ocean without any re-evaporation cycle on the way and  $\rho_o^{(k)}$  is the fraction of precipitation that comes from the ocean with  $k$  re-evaporation cycle(s) on the way ( $k = 1, \dots, n$ ). We confirm that

- The sum  $\rho_o + \rho_o^{(1)} + \rho_o^{(2)} + \dots + \rho_o^{(n)}$  is equal to 1. This is easy to interpret as all the precipitation in a location must have always come from the ocean (either directly or after a certain number of re-evaporation cycles).
- The sum  $\rho_o^{(1)} + \rho_o^{(2)} + \dots + \rho_o^{(n)}$  represents the fraction of precipitation that comes from the ocean with at least one re-evaporation cycle. It is equal to the continental recycling ratio  $\rho_c$  (see Sect. 2.3.1 and van der Ent et al., 2010).
- The sum  $\rho_o^{(2)} + \dots + \rho_o^{(n)}$  is the fraction of precipitation that comes from the ocean with at least two re-evaporation cycles. It is equal to  $\Delta P_c / P$ , introduced as the fraction of precipitation that has been evaporated at least twice on the continent (see Sect. 2.4).

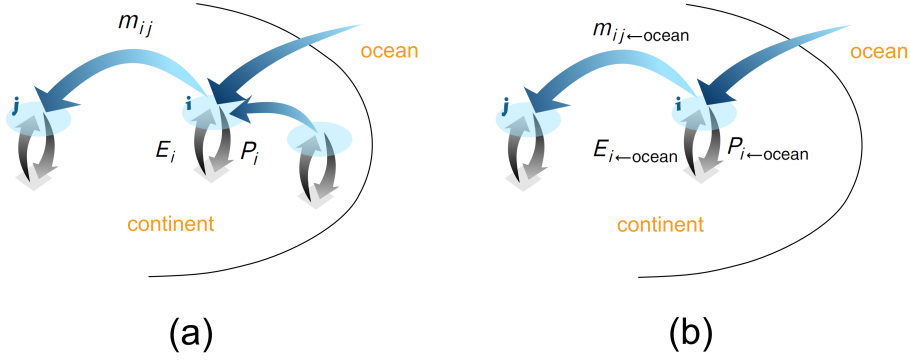


FIGURE B.1 Scheme explaining the removal of CMR. Originally, the precipitation in the grid cell  $i$  ( $P_i$ ) is composed of oceanic and continental moisture. The total incoming moisture is evaporated in  $i$  ( $E_i$ ) and some part of it contributes to precipitation in the grid cell  $j$  ( $m_{ij}$ ) (a). If we forbid the re-evaporation of continental precipitation, only the precipitation in  $i$  that has oceanic origin ( $P_{i←ocean}$ ) is evaporated in  $i$  ( $E_{i←ocean}$ ) and can contribute to precipitation in  $j$  ( $m_{ij←ocean}$ ). By doing so, we remove cascading recycling of continental moisture from the network.

We obtained thus the same results using different metrics. We cannot test the evaporation recycling ratio the same way because  $\Delta E_c/E$  quantifies the fraction of evapotranspiration that is involved in cascading moisture recycling (i.e., that comes from the continent and precipitates further over the continent), while  $\epsilon_o^{(2)} + \dots + \epsilon_o^{(n)}$  would be the fraction of evapotranspiration that runs through at least two re-evaporation cycles before precipitating over the ocean. This is also the reason why the two methodologies are needed even if they lead to the same results for the previously mentioned case.

### B.3 Quantifying cascading moisture recycling

To quantify the contribution of CMR in  $\Omega$  to total moisture in- and outflow, we modify the network such that the oceanic moisture (i.e., that has been last evaporated over the ocean) is only re-evaporated once in  $\Omega$ . By doing so, we remove CMR in  $\Omega$ . We then derive the corresponding reduction in total moisture inflow from  $\Omega$  or outflow towards  $\Omega$ :

$$\Delta P_{j←\Omega} = P_{j←\Omega} - P_{j←\Omega,o}, \quad (\text{B.7a})$$

$$\Delta E_{i→\Omega} = E_{i→\Omega} - E_{i→\Omega,o}, \quad (\text{B.7b})$$

where  $P_{j←\Omega} = \sum_{i \in \Omega} m_{ij}$  is the precipitation in  $j$  originating from  $\Omega$ ,  $E_{i→\Omega} = \sum_{j \in \Omega} m_{ij}$  is the evapotranspiration in  $i$  that precipitates over  $\Omega$ ,  $P_{j←\Omega,o} = \sum_{i \in \Omega} m_{ij←ocean}$  is the precipitation in  $j$  originating from the re-evaporation of oceanic moisture in  $\Omega$  and

$E_{i \rightarrow \Omega, o} = \sum_{j \in \Omega} m_{ij \leftarrow \text{ocean}}$  is the evapotranspiration of oceanic moisture in  $i$  that precipitates over  $\Omega$ . Thus,  $\Delta P_{j \leftarrow \Omega}$  is the precipitation in  $j$  originating from the re-evaporation of continental moisture in  $\Omega$  and  $\Delta E_{i \rightarrow \Omega}$  is the re-evaporation of continental moisture in  $i$  that precipitates over  $\Omega$ . If  $\Omega$  is the entire South American continent (the intermediary region),  $\Delta P_{j \leftarrow \Omega}$  becomes  $\Delta P_c$  ( $\Delta P_m$ ) and  $\Delta E_{i \rightarrow \Omega}$  becomes  $\Delta E_c$  ( $\Delta E_m$ ) as defined in Sect. 3.2.4.

To remove CMR in  $\Omega$ , we derive for each grid cell the evapotranspiration of moisture from oceanic origin as in Eq. (3.1):

$$E_{i \leftarrow \text{ocean}} = \frac{E_i}{P_i} \cdot P_{i \leftarrow \text{ocean}}, \quad (\text{B.8})$$

where  $P_{i \leftarrow \text{ocean}}$  is the precipitation from oceanic origin in  $i$  ( $P_{j \leftarrow \text{ocean}} = P_j - P_{j \leftarrow \text{continent}}$  and  $P_{j \leftarrow \text{continent}} = \sum_{i \in \text{continent}} m_{ij}$ ; see Fig. B.1). Using the same assumption, we get the moisture transport between each pair of grid cells  $i$  and  $j$  that results from evapotranspiration of moisture from oceanic origin only:

$$m_{ij \leftarrow \text{ocean}} = \frac{m_{ij}}{E_i} \cdot E_{i \leftarrow \text{ocean}}. \quad (\text{B.9})$$

At this stage,  $m_{ij \leftarrow \text{ocean}}$  can be interpreted as the evapotranspiration in  $i$  that precipitates in  $j$  and that has been evaporated from the ocean before that ( $m_{ij \leftarrow \text{ocean}} < m_{ij}$ ).

## B.4 Complex network analysis

### B.4.1 Clustering coefficient associated with Middleman motifs

Mathematically, the clustering coefficient  $C$  of the grid cell  $i$  is

$$C_i = \frac{t_i}{T_i}, \quad (\text{B.10})$$

where  $t_i$  is the number of Middleman motifs that  $i$  forms and  $T_i$  is the total number of that motif that  $i$  could have formed according to its number of incoming and outgoing arrows. To give more weight to a motif involved in the transport of a larger amount of moisture, we assign a weight to each motif. In agreement with Fagiolo [2007], the weight of a motif is defined as the geometric mean of the weights of the three involved arrows. The weighted counterpart of Eq. (B.10) is

$$\tilde{C}_i = \frac{\tilde{t}_i}{\tilde{T}_i}, \quad (\text{B.11})$$

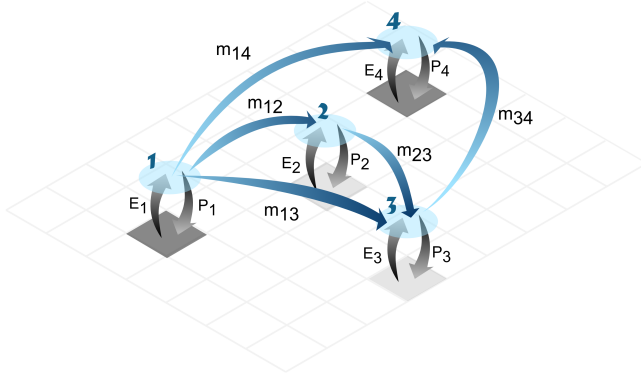


FIGURE B.2 Different CMR pathways from grid cell 1 to grid cell 4. The contribution of the direct pathway is  $W_{1,4} = m_{14}/P_4$ , the contribution of the path involving one re-evaporation cycle in grid cell 3 is  $W_{1,3,4} = m_{13}/P_3 \cdot m_{14}/P_4$  and the contribution of the path involving re-evaporation cycles in grid cells 2 and 3 is  $W_{1,2,3,4} = m_{12}/P_2 \cdot m_{13}/P_3 \cdot m_{14}/P_4$ . The legend is the same as that in Fig. 3.3.

with  $\tilde{t}_i$  the weighted counterpart of  $t_i$  (i.e., the sum of the weights of the Middleman motifs that is formed by  $i$ ).

The calculation of the clustering coefficient is derived from the methodology of a previous study [Fagiolo, 2007, Table 1] and has been corrected in order to account for the irregular sizes of the portion of the Earth's surface covered by the grid cells as explained in Zemp et al. [2014b].

We define the matrix  $\mathbf{P} = \{p_{ij}^{1/3}\}$  obtained by taking the cubic root of each entry  $p_{ij}$ , with  $p_{ij}$  being the weight of the arrow originating from  $i$  and pointing towards  $j$ . Here, in order to avoid a strong correlation between the clustering coefficient and the mean evapotranspiration and precipitation, we chose this weight to be  $p_{ij} = m_{ij}^2/(E_i P_j)$ . According to Fagiolo [2007], the numerator of Eq. (B.11) is derived as the  $i$ th element of the main diagonal of a product of matrices  $\tilde{t}_i = (\mathbf{P}\mathbf{P}^T\mathbf{P})_{ii}$ , where  $\mathbf{P}^T$  is the transpose of  $\mathbf{P}$ .

The denominator of Eq. (B.11) is  $T_i = k_i^{\text{in}} k_i^{\text{out}}$ , where  $k_i^{\text{in}}$  is the number of arrows pointing towards  $i$  and  $k_i^{\text{out}}$  the number of arrows originating from  $i$ :

$$k_i^{\text{in}} = \sum_{j \neq i} a_{ji}, \quad (\text{B.12a})$$

$$k_i^{\text{out}} = \sum_{j \neq i} a_{ij}, \quad (\text{B.12b})$$

where  $a_{ij} = 1$  if there is an arrow originating from  $i$  and pointing towards  $j$ ; otherwise,  $a_{ij} = 0$ . In order to compare the results for the two seasons, we normalize  $\tilde{C}$  with the maximum observed value for each network.

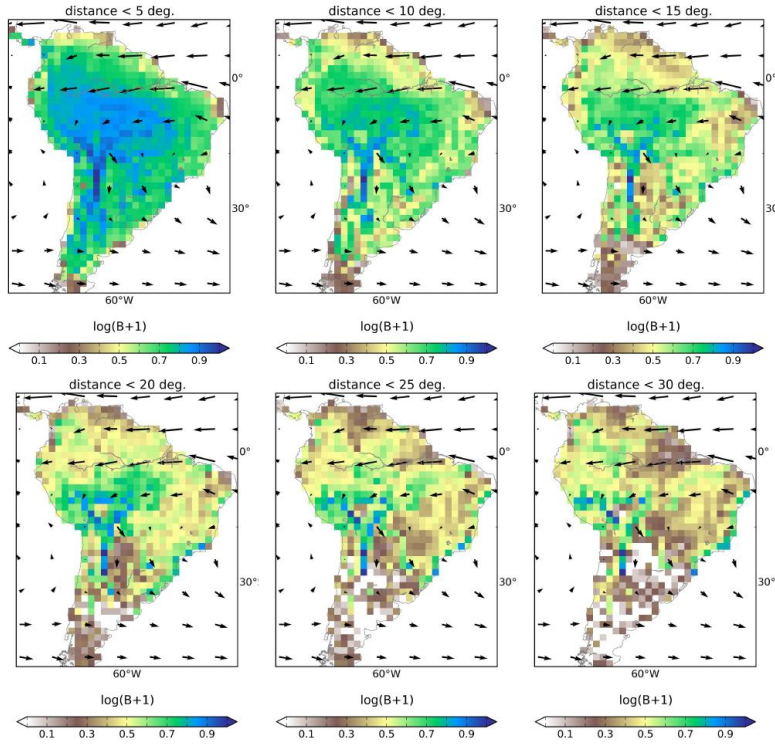


FIGURE B.3 Betweenness centrality ( $B$ ) obtained for different thresholds (yearly average for the input MOD).

### B.4.2 Optimal pathway

In complex network theory, many centrality measures (e.g., closeness and betweenness) are based on the concept of the shortest path. The shortest path is usually defined as the pathway between nodes that has the minimum cost. In this work, it is defined as the pathway that contributes most to the moisture transport between two grid cells. As this pathway is not necessarily the shortest one in terms of geographical distance, we will call it optimal pathway to avoid confusion.

Let  $(r_1, r_2, \dots, r_n)$  be the intermediary grid cells in a CMR pathway from grid cell  $i$  to grid cell  $j$ . The contribution of this pathway is defined as the fraction of precipitation in  $j$  that comes from evapotranspiration in  $i$  through CMR:

$$W_{i,r_1,\dots,r_n,j} = \frac{m_{ir_1}}{P_{r_1}} \cdot \prod_{l=1}^{n-1} \frac{m_{r_l r_{l+1}}}{P_{r_{l+1}}} \cdot \frac{m_{r_n j}}{P_j}. \quad (\text{B.13})$$

An example of pathway contributions is provided in Fig. B.2. The contribution of each existing pathway is calculated between any pair of grid cells in the network. The optimal pathway is the path with the maximum contribution.

To find the optimal pathway, we use the method `shortest_paths` in the package `iGraph` for Python based on an algorithm proposed by Dijkstra [1959]. In this method, the cost

of a pathway is calculated as the sum of the weight of its arrows. In order to adapt the method to our purpose, we chose the weight of the arrows as  $w_{r_l r_{l+1}} = -\log\left(\frac{m_{r_l r_{l+1}}}{P_{r_{l+1}}}\right)$ . The cost of a pathway from grid cell  $i$  to grid cell  $j$  as calculated in iGraph becomes

$$\begin{aligned}
 W'_{i,r_1,\dots,r_n,j} &= w_{ir_1} + \sum_{l=1}^{n-1} w_{r_l r_{l+1}} + w_{r_n j} \\
 &= -\log\left(\frac{m_{ir_1}}{P_{r_1}}\right) - \sum_{l=1}^{n-1} \log\left(\frac{m_{r_l r_{l+1}}}{P_{r_{l+1}}}\right) \\
 &\quad - \log\left(\frac{m_{r_n j}}{P_j}\right) \\
 &= \log\left(\frac{1}{\frac{m_{ir_1}}{P_{r_1}} \cdot \prod_{l=1}^{n-1} \left(\frac{m_{r_l r_{l+1}}}{P_{r_{l+1}}}\right) \cdot \frac{m_{r_n j}}{P_j}}\right) \\
 &= \log\left(\frac{1}{W_{i,r_1,\dots,r_n,j}}\right).
 \end{aligned}$$

Because the optimal pathway is defined as the pathway with the minimum cost  $W'$ , it corresponds to the pathway with the maximum contribution  $W$  as defined above.

### B.4.3 Betweenness centrality

Mathematically, betweenness of the grid cell  $i$  is the number of optimal pathways between any pair of grid cells that pass through  $i$ :

$$B_i = \sum_{jk} \frac{\sigma_{jk}(i)}{\sigma_{jk}}, \quad (\text{B.14})$$

where  $\sigma_{jk}$  is the total number of optimal pathways that connect  $j$  and  $k$  in the network and  $\sigma_{jk}(i)$  is the number of these optimal pathways that pass through the grid cell  $i$ .  $B$  reaches values between 0 and  $\binom{N-1}{2} = (N^2 - 3N + 2)/2$  with  $N$  the number of grid cells. To calculate it, we used the method `betweenness` in the package iGraph for Python following the algorithm proposed by [Newman, 2001]. This measure is then shifted to a logarithm scale ( $\log_{10}(B + 1)$ ) and normalized by the maximum obtained value. Figure B.3 shows the  $B$  for different thresholds in the geographical distance of the links excluded from the network.





## Appendix C

# Supplementary figures to chapter 4

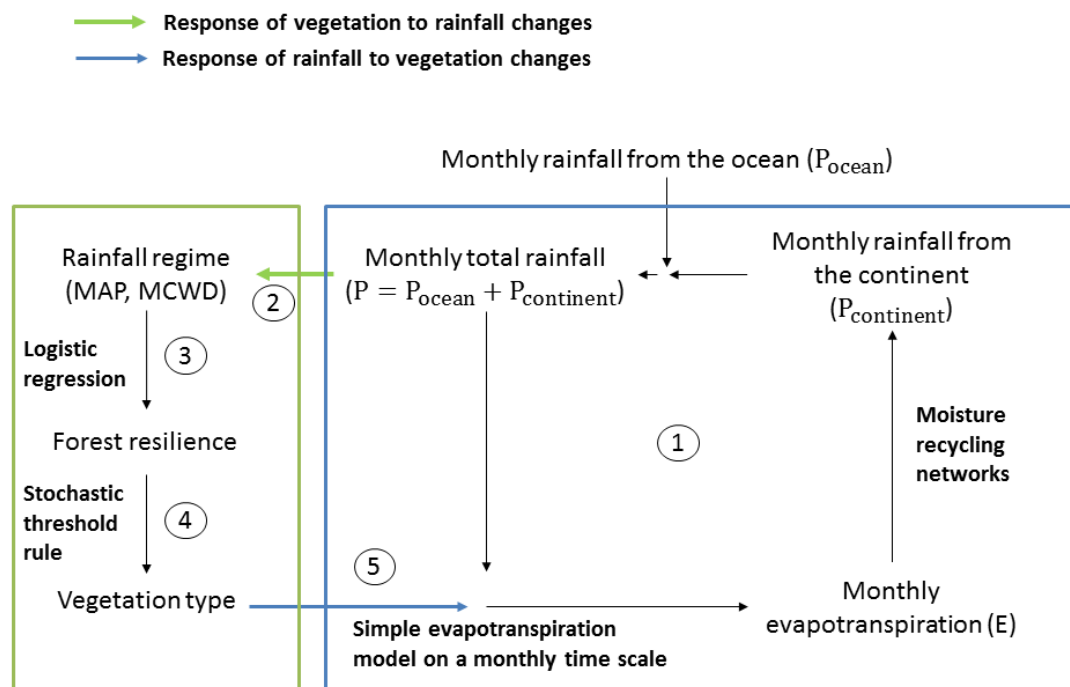
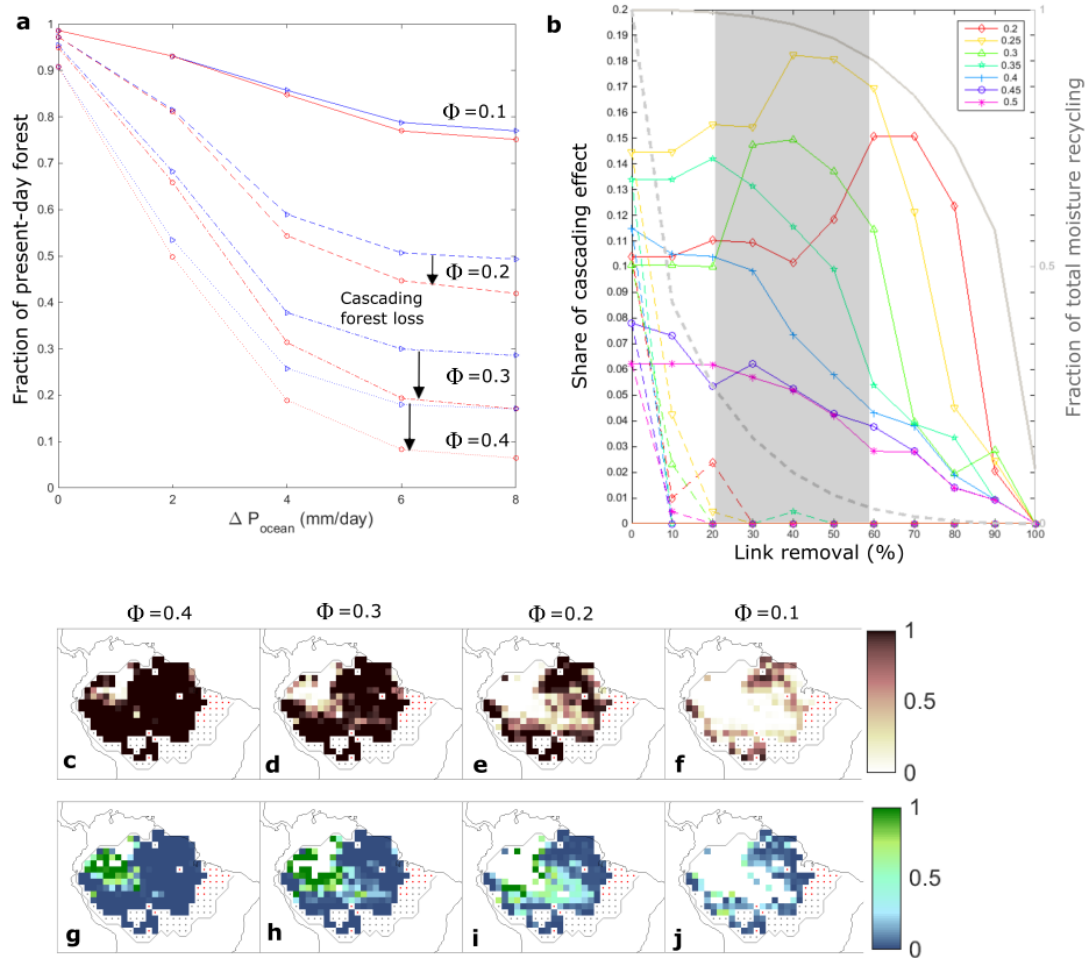
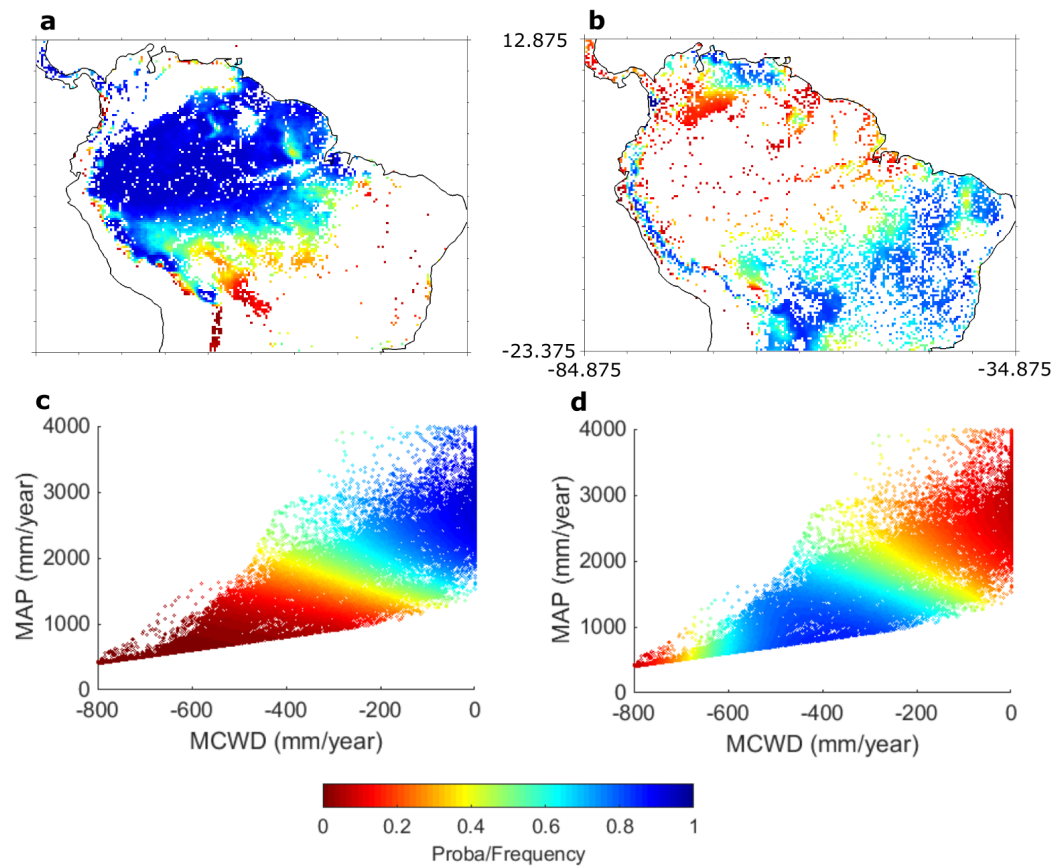


**FIGURE C.1 Cascade model scheme.** A simulation run comprises the following steps: (1) moisture from oceanic origin propagates through the network on a monthly time scale by moisture transport involving re-evaporation cycles. (2) Rainfall regime characterized by the mean annual precipitation (MAP) and Maximum Cumulative Water Deficit (MCWD) is calculated on a grid-cell basis. (3) The probability to find forest (tree cover  $\geq 55\%$ ) for a given rainfall regime (forest resilience) is calculated for each grid-cell using the output of a logistic regression on remotely sensed data. (4) A critical transition occurs in all grid cells for which the forest resilience crosses the individual threshold. (5) Local evapotranspiration is updated in grid cells where shifts occurred. If “cascade-mode on” (see Methods) and if there are shifts in the vegetation, go to step 1. The model runs until equilibrium is reached.



---

FIGURE C.2 (*previous page*) **Sensitivity of the results to mean resilience thresholds ( $\Phi$ ).** **a**, Fraction of remaining tropical Amazon forest area as a function of monthly oceanic moisture inflow reduction during the extended dry-season ( $\Delta P_{ocean}$ ) with cascade-mode off (blue line) and on (red lines). Results are shown for 100 realizations and for  $\sigma = 0.05$ . Note that quantitative projection of cascading forest loss remains almost unchanged using different plausible values of  $\Phi$  (between 0.2 and 0.4). **b**, Share of cascading effect with link removal in ascending order (short links removed first, solid lines) and descending order (large links removed first, dashed lines) with an increment of 10% link density. As in the main text, here  $\sigma = 0$ . The corresponding relative decrease of the total rainfall recycling over the Amazon is also shown (gray lines, right axis). Note that the stabilizing effect of long-range moisture links is also found using other values of  $\Phi$ . **c-f**, Shifting frequency and **g-j**, share of cascading effect for  $\Delta P_{ocean}=6$  mm/day. Results are shown for **c,g**,  $\Phi = 0.4$ , **d,h**,  $\Phi = 0.3$ , **e,i**,  $\Phi = 0.2$  and **f,k**,  $\Phi = 0.1$  and for  $\sigma = 0.05$ . Although the projection of forest loss varies using different values of  $\Phi$ , similar dynamics of the vegetation-rainfall system are found.



**e**

Coefficient	$\beta_0$	$\beta_1$	$\beta_2$	$\beta_3$	$\beta_4$
Estimates forest	3.3226	0.0065	0.0000	-0.0026	-0.0000
Std error forest	8.0921	0.0181	0.0000	0.0096	-0.0000
Estimates savanna	4.0700	-0.0075	-0.0000	-0.0045	0.0000
Std error savanna	4.4797	0.0083	0.0000	0.0046	0.0000

FIGURE C.3 **Vegetation resilience.** Probability to find (a,c) forest or (b,d) savanna as calculated by the logistic regression for the rainfall regime for the period 2001-2010 (see SI Sect. 1.3) presented (a,b) in maps and (c,d) in the mean annual precipitation (MAP) and maximum climatological water deficit (MCWD) space. Results are only shown for grid cells covered currently by the given vegetation state (see maps in Fig. C.7b). Artificial landscapes were excluded from the analysis using GLC2000 and data points with extreme hydro-climatic values (MAP > 4000 mm/month, MCWD = 0 and MCWD < - 800 mm) were also excluded from the analysis (but are shown in the maps). e, Coefficient estimates and standard errors in the logistic regression model.

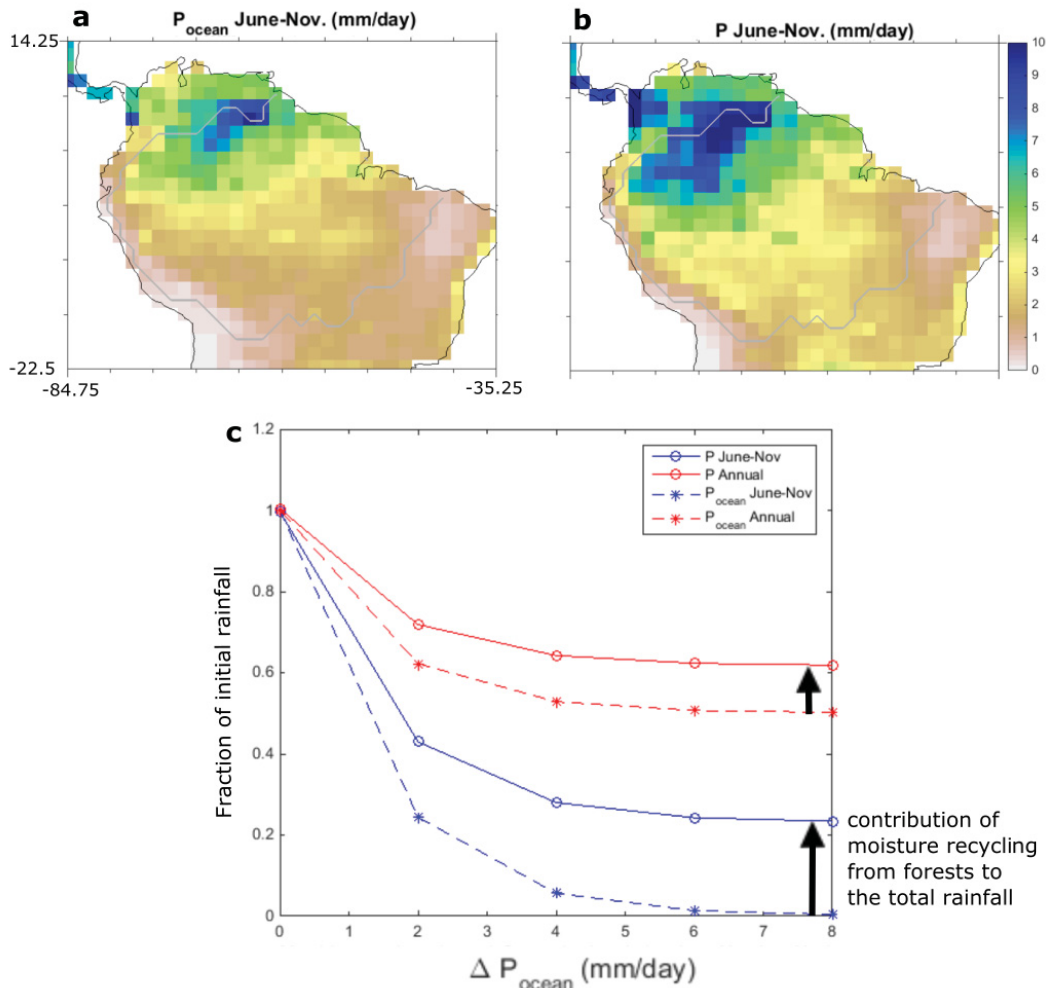


FIGURE C.4 **Results of dry-season intensification experiment with cascade-mode off.** (a) Rainfall coming from oceanic origin ( $P_{ocean}$ ) and (b) total rainfall ( $P$ ) during the extended dry-season (June-November) as found in the input data of the cascade model for the historical rainfall regime (see SI Sect. 1.1.3). (c) Relative changes of rainfall coming from oceanic moisture (dashed lines) and total rainfall (solid lines) averaged over the Amazon basin (gray boundaries in maps) during the year (red lines) and during the extended dry-season (June-November) (blue lines) as a function of monthly oceanic moisture inflow reduction during the extended dry-season ( $\Delta P_{ocean}$ ). The difference between rainfall from oceanic moisture and total rainfall (black arrows) corresponds to hypothetic contribution of moisture recycling from evapotranspiration by Amazon forests if they would not be lost due to the imposed rainfall reduction. Note the increasing contribution of moisture recycling to total rainfall with decreasing oceanic moisture inflow.

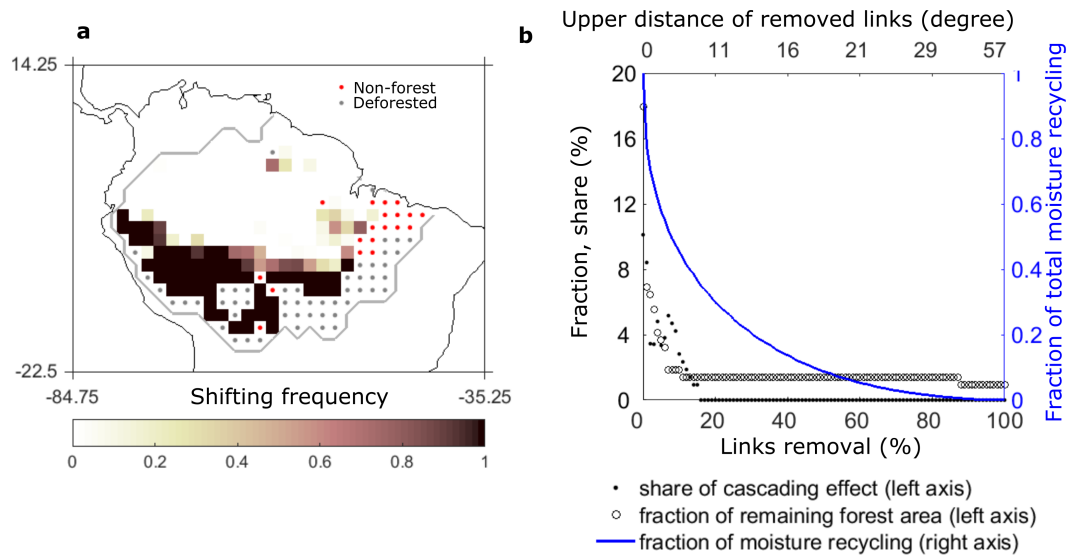
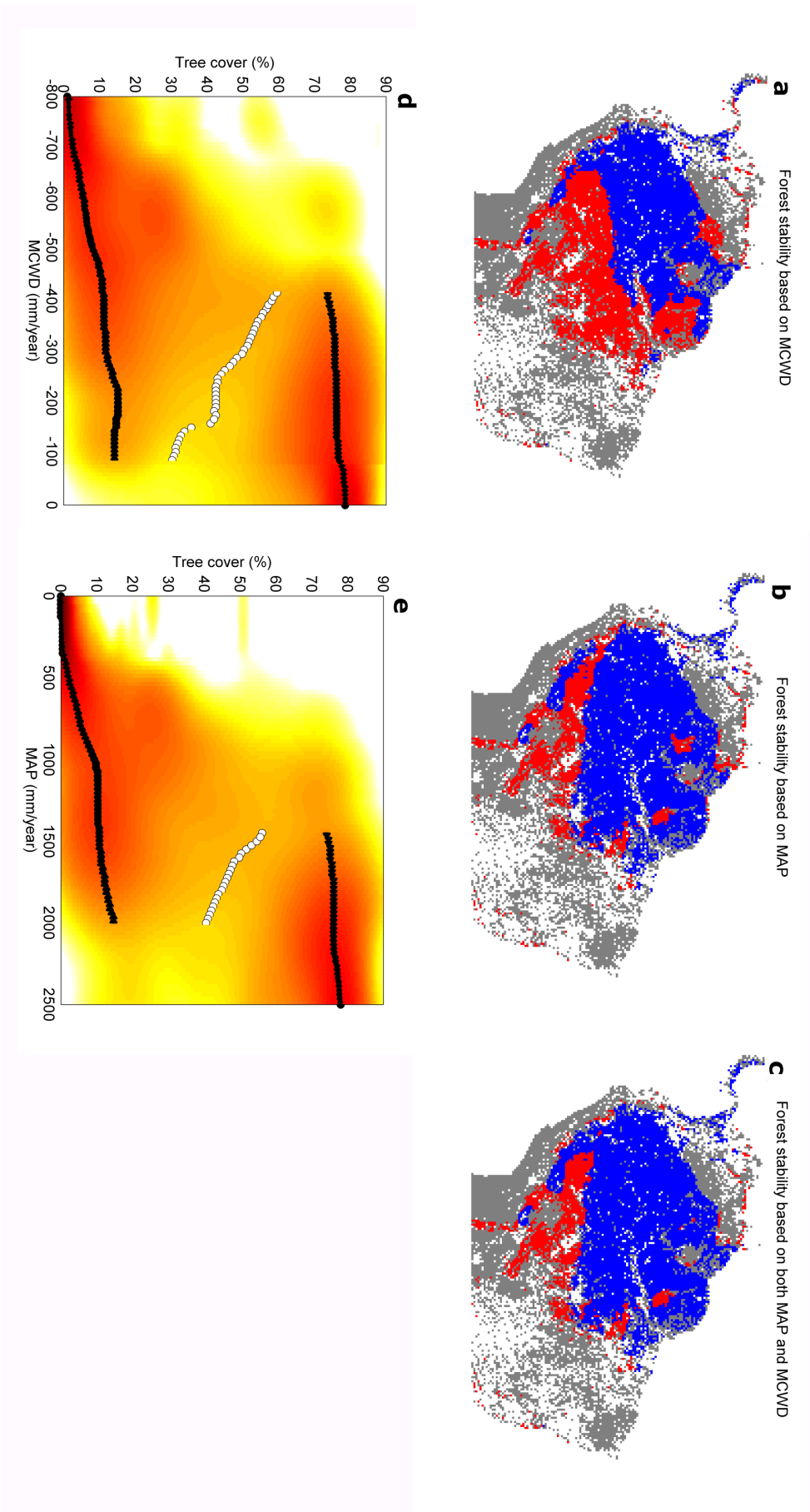
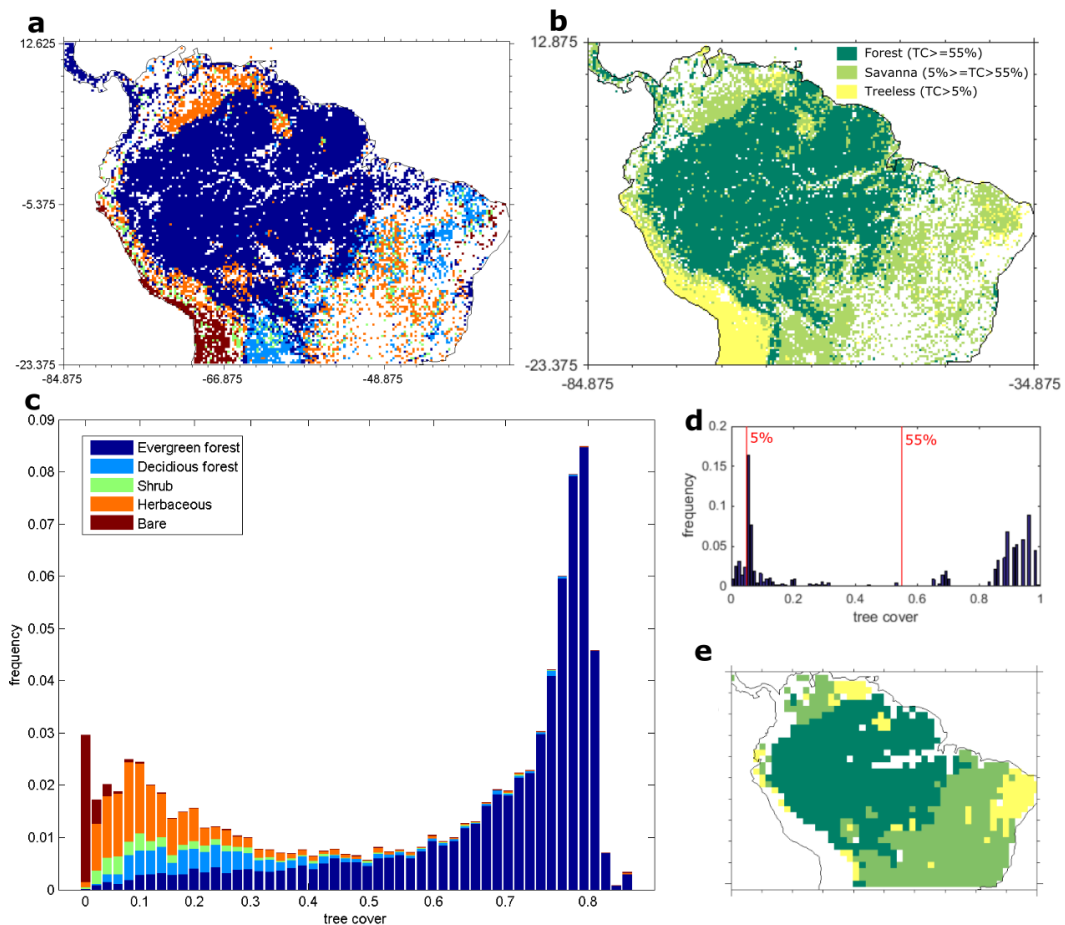


FIGURE C.5 **Additional results on links removal experiments.** **a**, Shifting frequency if all moisture recycling links are removed from the network such that rainfall is only provided by direct oceanic moisture inflow. For a direct comparison with Fig. 3a in the main text, the results are shown for the historical rainfall regime and with  $\Phi = 0.3$  and  $\sigma = 0.05$ . **b**, Share of cascading effect (black dots) and fraction of remaining forest area (black circles) when gradually removing moisture recycling links that bring rain over the Amazon basin with an increment of 1% link density. Links are removed according to their geographic distance in ascending order (short links removed first). As in the main text, the results are shown for an experiment of 6 mm/day reduction of oceanic moisture inflow during the extended dry-season (June-November) and with  $\Phi = 0.3$  and  $\sigma = 0$ .

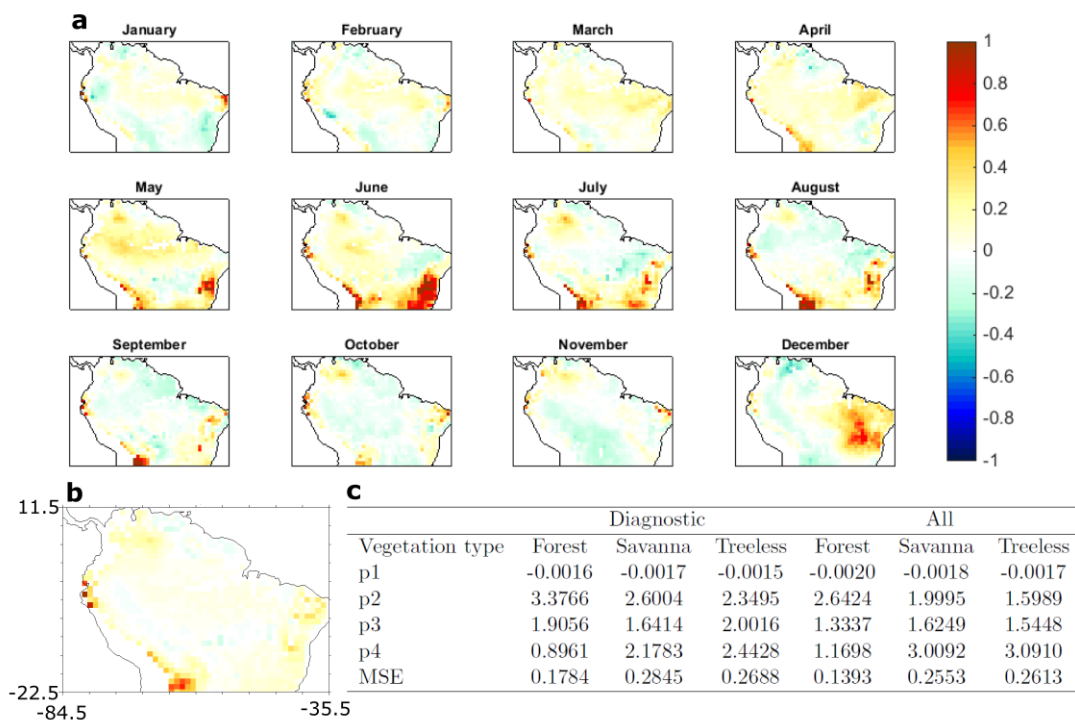


**FIGURE C.6 Rainfall regimes where forest and savanna are alternative stable states.** Range where the forest is bistable (red) and stable (blue) computed from the data using **a**, the maximum climatological water deficit (MCWD), **b**, the mean annual precipitation (MAP) and **c**, the combination of MAP and MCWD. Potential landscape of tree cover in relation to **d**, MCWD and **e**, MAP. Solid dots correspond to stable states and open dots to unstable states. Reddish colors indicates regions of high point density at a given value of MAP or MCWD.

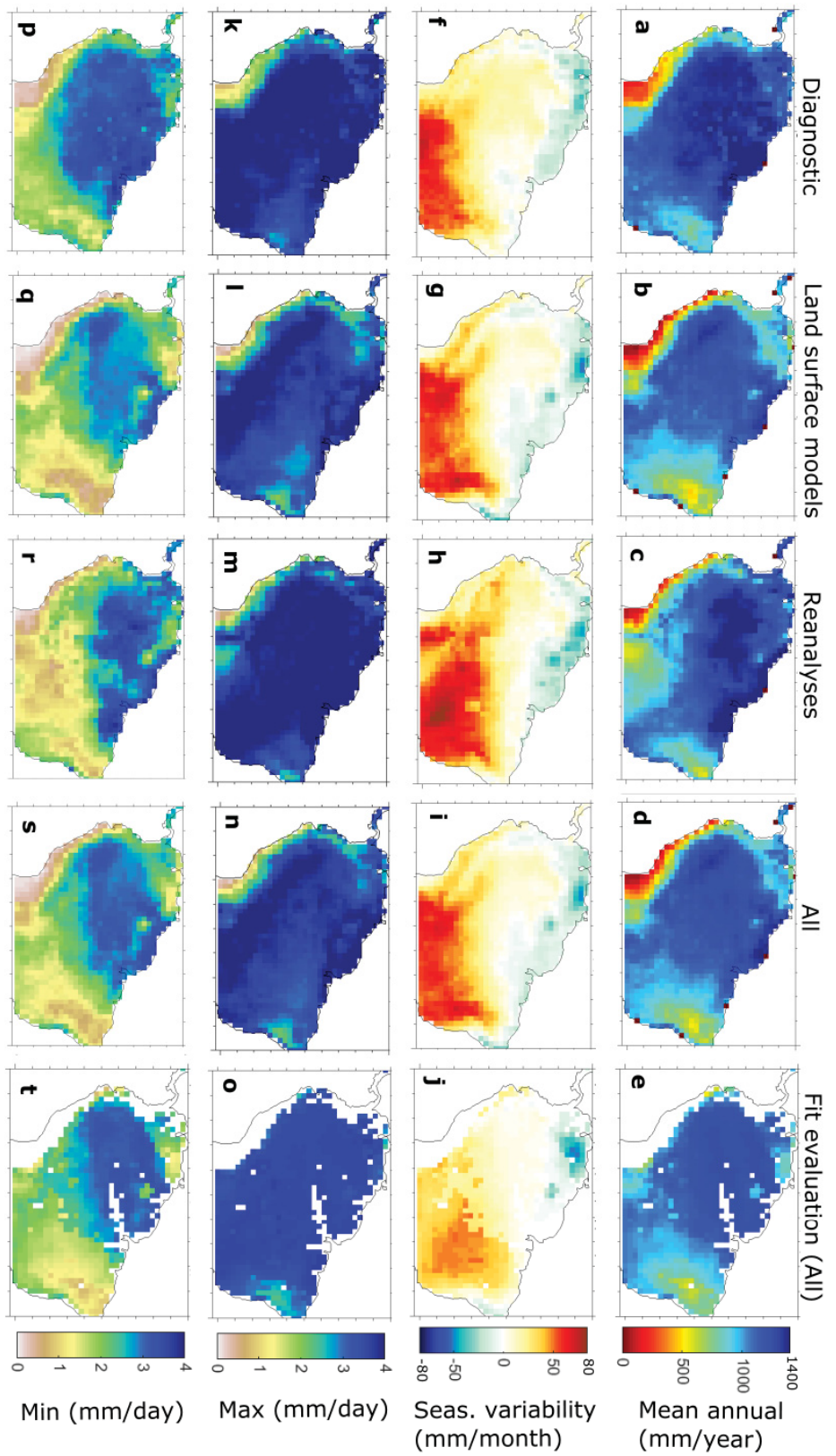




**FIGURE C.7 Frequency distribution of tree cover in tropical South America.** **a-c**, Sub-sample of 1km resolution data used for the calculation of the vegetation resilience (SI Sect. 1.3). **a**, Land-cover GLC2000 for the year 2001 and **b**, three alternative stable states obtained from tree-cover distribution from MOD44B v5 averaged for the period 2001–2010. White areas are artificial landscapes and water bodies and are excluded from the analysis. **c**, Frequency distribution of the arcsine transformed tree cover: forest ( $\geq 55\%$  tree cover), savanna ( $5\% \leq \text{tree cover} < 55\%$ ) (including deciduous forest, shrub and herbaceous) and treeless ( $< 5\%$  tree cover) (bare soil). **d,e**, Tree cover from MOD44B v5 data upscaled to  $1^\circ$  longitude and latitude using the most frequent value in the original dataset and used to calibrate the simple evapotranspiration model (SI Sect. 1.2). **d**, Frequency distribution of the arcsine transformed tree cover and **d**, corresponding three alternative stable states. White areas are the Andes mountain and are excluded from the analysis. Due to differences in the spatial distribution of the vegetation states (**b,e**), we do not distinguish shifts between savanna and treeless in the cascade model (see SI Sect. 1.1.2).



**FIGURE C.8 Relative difference between evapotranspiration from the Landflux-EVAL data and the fit evaluation for the period 1989 - 1995.** Red color indicate over-estimation, while blue color indicate under-estimation of the fit evaluation compared to the Landflux-EVAL data (all categories) for the monthly scale (a) and the annual scale (b). c, Parameter estimates and average mean squared error (MSE) of the fit to the Landflux-EVAL data containing diagnostic only or all categories (diagnostic, reanalysis and land-surface models). The deviance of the fit is 7.5825. See SI Sect. 1.2 for a description of the data and the fit and SI Sect. 2.1 for a discussion of these results.



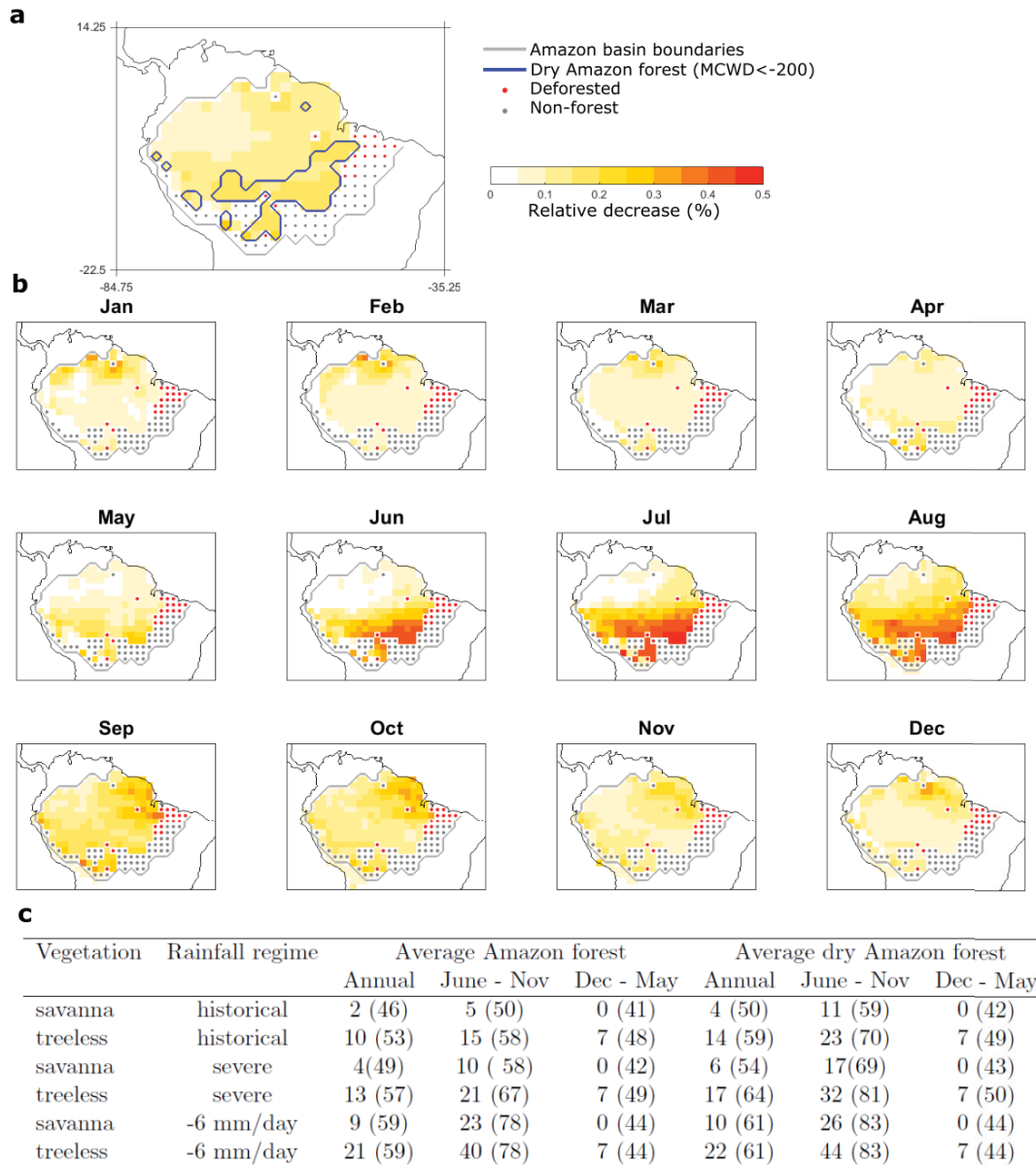


**FIGURE C.10 Effect of deforestation on evapotranspiration.** **a,b**, Relative decrease in evapotranspiration (in %) after replacement of the Amazon forest by a treeless state for historical rainfall regime (1989 - 1995) on the annual (**b**) and monthly (**a**) scale. **c** Relative decrease in evapotranspiration (in %) after replacement of the Amazon forest by savanna or a treeless state for historical rainfall regime, severe dry-season intensification scenario and -6 mm/day reduction of oceanic moisture inflow during the extended dry-season (June-November) calculated using the step 1 of the cascade model (See Extended Data Fig. 1). Results are given for the average of the Amazon forest or only its drier part (forest grid cells where MCWD < -200 mm/day currently, see blue boundary). The 95% upper bound is given in brackets. See SI Sect. 2.3 for comparison with flux tower measurements.

# Appendix D

## Supplementary information to chapter 4

### D.1 Supplementary Methods

#### D.1.1 Cascade model

##### D.1.1.1 Cascade model description

The input data cover the tropical South America (between  $14.25^\circ$  North and  $23.5^\circ$  South) with  $1.5^\circ$  resolution in longitude and latitude. The input data are vegetation cover (forest, savanna or treeless), potential evapotranspiration, monthly oceanic moisture inflow and monthly moisture recycling networks (see Sec. D.1.1.3). In addition, we use the output of the fitting procedure for the evaluation of evapotranspiration (see Sec. D.1.2.5) and the output of the logistic regression for the calculation of the forest resilience (see Sec. D.1.3.3) for each vegetation type. We perform 1000 model realizations. For each of the realizations, we assign a resilience threshold to each grid-cell below which the forest shifts. This threshold is a random number from a normal distribution with mean  $\Phi$  and standard deviation  $\sigma$ . The thresholds are fixed for the duration the model realization. The model steps are described in Fig. C1.

##### D.1.1.2 Notes on treeless vegetation type

We note that the vegetation cover classification used for the different analysis (Fig. C7) were not exactly the same. In particular savanna and treeless patterns are different. This discrepancy is explained by two factors. First, the areas excluded from the analyses were

not the same. For Fig. C7b, artificial landscapes were excluded from the analysis to better account for natural distribution of alternative stable states in relation to rainfall regime. We note that most of the treeless cover was found in the Andes. For Fig. C7e, the Andes were excluded from the analysis as evapotranspiration in this region is mainly determined by temperature rather than rainfall. Artificial landscapes were not excluded. Second, the preprocessing procedures of the data are different. In one case the original tree cover data at 1km resolution was sampled (see Sec. D.1.3.1) to evaluate the rainfall control on small-scale vegetation distribution; in the other case it was up-scaled using the most frequent value (see Sec. D.1.2.2) to account for spatial variability in evapotranspiration.

For this reason we do not distinguish between savanna and treeless in the step 4 of our cascade model (see Fig. C1). Rather, shifts occur between forest and “non-forest” (savanna or treeless) states. Under the rainfall regime under study, forest would probably shift to savanna rather than treeless. Therefore, by default in the experiments forest is replaced by savanna after a shift. We also perform deforestation experiments for which forest is systematically replaced by treeless rather than savanna after a shift. The settings of forest being replaced by savanna or treeless matter for the evaluation of the evapotranspiration after the shifts.

### D.1.1.3 Input data

The moisture recycling networks are obtained from a numerical atmospheric moisture tracking experiment as described in Sec. D.1.4.1 and D.1.4.2. For experiments under historical rainfall regime, we use the monthly oceanic moisture inflow found using a numerical atmospheric moisture tracking experiment for the period 1989–1995. For experiments under dry-season intensification, we decrease the monthly oceanic moisture inflow as described in the main text (Methods). The initial vegetation cover within the Amazon basin (forest, deforested and non-forest) is derived from satellite monitoring of the vegetation available [Soares-Filho et al., 2006] <http://www.csr.ufmg.br/simamazonia/> for the year 2003. Here, the deforested areas are set to treeless and non-forest to savanna. Outside the Amazon basin, we use a vegetation cover based on cut-off level in tree-cover (5 and 55% in MOD44B v5 data as described below). The vegetation cover data were up-scaled to  $1.5^\circ$  grid by selecting the most frequent value found in the original data.

Monthly potential evapotranspiration data for the period 1989–1995 is the same product as described in Sec. D.1.2.1 but interpolated to  $1.5^\circ$  grid using a nearest neighbors algorithm.

## D.1.2 Simple empirical evapotranspiration model on a monthly time scale

### D.1.2.1 Data

The precipitation dataset is an average of four observation-based products: Climate Research Unit (CRU) [New et al., 2000], the Global Precipitation Climatology Centre (GPCC) [Adler et al., 2003, Huffman et al., 1995], the Global Precipitation Climatology Project (GPCP) [Adler et al., 2003] and the unified climate prediction center (CPC) from the National Oceanic and Atmospheric Administration (NOAA) [Chen et al., 2008]. An overview of the precipitation dataset and the links to download the data are provided in Mueller et al. [2013] (Appendix A and acknowledgments).

The potential evapotranspiration data is based on the Penman-Monteith algorithm forced by temperature, humidity and wind speed from NCEP-NCAR reanalysis data [Kalnay et al., 1996] corrected to remove biases at various time scales by merging with observation-based data [Sheffield et al., 2006, 2012]. The data is available at monthly time scale for the period 1948–2008 at  $1^\circ$  resolution and can be downloaded at <http://hydrology.princeton.edu/data.pdsi.php>.

For the evapotranspiration data, we used a merged synthesis product from the LandFlux initiative (LandFlux-Eval, Mueller et al. [2013]). The Landflux-EVAL dataset merges products from different categories: satellite and/or in situ observations (diagnostic), calculated via land-surface models (LSMs), output from atmospheric reanalyses (reanalyses) or all categories together (all) (see Fig. C9). The short version of the Landflux-EVAL dataset covers the time period 1989–1995 and contains forty different products. All the versions of the dataset are available at  $1^\circ$  resolution can be downloaded at <https://data.iac.ethz.ch/landflux/>.

We now describe briefly the products from the diagnostic category included in the short Landflux-EVAL data for the Amazon region:

- The PT-JPL dataset [Fisher et al., 2008] is based on the Priestley-Taylor (1972) method in combination with bio-meteorological remote sensing metrics: net radiation, normalized difference vegetation index, soil adjusted vegetation index, maximum air temperature and water vapor pressure. The input data are from International Satellite Land-Surface Climatology Project, Initiative II (ISLSCP-II) and the Advanced Very High Resolution Spectroradiometer (AVHRR). Comparison of this model output with measurement from twelve tropical eddy-covariance sites located within Amazonia showed that the PT-JPL product performs overall best among thirteen different models [Fisher et al., 2009].

- The MAUNI dataset [Wang and Liang, 2008] is simple regression based on satellite determination of surface net radiation, vegetation index, temperature, and soil moisture from the International Satellite Land Surface Climatology Project (ISLSCP) Initiative II global interdisciplinary monthly dataset.
- The PRUNI dataset [Sheffield et al., 2010] is based on the Penman-Monteith algorithm forced by radiation and meteorological data from the International Satellite Cloud Climatology Project (ISCCP) and vegetation distribution derived from Advanced Very High Resolution Radiometer (AVHRR) products. This dataset has been described and evaluated only for Mexico but is available on a global scale.
- The MPIBGC dataset [Jung et al., 2009] is an empirical up-scaling of FLUXNET eddy covariance observations among which sites are located in the American tropics.
- The CSIRO dataset [Zhang et al., 2010] is based on the Penman-Monteith energy balance equation, gridded meteorology, and a simple biophysical model for surface conductance. This conductance is a function of evaporation from the soil surface, leaf area index, absorbed photosynthetically active radiation, atmospheric water vapor pressure deficit, and maximum stomatal conductance. This dataset has been described and evaluated only for Australia but is available on a global scale.
- The GLEAM v1A dataset [Miralles et al., 2011] is based on Priestley-Taylor equation combining input from microwave-derived soil moisture, land surface temperature and vegetation density, as well as estimation of rainfall interception loss. Comparison with FLUXNET eddy covariance observations showed low correlation for the Amazonian site due to lack of seasonal cycle.
- The AWB dataset [Mueller et al., 2011] uses an atmospheric water balance approach based on GPCP and total column water vapor and water vapor flux divergence from the European Center for Medium-Range Weather Forecasts (ECMWF) reanalysis ERA-Interim.

The merged rainfall data that we use has been considered as forcing for the diagnostic product of Landflux-EVAL data [Mueller et al., 2013]. In the preparation of the merged Landflux-EVAL data, Mueller et al. [2013] constrained the long-term evapotranspiration by the energy balance (latent heat flux cannot exceed net surface radiation) but not by the available water (evapotranspiration can exceed precipitation).



### D.1.2.2 Vegetation cover data

We built a vegetation cover map using the tree cover data from the Moderate Resolution Imaging Spectroradiometer (MODIS) Vegetation Continuous Fields MOD44B v5 at 1km resolution longitude and latitude (see notes in Sec. D.1.1.2). Following Staal et al. [2015], we up-scale this product to 1° longitude and latitude grid by selecting the most frequent tree cover value in the original dataset (see Fig. C7a-c). We classified as ‘tropical forest’ all cells with tree cover  $\geq 55\%$ , ‘savanna’ all cells with tree cover ( $\geq 5\%$  and  $< 55\%$ ) and ‘treeless’ all cells with tree cover  $< 5\%$ . To exclude the Andes from the analysis, we use a natural vegetation cover map that is based on a consensus of two global natural vegetation maps widely used in climate studies, as well as several regional maps from different sources [Lapola et al., 2008]. The data is available at 1° resolution, accessible from Instituto Nacional de Pesquisas Espaciais (INPE) – Centro de Previsão de Tempo e Estudos Climáticos (CPTEC). The classes that represent the Andes region and that were excluded from the analysis are ‘desert’, ‘semi-desert’, ‘tundra’ and ‘grasslands’.

### D.1.2.3 Gerrits’s equations

This section describes the analytical derivation of the monthly interception and transpiration process from a previous study [Gerrits et al., 2009]. Evapotranspiration ( $E$ ) includes evaporation of intercepted water by the surfaces (canopy, understory, forest floor and the top layer of the soil) ( $E_i$ ) and transpiration by the vegetation ( $E_t$ ), while evaporation from deeper soil and open water are neglected. The authors showed that monthly transpiration can be modeled as a simple threshold process that is a function of monthly precipitation  $P$ :

$$E_t = \min(F_{CO} + B_t(P - E_i), D_t) \quad (\text{D.1})$$

$F_{CO}$  is a carry-over factor that represents the transpiration rate at  $P = 0$  and relates to the access of the vegetation to subsurface water during seasonal drought. It depends on the vegetation rooting depth and soil moisture.  $B_t$  is the slope between effective rainfall (rainfall minus interception evaporation) and transpiration. This slope can be estimated as  $B_t = 1 - \omega - \omega(\exp(-\omega))$  with  $\omega = S_b/D_t$  where  $S_b$  is the soil moisture below which transpiration is soil moisture constrained.  $D_t$  is the monthly potential transpiration (i.e., the atmospheric demand for evaporation once the interception process has first absorbed its part of the available energy). Gerrits et al. [2009] also showed that monthly evaporation from interception can be modeled as:

$$E_i = P(1 - \exp(-B_i/P)) \quad (\text{D.2})$$

where  $B_i$  is the potential amount of monthly interception (in term of storage capacity). The authors also provide numerical derivation of the processes that takes into account the distribution of the expected number of rain days per month. For simplicity, we only use in our study the analytical derivation.

#### D.1.2.4 Our equations

Here, we assume that limits of the  $E_i$  and  $E_t$  can be combined to derive the overall limiting factors of  $E$ : because there is no interception with no rainfall,  $E$  is limited at  $P = 0$  by  $F_{CO}$ . In addition, the maximum limit of  $E$  is the potential evapotranspiration  $E_{pot}$ . We can thus model  $E$  as:

$$E = E_i + E_t \quad (D.3)$$

$$= E_i + \min(F_{CO} + B_t(P - E_i), D_t) \quad (D.4)$$

$$= \min(F_{CO} + E_i + B_t(P - E_i), E_{pot}) \quad (D.5)$$

$$= \min(F_{CO} + P(1 - \exp(-B_i/P)) + B_t(P - P(1 - \exp(-B_i/P))), E_{pot}) \quad (D.6)$$

$$= \min(F_{CO} + P(1 - \exp(-B_i/P) + B_t(1 - (1 - \exp(-B_i/P)))), E_{pot}) \quad (D.7)$$

$$= \min(F_{CO} + P(1 - \exp(-B_i/P) + B_t(\exp(-B_i/P))), E_{pot}) \quad (D.8)$$

$$= \min(F_{CO} + P(1 - \exp(-B_i/P)(1 - B_t)), E_{pot}) \quad (D.9)$$

Here, we consider that  $F_{CO}$  is a linear function of the climatological water deficit ( $C_{WD}$ , see Sec. D.1.3.2).  $C_{WD}$  is estimated individually for each year (rather than on the average for the entire period). We call  $p_1 = 1/(1 - B_t) = 1/\omega(1 - \exp(-\omega))$  and  $p_2 = B_{int}$ . Our evapotranspiration model becomes:

$$E = \min(F_{CO} + P/p_1 * (1 - \exp(-p_2/P)), E_{pot}) \quad (D.10)$$

$$F_{CO} = -p_3 * C_{WD} + p_4 \quad (D.11)$$

with  $p_1, p_2, p_3, p_4$  parameters.

#### D.1.2.5 Data fitting

We fit Equ. 10-11 to the monthly data for the period 1989–1995 (see Sec. D.1.2.1) considering all grid cells together for each vegetation state. The parameters ( $p_1, p_2, p_3, p_4$ ) are estimated using iterative least-squares estimation, with initial values (1, 1, 1, 0). Since rooting depths in land-surface models are usually fixed parameters and set arbitrarily, we

compared the output of the fit for different dataset categories included in the Landflux-EVAL data (see Fig. C8). Because the results are not greatly affected by the choice of the underlying dataset, we decide to use the Landflux-EVAL product containing all categories.

### D.1.3 Vegetation Resilience

#### D.1.3.1 Data

We use the monthly precipitation data from the Tropical Rainfall Measuring Mission (TRMM) 3B-42 v7 [Huffman et al., 2007] for the years 2000–2012. We chose this data for its fine resolution ( $0.25^\circ$  longitude and latitude) and its ability to represent temporal and spatial variability over South America [Franchito et al., 2009, Rozante et al., 2010]. We use also tree cover data from the Moderate Resolution Imaging Spectroradiometer (MODIS) Vegetation Continuous Fields MOD44B v5 at 1km resolution longitude and latitude averaged for the years 2001–2010. Finally, we use the global land-cover map from GLC2000 database from the European Commission Joint Research Centre available at <http://www-gem.jrc.it/glc2000> for the year 2001 at 1km resolution longitude and latitude. All the data cover the South American continent between  $23.375^\circ\text{S}$  and  $12.875^\circ\text{S}$ . In order to sample the high resolution data, we selected the MODIS and GLC2000 grid cell located at the centroid of each TRMM grid cell. We excluded human-modified landscapes and water bodies (classes 16–18 and 20–23 from GLC2000). The tree cover distribution has been arc-sin transformed.

#### D.1.3.2 Rainfall regime characteristic

We compute the mean annual precipitation (MAP) and the Maximum Climatological Water Deficit (MCWD) for the entire period that are the best hydrological indicators to explain the variability of vegetation distribution in the Tropics [Malhi et al., 2009]. The MCWD is the most negative cumulative value of water cumulated deficit (CWD). For the month  $n$  [Aragão et al., 2007]:

$$CWD_n = CMD_{n-1} + P_n - E_n \quad (\text{D.12})$$

$$\max(CWD_n) = 0 \quad (\text{D.13})$$

$$CWD_0 = CDW_n \quad (\text{D.14})$$

$$MCWD = \min(CWD_1, CWD_2, \dots, CWD_{12}) \quad (\text{D.15})$$

with  $P_n$  and  $E_n$  the monthly precipitation and evapotranspiration. We calculate MCWD on monthly rainfall data averaged for the entire period rather than for each year individually. The MCWD will be used as an indicator of a “meteorological induced” water stress [Aragão et al., 2007] and correlates with tree mortality in Amazonian forests [Phillips et al., 2010]. We use a fixed evapotranspiration value of  $E_{fix} = 100$  mm/month rather than a spatio-temporal evapotranspiration data that include already vegetation adaptation.  $E_{fix}$  is an approximation of the evapotranspiration rate below which the vegetation is in water stress. Using the Landflux-EVAL data we found that  $E_{fix}$  ( 3.3 mm/day) is reached or exceeded both in forest and savanna regions (see Fig. C8).

### D.1.3.3 Calculation of the vegetation resilience

Following Hirota et al. [2011], Staver et al. [2011], the frequency distribution of tropical tree cover is used to distinguish existence of three alternative stable states: ‘forest’ ( $\geq 55\%$  tree cover), ‘savanna’ ( $5 \geq \text{tree cover} < 55\%$ ) containing a combination of deciduous forest, shrub and herbaceous and ‘treeless’ ( $< 5\%$  tree cover) containing mainly bare soil in Andean deserts (see Fig. C7c).

We calculate the resilience of the vegetation based on Hirota et al. [2011], but including MCWD in the calculation as well instead of MAP only. We exclude the data points with extreme hydro-climatic values (MAP  $> 4000$  mm/month, MCWD = 0 and MCWD  $< -800$  mm) from the analysis. 10602 data points were used in total. We quantify the relative frequency of these vegetation states in equi-frequent rainfall regime classes of combined increasing MAP and MCWD values. To get the classes, the original TRMM data were first divided in classes of 1000 grid cells according to the rank of MAP values. Then, sub-classes of 100 grid cells were defined according to the rank of MCWD values. This resulted in the creation of 100 equi-frequent rainfall regime classes. We then fit the frequency of each vegetation states to a multinomial logistic regression model:

$$f(z) = \frac{1}{1 + \exp(-z)} \quad (\text{D.16})$$

$$z = \beta_0 + \beta_1 x + \beta_2 x^2 + \beta_3 y + \beta_4 y^2 \quad (\text{D.17})$$

$$(\text{D.18})$$

with  $x$  the MAP and  $y$  the MCWD mean values of the rainfall regime classes. We use the function “mnrfit” in Matlab. See fit output in Fig. C3.

#### **D.1.3.4 Potential landscapes**

We estimated under which conditions forest and savanna are alternative stable states by performing potential analysis [Livina et al., 2010] on the tree-cover dataset following the method of Hirota et al. [2011]. We computed stability landscapes of tree cover by determining how the probability density of tree cover changes with MAP (0 to 2500 mm/yr in steps of 25 mm/yr) and MCWD (-800 to 0 mm/yr in steps of 80 mm/yr). At each step of the climatic variable (MAP or MCWD), tree-cover values were weighted by applying a Gaussian kernel on the climatic variable with a standard deviation of 5% of the total range considered. Subsequently, the probability density of tree cover was estimated using the Kernel smoothing function in MATLAB (`ksdensity`) with a bandwidth according to Silverman's rule of thumb. Maxima (minima) in these probability densities are considered to be stable (unstable) states, whereby local fluctuations in the densities were filtered out (see Hirota et al. [2011]). Forest is bistable under climatic conditions below the highest values of MAP and MCWD at which a stable savanna is inferred (respectively 2000 mm/yr and -88 mm/yr) (see Fig. C6).

#### **D.1.4 Moisture recycling**

##### **D.1.4.1 Atmospheric moisture tracking model and input data**

We use the Eulerian atmospheric moisture tracking model WAM-2layers (Water Accounting Model-two layers) version 2.3.01 [van der Ent et al., 2010, 2014] to build moisture recycling networks. The input data are the same monthly precipitation and evapotranspiration products as used in the evapotranspiration model (Landflux-EVAL all categories and the average of CRU, GPCC, GPCP and CPC, see description in section D.1.2.1). In addition, we use 6-hourly wind and specific humidity data from ERA-Interim reanalysis product [Dee et al., 2011]. All the data cover the period 1989-1995. As requested by WAM-2layers settings, all the data have been spatially interpolated to 1.5° longitude and latitude grid using the nearest neighbor algorithm. In addition, data have been temporally down-scaled to the finest temporal dynamics of ERA-Interim products (3 hours for the evapotranspiration and precipitation). Following Zemp et al. [2014a], moisture recycling networks were built with WAM-2layers by tracking individually moisture evaporating from each grid cell covering the South American continent.

### D.1.4.2 Moisture recycling networks

A description of the network construction based on the output of the WAM-2layers is given in Zemp et al. [2014a]. Here, the nodes represent the grid cells and the arrows between nodes indicate the fraction of evapotranspiration in the origin that contributes to rainfall in the destination. For each pair of nodes  $j$  and  $k$  and for a given month, the arrow originating from  $j$  and pointing towards  $k$  has the weight  $w_{j,k} = m_{j,k}/E_j$  where  $m_{j,k}$  is the monthly amount of water that comes from evapotranspiration in  $j$  and falls as rain over  $k$  and  $E_j$  is the total monthly evapotranspiration in  $j$ . We note that for each grid cell  $j$  and for each month, the sum of all incoming arrows  $\epsilon_j = \sum_k(w_{j,k})$  is the total fraction of total monthly evapotranspiration in  $j$  that contributes to rainfall over the continent. On the other hand,  $P_{continent_k} = \sum_j(m_{j,k}) = \sum_i(w_{j,k} * E_j)$  is the part of monthly rainfall in  $k$  that comes from continental origin. Thus,  $\rho_k = P_{continent_k}/P_k$  (with  $P_k$  the total monthly precipitation in  $k$ ) is the fraction of total monthly precipitation in  $k$  that comes from continental origin.  $\rho$  and  $\epsilon$  correspond to the continental precipitation recycling ratio and continental evapotranspiration recycling ratio, respectively [van der Ent et al., 2010].

### D.1.4.3 Propagation of moisture through cascading moisture recycling in the cascade model

We note that  $w_{j,k}$  for each  $j$  and  $k$  are considered static in the entire experiment. Thus, after a change in the evapotranspiration in cell  $j$  from  $E_j$  to  $E_{j_2}$ , the amount of recycled moisture from  $j$  to  $k$  becomes  $m_{j,k_2} = w_{j,k} * E_{j_2}$ . This implies firstly that atmospheric circulation following vegetation shifts are not considered and secondly that rainfall is assumed linearly correlated to atmospheric moisture.

## D.2 Supplementary Discussion

### D.2.1 Comparison between fit evaluation and data

We compare the fit evaluation of the evapotranspiration model (see Sect. D.1.2.5) with the original data (Fig. C8). The fit evaluation reproduces well the evapotranspiration data on the annual scale (+1% averaged over forests and -4% over savanna and +9% in treeless). We note however an over-estimation of evapotranspiration during the dry season in savannas and in particular in Bolivia and Paraguay. A reason for this bias might be a mismatch between vegetation cover maps (for example this regions is sometimes

classified as Caatinga [Lapola et al., 2008] and seasonal forests (GLC2000)). Nevertheless, it is not the absolute values but rather the relative changes in evapotranspiration between the dry and the wet season on the one hand, and among vegetation types on the other hand that really matters for our study. In this respect, the fit evaluation reproduces well the patterns found in the data (see Fig. C9).

## D.2.2 Minimum evapotranspiration values

The minimum evapotranspiration value, even though not directly comparable to the carry-over factor (Equ. D.11), is an indicator of the capacity of the vegetation to access subsurface water during seasonal drought. Our results (see Fig. C9t) are comparable with Large Scale Biosphere-Atmosphere Experiment in Amazonia experiments where evapotranspiration during dry-season was measured as low as 1 mm/day in savanna (22° N, 48° W), 2.5 mm/day in transitional forests in southern Amazonia (11°N, 55°W) and up to 4 mm/day in tropical humid forests of central Amazonia (2-3°N, 54-60°W) [Da Rocha et al., 2009].

## D.2.3 Effect of deforestation on evapotranspiration

Our approach allows considering the depletion of subsurface water storage with changing rainfall regime and the different access to this subsurface water depending on tree cover densities. These effects are still poorly represented in most hydrological models [Miguez-Macho and Fan, 2012]. The evapotranspiration change after a replacement of all the tropical forests by a treeless state is shown in Fig. C10. Flux tower measurements showed a relative decrease of 20% during the wet season and 41% during the dry season of latent heat in pasture compared to forest in south-western Amazon (10°S, 61-62°W) [Von Randow et al., 2004]. Our experiments for this location indicate a decrease of 2% and 33%, respectively.





# Bibliography

- Adler, R. F., Huffman, G. J., Chang, A., Ferraro, R., Xie, P.-P., Janowiak, J., Rudolf, B., Schneider, U., Curtis, S., Bolvin, D., Gruber, A., Susskind, J., Arkin, P., and Nelkin, E. (2003). The version-2 global precipitation climatology project (gpcp) monthly precipitation analysis (1979-present). *Journal of hydrometeorology*, 4:1147–1167.
- Aguiar, A. P., Tejada, G., Assis, T., and Dalla-Nora, E. (2014). AMAZALERT project deliverable 4.2. Set of land-use scenarios for Brazil, linked to implications for policies: Final report. Technical report, Instituto Nacional de Pesquisas Espaciais.
- Aragão, L. E. O., Malhi, Y., Barbier, N., Lima, A., Shimabukuro, Y., Anderson, L., and Saatchi, S. (2008). Interactions between rainfall, deforestation and fires during recent years in the Brazilian Amazonia. *Philosophical Transactions of the Royal Society B: Biological Sciences*, 363:1779–1785.
- Aragão, L. E. O. C., Malhi, Y., Roman-Cuesta, R. M., Saatchi, S., Anderson, L. O., and Shimabukuro, Y. E. (2007). Spatial patterns and fire response of recent Amazonian droughts. *Geophysical Research Letters*, 34(L07701).
- Arraut, J. M., Nobre, C., Barbosa, H. M., Obregon, G., and Marengo, J. (2012). Aerial rivers and lakes: looking at large-scale moisture transport and its relation to Amazonia and to subtropical rainfall in South America. *Journal of Climate*, 25:543–556.
- Arraut, J. M. and Satyamurty, P. (2009). Precipitation and water vapor transport in the southern hemisphere with emphasis on the South American region. *Journal of Applied Meteorology and Climatology*, 48:1902–1912.
- Asner, G. P. and Alencar, A. (2010). Drought impacts on the Amazon forest: the remote sensing perspective. *New Phytologist*, 187:569–578.
- Bagley, J. E., Desai, A. R., Harding, K. J., Snyder, P. K., and Foley, J. A. (2014). Drought and deforestation: Has land cover change influenced recent precipitation extremes in the Amazon? *Journal of Climate*, 27:345–361.

- Baskaran, T., Blöchl, F., Brück, T., and Theis, F. J. (2011). The heckscher–ohlin model and the network structure of international trade. *International Review of Economics and Finance*, 20:135–145.
- Bertram, J. and Dewar, R. C. (2013). Statistical patterns in tropical tree cover explained by the different water demand of individual trees and grasses. *Ecology*, 94:2138–2144.
- Betts, R., Cox, P., Collins, M., Harris, P., Huntingford, C., and Jones, C. (2004). The role of ecosystem-atmosphere interactions in simulated Amazonian precipitation decrease and forest dieback under global climate warming. *Theoretical and Applied Climatology*, 78:157–175.
- Boccaletti, S., Latora, V., Moreno, Y., Chavez, M., and Hwang, D.-U. (2006). Complex networks: Structure and dynamics. *Physics Reports*, 424:175–308.
- Boers, N., Bookhagen, B., Barbosa, H., Marwan, N., Kurths, J., and Marengo, J. (2014). Prediction of extreme floods in the eastern central andes based on a complex networks approach. *Nature communications*, 5(5199).
- Boers, N., Bookhagen, B., Marwan, N., Kurths, J., and Marengo, J. (2013). Complex networks identify spatial patterns of extreme rainfall events of the South American monsoon system. *Geophysical Research Letters*, 40:4386–4392.
- Boisier, J. P., Ciais, P., Ducharne, A., and Guimberteau, M. (2015). Projected strengthening of Amazonian dry season by constrained climate model simulations. *Nature Climate Change*, 5:656–660. doi:10.1038/nclimate2658.
- Bonan, G. B. (2008). Forests and climate change: forcings, feedbacks, and the climate benefits of forests. *science*, 320:1444–1449.
- Bond, W. J. and Keeley, J. E. (2005). Fire as a global ‘herbivore’: the ecology and evolution of flammable ecosystems. *Trends in Ecology and Evolution*, 20:387 – 394.
- Bosilovich, M. G. and Chern, J.-D. (2006). Simulation of water sources and precipitation recycling for the mackenzie, mississippi, and Amazon river basins. *Journal of Hydrometeorology*, 7:312–329.
- Brando, P. M., Balch, J. K., Nepstad, D. C., Morton, D. C., Putz, F. E., Coe, M. T., Silvério, D., Macedo, M. N., Davidson, E. A., Nóbrega, C. C., et al. (2014). Abrupt increases in Amazonian tree mortality due to drought–fire interactions. *Proceedings of the National Academy of Sciences*, 111:6347–6352.
- Brando, P. M., Nepstad, D. C., Davidson, E. A., Trumbore, S. E., Ray, D., and Carmargo, P. (2008). Drought effects on litterfall, wood production and belowground

- carbon cycling in an Amazon forest: results of a throughfall reduction experiment. *Philosophical Transactions of the Royal Society B: Biological Sciences*, 363:1839–1848.
- Brovkin, V. and Claussen, M. (2008). Comment on “Climate-driven ecosystem succession in the Sahara: The past 6000 years”. *Science*, 322:1326–1326.
- Brovkin, V., Claussen, M., Petoukhov, V., and Ganopolski, A. (1998). On the stability of the atmosphere-vegetation system in the sahara/sahel region. *Journal of Geophysical Research-Atmospheres*, 103:31613–31624.
- Brubaker, K. L., Entekhabi, D., and Eagleson, P. (1993). Estimation of continental precipitation recycling. *Journal of Climate*, 6:1077–1089.
- Bruno, R. D., Da Rocha, H. R., De Freitas, H. C., Goulden, M. L., and Miller, S. D. (2006). Soil moisture dynamics in an eastern Amazonian tropical forest. *Hydrological Processes*, 20:2477–2489.
- Burde, G. and Zangvil, A. (2001). The estimation of regional precipitation recycling. part i: Review of recycling models. *Journal of Climate*, 14:2497–2508.
- Burde, G. I., Gandush, C., and Bayarjargal, Y. (2006). Bulk recycling models with incomplete vertical mixing. Part II: Precipitation recycling in the Amazon basin. *Journal of Climate*, 19:1473–1489.
- Capocci, A., Servedio, V. D. P., Colaiori, F., Buriol, L. S., Donato, D., Leonardi, S., and Caldarelli, G. (2006). Preferential attachment in the growth of social networks: The internet encyclopedia wikipedia. *Physical Review E*, 74(036116).
- Chen, M., Shi, W., Xie, P., Silva, V. B. S., Kousky, V. E., Wayne Higgins, R., and Janowiak, J. E. (2008). Assessing objective techniques for gauge-based analyses of global daily precipitation. *Journal of Geophysical Research: Atmospheres*, 113(D04110).
- Claussen, M., Bathiany, S., Brovkin, V., and Kleinen, T. (2013). Simulated climate-vegetation interaction in semi-arid regions affected by plant diversity. *Nature Geoscience*, 6:954–958.
- Cochrane, M. A. and Laurance, W. F. (2008). Synergisms among fire, land use, and climate change in the Amazon. *AMBIO: A Journal of the Human Environment*, 37:522–527.
- Coe, M. T., Marthews, T. R., Costa, M. H., Galbraith, D. R., Greenglass, N. L., Imbuzeiro, H. M., Levine, N. M., Malhi, Y., Moorcroft, P. R., Muza, M. N., et al. (2013). Deforestation and climate feedbacks threaten the ecological integrity of

- south-southeastern Amazonia. *Philosophical Transactions of the Royal Society B*, 368(20120155).
- Cox, P. M., Betts, R., Collins, M., Harris, P., Huntingford, C., and Jones, C. (2004). Amazonian forest dieback under climate-carbon cycle projections for the 21st century. *Theoretical and Applied Climatology*, 78:137–156.
- Cox, P. M., Betts, R. A., Jones, C. D., Spall, S. A., and Totterdell, I. J. (2000). Acceleration of global warming due to carbon-cycle feedbacks in a coupled climate model. *Nature*, 408:184–187.
- Cox, P. M., Harris, P. P., Huntingford, C., Betts, R. A., Collins, M., Jones, C. D., Jupp, T. E., Marengo, J. A., and Nobre, C. A. (2008). Increasing risk of Amazonian drought due to decreasing aerosol pollution. *Nature*, 453:212–215.
- Cramer, W., Bondeau, A., Schaphoff, S., Lucht, W., Smith, B., and Sitch, S. (2004). Tropical forests and the global carbon cycle: impacts of atmospheric carbon dioxide, climate change and rate of deforestation. *Philosophical Transactions of the Royal Society B: Biological Sciences*, 359:331–343.
- da Costa, A. C. L., Galbraith, D., Almeida, S., Portela, B. T. T., da Costa, M., de Athaydes Silva Junior, J., Braga, A. P., de Gonçalves, P. H., de Oliveira, A. A., Fisher, R., et al. (2010). Effect of 7 yr of experimental drought on vegetation dynamics and biomass storage of an eastern Amazonian rainforest. *New Phytologist*, 187:579–591.
- Da Rocha, H. R., Manzi, A. O., Cabral, O. M., Miller, S. D., Goulden, M. L., Saleska, S. R., R-Coupe, N., Wofsy, S. C., Borma, L. S., Artaxo, P., et al. (2009). Patterns of water and heat flux across a biome gradient from tropical forest to savanna in Brazil. *Journal of Geophysical Research: Biogeosciences*, 114(G00B12).
- Da Silva, R. R., Werth, D., and Avissar, R. (2008). Regional impacts of future land-cover changes on the Amazon basin wet-season climate. *Journal of Climate*, 21:1153–1170.
- Da Silveira Lobo Sternberg, L. (2001). Savanna-forest hysteresis in the tropics. *Global Ecology and Biogeography*, 10:369–378.
- Dai, A. (2013). Increasing drought under global warming in observations and models. *Nature Climate Change*, 3:52–58.
- Dall’Olio, A., Salati, E., Azevedo, C., and Matsui, E. (1979). Modelo de fracionamento isotópico da água na bacia amazônica (primeira aproximação). *Acta Amazonica*, 9:675–687.

- Davidson, E. A., de Araújo, A. C., Artaxo, P., Balch, J. K., Brown, I. F., Bustamante, M. M., Coe, M. T., DeFries, R. S., Keller, M., Longo, M., et al. (2012). The Amazon basin in transition. *Nature*, 481:321–328.
- Dee, D. and Uppala, S. (2008). Variational bias correction in era-interim. Technical Report 575.
- Dee, D., Uppala, S., Simmons, A., Berrisford, P., Poli, P., Kobayashi, S., Andrae, U., Balmaseda, M., Balsamo, G., Bauer, P., et al. (2011). The era-interim reanalysis: Configuration and performance of the data assimilation system. *Quarterly Journal of the Royal Meteorological Society*, 137:553–597.
- Dijkstra, E. W. (1959). A note on two problems in connexion with graphs. *Numerische Mathematik*, 1:269–271.
- Dirmeyer, P. A., Brubaker, K. L., and DelSole, T. (2009). Import and export of atmospheric water vapor between nations. *J. Hydrol.*, 365:11–22.
- Dolman, A. and De Jeu, R. (2010). Evaporation in focus. *Nature Geoscience*, 3:296–296.
- Donges, J. F., Schultz, H. C. H., Marwan, N., Zou, Y., and Kurths, J. (2011). Investigating the topology of interacting networks. *The European Physical Journal B*, 84:635–651.
- Donges, J. F., Zou, Y., Marwan, N., and Kurths, J. (2009a). The backbone of the climate network. *Europhysics Letters*, 87(48007).
- Donges, J. F., Zou, Y., Marwan, N., and Kurths, J. (2009b). Complex networks in climate dynamics. *European Physical Journal-Special Topics*, 174:157–179.
- Doughty, C. E. (2011). An in situ leaf and branch warming experiment in the Amazon. *Biotropica*, 43:658–665.
- Drumond, A., Marengo, J., Ambrizzi, T., Nieto, R., Moreira, L., and Gimeno, L. (2014). The role of the Amazon basin moisture in the atmospheric branch of the hydrological cycle: a lagrangian analysis. *Hydrology and Earth System Sciences*, 18:2577.
- Drumond, A., Nieto, R., Gimeno, L., and Ambrizzi, T. (2008). A lagrangian identification of major sources of moisture over central Brazil and La Plata basin. *Journal of Geophysical Research*, 113(D1412).
- Eltahir, E. A. and Bras, R. L. (1994). Precipitation recycling in the Amazon basin. *Quarterly Journal of the Royal Meteorological Society*, 120:861–880.
- Fagiolo, G. (2007). Clustering in complex directed networks. *Physical Review E*, 76(026107).

- Fearnside, P. M. (2015). Deforestation soars in the Amazon. *Nature*, 521:423–423.
- Feldpausch, T. R., Lloyd, J., Lewis, S. L., Brien, R. J. W., Gloor, M., Monteagudo Mendoza, A., Lopez-Gonzalez, G., Banin, L., Abu Salim, K., Affum-Baffoe, K., Alexiades, M., Almeida, S., Amaral, I., Andrade, A., Aragão, L. E. O. C., Araujo Murakami, A., Arets, E. J. M. M., Arroyo, L., Aymard, C., G. A., Baker, T. R., Bánki, O. S., Berry, N. J., Cardozo, N., Chave, J., Comiskey, J. A., Alvarez, E., de Oliveira, A., Di Fiore, A., Djangbletey, G., Domingues, T. F., Erwin, T. L., Fearnside, P. M., França, M. B., Freitas, M. A., Higuchi, N., C., E. H., Iida, Y., Jiménez, E., Kassim, A. R., Killeen, T. J., Laurance, W. F., Lovett, J. C., Malhi, Y., Marimon, B. S., Marimon-Junior, B. H., Lenza, E., Marshall, A. R., Mendoza, C., Metcalfe, D. J., Mitchard, E. T. A., Neill, D. A., Nelson, B. W., Nilus, R., Nogueira, E. M., Parada, A., Peh, K. S.-H., Pena Cruz, A., Peñuela, M. C., Pitman, N. C. A., Prieto, A., Quesada, C. A., Ramírez, F., Ramírez-Angulo, H., Reitsma, J. M., Rudas, A., Saiz, G., Salomão, R. P., Schwarz, M., Silva, N., Silva-Espejo, J. E., Silveira, M., Sonké, B., Stropp, J., Taedoung, H. E., Tan, S., ter Steege, H., Terborgh, J., Torello-Raventos, M., van der Heijden, G. M. F., Vásquez, R., Vilanova, E., Vos, V. A., White, L., Willcock, S., Woell, H., and Phillips, O. L. (2012). Tree height integrated into pantropical forest biomass estimates. *Biogeosciences*, 9:3381–3403.
- Figuerola, S. N. and Nobre, C. A. (1990). Precipitation distribution over central and western tropical South America. *Climanálise*, 5:36–45.
- Fisher, J. B., Malhi, Y., Bonal, D., Da Rocha, H. R., De Araujo, A. C., Gamo, M., Goulden, M. L., Hirano, T., Huete, A. R., Kondo, H., et al. (2009). The land-atmosphere water flux in the tropics. *Global Change Biology*, 15:2694–2714.
- Fisher, J. B., Tu, K. P., and Baldocchi, D. D. (2008). Global estimates of the land-atmosphere water flux based on monthly AVHRR and ISLSCP-II data, validated at 16 FLUXNET sites. *Remote Sensing of Environment*, 112:901–919.
- Franchito, S. H., Rao, V. B., Vasques, A. C., Santo, C. M., and Conforte, J. C. (2009). Validation of TRMM precipitation radar monthly rainfall estimates over Brazil. *Journal of Geophysical Research: Atmospheres*, 114(D0210).
- Freeman, L. C. (1977). A set of measures of centrality based on betweenness. *Sociometry*, 40:35–41.
- Fu, R., Yin, L., Li, W., Arias, P. A., Dickinson, R. E., Huang, L., Chakraborty, S., Fernandes, K., Liebmann, B., Fisher, R., et al. (2013). Increased dry-season length over southern Amazonia in recent decades and its implication for future climate projection. *Proceedings of the National Academy of Sciences*, 110:18110–18115.

- Galbraith, D., Levy, P. E., Sitch, S., Huntingford, C., Cox, P., Williams, M., and Meir, P. (2010). Multiple mechanisms of Amazonian forest biomass losses in three dynamic global vegetation models under climate change. *New Phytologist*, 187:647–665.
- Gat, J. and Matsui, E. (1991). Atmospheric water balance in the Amazon basin: an isotopic evapotranspiration model. *Journal of Geophysical Research: Atmospheres*, 96:13179–13188.
- Gerrits, A., Savenije, H., Veling, E., and Pfister, L. (2009). Analytical derivation of the budyko curve based on rainfall characteristics and a simple evaporation model. *Water Resources Research*, 45(W04403).
- Ghazoul, J., Sheil, D., Ghazoul, J., and Ghazoul, J. (2010). *Tropical rain forest ecology, diversity, and conservation*. Oxford University Press Oxford.
- Goessling, H. F. and Reick, C. H. (2013). Continental moisture recycling as a poisson process. *Hydrology and Earth System Sciences*, 17:4133–4142.
- Good, P., Jones, C., Lowe, J., Betts, R., and Gedney, N. (2013). Comparing Tropical Forest Projections from Two Generations of Hadley Centre Earth System Models, HadGEM2-ES and HadCM3LC. *Journal of Climate*, 26:495–511.
- Gozolchiani, A., Havlin, S., and Yamasaki, K. (2011). Emergence of el niño as an autonomous component in the climate network. *Physical Review Letter*, 107:148501–1 – 148501–5.
- Gozolchiani, A., Yamasaki, K., Gazit, O., and Havlin, S. (2008). Pattern of climate network blinking links follows el nino events. *Europhysics Letter*, 83:28005–p1 – 28005–p5.
- Graham, E. A., Mulkey, S. S., Kitajima, K., Phillips, N. G., and Wright, S. J. (2003). Cloud cover limits net co2 uptake and growth of a rainforest tree during tropical rainy seasons. *Proceedings of the National Academy of Sciences*, 100:572–576.
- Grimm, A., Vera, C., and Mechoso, C. (2004). The South American monsoon system. In *The Third International Workshop on Monsoons*, Hangzhou. World Meteorological Organizations.
- Guan, K., Pan, M., Li, H., Wolf, A., Wu, J., Medvigy, D., Caylor, K. K., Sheffield, J., Wood, E. F., Malhi, Y., et al. (2015). Photosynthetic seasonality of global tropical forests constrained by hydroclimate. *Nature Geoscience*, 8:284–289.
- Hanan, N. P., Tredennick, A. T., Prihodko, L., Bucini, G., and Dohn, J. (2014). Analysis of stable states in global savannas: is the CART pulling the horse? *Global ecology and biogeography*, 23:259–263.

- Hasler, N., Werth, D., and Avissar, R. (2009). Effects of tropical deforestation on global hydroclimate: A multimodel ensemble analysis. *Journal of Climate*, 22:1124–1141.
- Heitzig, J., Donges, J. F., Zou, Y., Marwan, N., and Kurths, J. (2012). Node-weighted measures for complex networks with spatially embedded, sampled, or differently sized nodes. *The European Physical Journal B*, 85:38.
- Hilker, T., Lyapustin, A. I., Tucker, C. J., Hall, F. G., Myneni, R. B., Wang, Y., Bi, J., de Moura, Y. M., and Sellers, P. J. (2014). Vegetation dynamics and rainfall sensitivity of the Amazon. *Proceedings of the National Academy of Sciences*, 111:16041–16046.
- Hirota, M., Holmgren, M., Van Nes, E. H., and Scheffer, M. (2011). Global resilience of tropical forest and savanna to critical transitions. *Science*, 334:232–235.
- Hirota, M., Nobre, C., Oyama, M. D., and Bustamante, M. (2010). The climatic sensitivity of the forest, savanna and forest–savanna transition in tropical South America. *New Phytologist*, 187:707–719.
- Holmgren, M., Hirota, M., van Nes, E. H., and Scheffer, M. (2013). Effects of interannual climate variability on tropical tree cover. *Nature Climate Change*, 3:755–758.
- Hopkins, M. J. (2007). Modelling the known and unknown plant biodiversity of the Amazon basin. *Journal of Biogeography*, 34:1400–1411.
- Huete, A. R., Didan, K., Shimabukuro, Y. E., Ratana, P., Saleska, S. R., Hutyyra, L. R., Yang, W., Nemani, R. R., and Myneni, R. (2006). Amazon rainforests green-up with sunlight in dry season. *Geophysical Research Letters*, 33(L0640).
- Huffman, G. J., Adler, R. F., Rudolf, B., Schneider, U., and Keehn, P. R. (1995). Global precipitation estimates based on a technique for combining satellite-based estimates, rain gauge analysis, and NWP model precipitation information. *Journal of Climate*, 8:1284–1295.
- Huffman, G. J., Bolvin, D. T., Nelkin, E. J., Wolff, D. B., Adler, R. F., Gu, G., Hong, Y., Bowman, K. P., and Stocker, E. F. (2007). The TRMM multisatellite precipitation analysis (TMPA): Quasi-global, multiyear, combined-sensor precipitation estimates at fine scales. *Journal of Hydrometeorology*, 8:38–55.
- Huntingford, C., Zelazowski, P., Galbraith, D., Mercado, L. M., Sitch, S., Fisher, R., Lomas, M., Walker, A. P., Jones, C. D., Booth, B. B., et al. (2013). Simulated resilience of tropical rainforests to co<sub>2</sub>-induced climate change. *Nature Geoscience*, 6:268–273.
- Huntley, B. J. and Walker, B. H. (2012). *Ecology of tropical savannas*, volume 42. Springer Science & Business Media.



- Joetzjer, E., Delire, C., Douville, H., Ciais, P., Decharme, B., Fisher, R., Christoffersen, B., Calvet, J., da Costa, A., Ferreira, L., et al. (2014). Predicting the response of the Amazon rainforest to persistent drought conditions under current and future climates: a major challenge for global land surface models. *Geoscientific Model Development*, 7:2933–2950.
- Joetzjer, E., Douville, H., Delire, C., and Ciais, P. (2013). Present-day and future Amazonian precipitation in global climate models: CMIP5 versus CMIP3. *Climate dynamics*, 41:2921–2936.
- Jung, M., Reichstein, M., and Bondeau, A. (2009). Towards global empirical upscaling of FLUXNET eddy covariance observations: validation of a model tree ensemble approach using a biosphere model. *Biogeosciences*, 6:2001–2013.
- Kalnay, E., Kanamitsu, M., Kistler, R., Collins, W., Deaven, D., Gandin, L., Iredell, M., Saha, S., White, G., Woollen, J., Zhu, Y., Leetmaa, A., Reynolds, R., Chelliah, M., E. W., Higgins, W., Janowiak, J., Mo, K. C., Ropelewski, C., Wang, J., Jenne, R., and Joseph, D. (1996). The NCEP/NCAR 40-year reanalysis project. *Bulletin of the American meteorological Society*, 77:437–471.
- Keys, P., Ent, R., Gordon, L., Hoff, H., Nikoli, R., and Savenije, H. (2012). Analyzing precipitationsheds to understand the vulnerability of rainfall dependent regions. *Biogeosciences*, 9:733–746.
- Keys, P. W., Barnes, E. A., van der Ent, R. J., and Gordon, L. J. (2014). Variability of moisture recycling using a precipitationshed framework. *Hydrology and Earth System Sciences*, 18:3937–3950.
- Kim, J.-E. and Alexander, M. J. (2013). Tropical precipitation variability and convectively coupled equatorial waves on submonthly time scales in reanalyses and trmm. *Journal of Climate*, 26:3013–3030.
- Knox, R., Bisht, G., Wang, J., and Bras, R. (2011). Precipitation variability over the forest-to-nonforest transition in southwestern Amazonia. *Journal of Climate*, 24:2368–2377.
- Krinner, G., Viovy, N., de Noblet-Ducoudré, N., Ogée, J., Polcher, J., Friedlingstein, P., Ciais, P., Sitch, S., and Prentice, I. C. (2005). A dynamic global vegetation model for studies of the coupled atmosphere-biosphere system. *Global Biogeochemical Cycles*, 19(GB1015).
- Kröpelin, S., Verschuren, D., Lézine, A.-M., Eggermont, H., Cocquyt, C., Francus, P., Cazet, J.-P., Fagot, M., Rumes, B., Russell, J., et al. (2008). Climate-driven ecosystem succession in the sahara: the past 6000 years. *science*, 320:765–768.

- Lapola, D. M., Oyama, M. D., and Nobre, C. A. (2009). Exploring the range of climate biome projections for tropical South America: the role of CO<sub>2</sub> fertilization and seasonality. *Global Biogeochemical Cycles*, 23(GB3003).
- Lapola, D. M., Oyama, M. D., Nobre, C. A., and Sampaio, G. (2008). A new world natural vegetation map for global change studies. *Anais da Academia Brasileira de Ciências*, 80:397–408.
- Lawrence, D. and Vandecar, K. (2015). Effects of tropical deforestation on climate and agriculture. *Nature Climate Change*, 5:27–36.
- Lean, J. and Warrilow, D. (1989). Simulation of the regional climatic impact of Amazon deforestation. *Nature*, 342:411–413.
- Lee, J.-E., Frankenberg, C., van der Tol, C., Berry, J. A., Guanter, L., Boyce, C. K., Fisher, J. B., Morrow, E., Worden, J. R., Asefi, S., et al. (2013). Forest productivity and water stress in Amazonia: observations from gosat chlorophyll fluorescence. *Proceedings of the Royal Society of London B: Biological Sciences*, 280:20130171.
- Lettau, H., Lettau, K., and Molion, L. C. B. (1979). Amazonia's hydrologic cycle and the role of atmospheric recycling in assessing deforestation effects. *Monthly Weather Review*, 107:227–238.
- Lewis, S. L., Brando, P. M., Phillips, O. L., van der Heijden, G. M., and Nepstad, D. (2011). The 2010 Amazon drought. *Science*, 331:554–554.
- Liebmann, B., Kiladis, G. N., Marengo, J., Ambrizzi, T., and Glick, J. D. (1999). Sub-monthly convective variability over South America and the South Atlantic convergence zone. *Journal of Climate*, 12:1877–1891.
- Liebmann, B. and Marengo, J. (2001). Interannual variability of the rainy season and rainfall in the Brazilian Amazon basin. *Journal of Climate*, 14:4308–4318.
- Livina, V. N., Kwasniok, F., and Lenton, T. M. (2010). Potential analysis reveals changing number of climate states during the last 60 kyr. *Climate of the Past*, 6:77–82.
- Loarie, S. R., Lobell, D. B., Asner, G. P., Mu, Q., and Field, C. B. (2011). Direct impacts on local climate of sugar-cane expansion in Brazil. *Nature Climate Change*, 1:105–109.
- Ludescher, J., Gozolchiani, A., Bogachev, M. I., Bunde, A., Havlin, S., and Schellnhuber, H. J. (2013). Improved El Niño forecasting by cooperativity detection. *Proceedings of the National Academy of Sciences*, 110:11742–11745.

- Ludescher, J., Gozolchiani, A., Bogachev, M. I., Bunde, A., Havlin, S., and Schellnhuber, H. J. (2014). Very early warning of next El Niño. *Proceedings of the National Academy of Sciences*, 111:2064–2066.
- Maeda, E. E., Kim, H., Aragão, L. E. O. C., Famiglietti, J. S., and Oki, T. (2015). Disruption of hydroecological equilibrium in southwest Amazon mediated by drought. *Geophysical Research Letters*, 42. doi:10.1002/2015GL065252.
- Makarieva, A., Gorshkov, V., Sheil, D., Nobre, A., and Li, B.-L. (2013). Where do winds come from? A new theory on how water vapor condensation influences atmospheric pressure and dynamics. *Atmospheric Chemistry and Physics*, 13:1039–1056.
- Malhi, Y., Aragão, L. E., Galbraith, D., Huntingford, C., Fisher, R., Zelazowski, P., Sitch, S., McSweeney, C., and Meir, P. (2009). Exploring the likelihood and mechanism of a climate-change-induced dieback of the Amazon rainforest. *Proceedings of the National Academy of Sciences*, 106:20610–20615.
- Malik, N., Bookhagen, B., Marwan, N., and Kurths, J. (2012). Analysis of spatial and temporal extreme monsoonal rainfall over South Asia using complex networks. *Climate Dynamics*, 39:971–987.
- Marengo, J., Liebmann, B., Grimm, A., Misra, V., Silva Dias, P., Cavalcanti, I., Carvalho, L., Berbery, E., Ambrizzi, T., Vera, C., et al. (2012). Recent developments on the South American monsoon system. *International Journal of Climatology*, 32:1–21.
- Marengo, J. A. (2005). Characteristics and spatio-temporal variability of the Amazon river basin water budget. *Climate Dynamics*, 24:11–22.
- Marengo, J. A. (2006). On the hydrological cycle of the Amazon basin: A historical review and current state-of-the-art. *Revista Brasileira de Meteorologia*, 21:1–19.
- Marengo, J. A., Nobre, C. A., Tomasella, J., Oyama, M. D., Sampaio de Oliveira, G., De Oliveira, R., Camargo, H., Alves, L. M., and Brown, I. F. (2008). The drought of Amazonia in 2005. *Journal of Climate*, 21:495–516.
- Marengo, J. A., Soares, W. R., Saulo, C., and Nicolini, M. (2004). Climatology of the low-level jet east of the andes as derived from the ncep-ncar reanalyses: Characteristics and temporal variability. *Journal of Climate*, 17:2261–2280.
- Marengo, J. A., Tomasella, J., Alves, L. M., Soares, W. R., and Rodriguez, D. A. (2011). The drought of 2010 in the context of historical droughts in the Amazon region. *Geophysical Research Letters*, 38(12).
- Martinez, J. A. and Dominguez, F. (2014). Sources of atmospheric moisture for the La Plata river basin. *Journal of Climate*, 27:6737–6753.

- Medvigy, D., Walko, R. L., and Avissar, R. (2011). Effects of deforestation on spatiotemporal distributions of precipitation in South America. *Journal of Climate*, 24(8):2147–2163.
- Miguez-Macho, G. and Fan, Y. (2012). The role of groundwater in the amazon water cycle: 2. influence on seasonal soil moisture and evapotranspiration. *Journal of Geophysical Research: Atmospheres*, 117(D15114).
- Milo, R., Shen-Orr, S., Itzkovitz, S., Kashtan, N., Chklovskii, D., and Alon, U. (2002). Network motifs: simple building blocks of complex networks. *Science*, 298:824–827.
- Miralles, D., Holmes, T., De Jeu, R., Gash, J., Meesters, A., and Dolman, A. (2011). Global land-surface evaporation estimated from satellite-based observations. *Hydrology and Earth System Sciences*, 15:453–469.
- Monteith, J. (1965). Evaporation and environment. In *Symp. Soc. Exp. Biol*, volume 19, page 4.
- Morton, D. C., DeFries, R. S., Shimabukuro, Y. E., Anderson, L. O., Arai, E., del Bon Espirito-Santo, F., Freitas, R., and Morisette, J. (2006). Cropland expansion changes deforestation dynamics in the southern Brazilian Amazon. *Proceedings of the National Academy of Sciences*, 103:14637–14641.
- Morton, D. C., Nagol, J., Carabajal, C. C., Rosette, J., Palace, M., Cook, B. D., Vermote, E. F., Harding, D. J., and North, P. R. (2014). Amazon forests maintain consistent canopy structure and greenness during the dry season. *Nature*, 506:221–224.
- Mu, Q., Zhao, M., and Running, S. W. (2011). Improvements to a modis global terrestrial evapotranspiration algorithm. *Remote Sensing of Environment*, 115:1781–1800.
- Mueller, B., Hirschi, M., Jimenez, C., Ciais, P., Dirmeyer, P. A., Dolman, A. J., Fisher, J. B., Jung, M., Ludwig, F., Maignan, F., Miralles, D. G., McCabe, M. F., Reichstein, M., Sheffield, J., Wang, K., Wood, E. F., Zhang, Y., and Seneviratne, S. I. (2013). Benchmark products for land evapotranspiration: LandFlux-EVAL multi-data set synthesis. *Hydrology and Earth System Sciences*, 17:3707–3720.
- Mueller, B., Seneviratne, S. I., Jimenez, C., Corti, T., Hirschi, M., Balsamo, G., Ciais, P., Dirmeyer, P., Fisher, J. B., Guo, Z., Jung, M., Maignan, F., McCabe, M. F., Reichle, R., Reichstein, M., Rodell, M., Sheffield, J., Teuling, A. J., Wang, K., Wood, E. F., and Zhang, Y. (2011). Evaluation of global observations-based evapotranspiration datasets and IPCC AR4 simulations. *Geophysical Research Letters*, 38(L06402).
- Murphy, P. G. and Lugo, A. E. (1986). Ecology of tropical dry forest. *Annual review of ecology and systematics*, pages 67–88.

- Myers, N., Mittermeier, R. A., Mittermeier, C. G., Da Fonseca, G. A., and Kent, J. (2000). Biodiversity hotspots for conservation priorities. *Nature*, 403:853–858.
- Nepstad, D., McGrath, D., Stickler, C., Alencar, A., Azevedo, A., Swette, B., Bezerra, T., DiGiano, M., Shimada, J., da Motta, R. S., et al. (2014). Slowing Amazon deforestation through public policy and interventions in beef and soy supply chains. *Science*, 344:1118–1123.
- Nepstad, D. C., de Carvalho, C. R., Davidson, E. A., Jipp, P. H., Lefebvre, P. A., Negreiros, G. H., da Silva, E. D., Stone, T. A., Trumbore, S. E., and Vieira, S. (1994). The role of deep roots in the hydrological and carbon cycles of Amazonian forests and pastures. *Nature*, 372:666–669.
- Nepstad, D. C., Stickler, C. M., Soares-Filho, B., and Merry, F. (2008). Interactions among Amazon land use, forests and climate: prospects for a near-term forest tipping point. *Philosophical Transactions of the Royal Society B: Biological Sciences*, 363(1498):1737–1746.
- Nepstad, D. C., Tohver, I. M., Ray, D., Moutinho, P., and Cardinot, G. (2007). Mortality of large trees and lianas following experimental drought in an Amazon forest. *Ecology*, 88:2259–2269.
- New, M., Hulme, M., and Jones, P. (2000). Representing twentieth-century space-time climate variability. Part II: Development of 1901–96 monthly grids of terrestrial surface climate. *Journal of Climate*, 13:2217–2238.
- Newman, M. E. and Park, J. (2003). Why social networks are different from other types of networks. *Physical Review E*, 68:036122.
- Newman, M. E. J. (2001). Scientific collaboration networks. II. Shortest paths, weighted networks, and centrality. *Physical Review E*, 64:016132.
- Nobre, C. A., Sellers, P. J., and Shukla, J. (1991). Amazonian deforestation and regional climate change. *Journal of Climate*, 4:957–988.
- Nobre, P., Malagutti, M., Urbano, D. F., de Almeida, R. A., and Giarolla, E. (2009). Amazon deforestation and climate change in a coupled model simulation. *Journal of Climate*, 22:5686–5697.
- Norby, R. J., De Kauwe, M. G., Domingues, T. F., Duursma, R. A., Ellsworth, D. S., Goll, D. S., Lapola, D. M., Luus, K. A., MacKenzie, A. R., Medlyn, B. E., Pavlick, R., Rammig, A., Smith, B., Thomas, R., Thonicke, K., Walker, A. P., Yang, X., and Zaehle, S. (2015). Model–data synthesis for the next generation of forest free-air CO<sub>2</sub> enrichment (FACE) experiments. *New Phytologist*. doi:10.1111/nph.13593.

- Numaguti, A. (1999). Origin and recycling processes of precipitating water over the Eurasian continent: Experiments using an atmospheric general circulation model. *Journal of Geophysical Research: Atmospheres*, 104:1957–1972.
- Oliveira, R. S., Dawson, T. E., Burgess, S. S., and Nepstad, D. C. (2005). Hydraulic redistribution in three Amazonian trees. *Oecologia*, 145:354–363.
- Ortiz, J., Guilderson, T., Adkins, J., Sarnthein, M., Baker, L., Yarusinsky, M., et al. (2000). Abrupt onset and termination of the African humid period: rapid climate responses to gradual insolation forcing. *Quaternary Science Reviews*, 19:347–361.
- Oyama, M. D. and Nobre, C. A. (2003). A new climate-vegetation equilibrium state for tropical South America. *Geophysical Research Letters*, 30(23).
- Phillips, O. L., Aragão, L. E., Lewis, S. L., Fisher, J. B., Lloyd, J., López-González, G., Malhi, Y., Monteagudo, A., Peacock, J., Quesada, C. A., et al. (2009). Drought sensitivity of the Amazon rainforest. *Science*, 323:1344–1347.
- Phillips, O. L., van der Heijden, G., Lewis, S. L., López-González, G., Aragão, L. E. O. C., Lloyd, J., Malhi, Y., Monteagudo, A., Almeida, S., Dávila, E. A., Amaral, I., Andelman, S., Andrade, A., Arroyo, L., Aymard, G., Baker, T. R., Blanc, L., Bonal, D., de Oliveira, t. C. A., Chao, K.-J., Cardozo, N. D., da Costa, L., Feldpausch, T. R., Fisher, J. B., Fyllas, N. M., Freitas, M. A., Galbraith, D., Gloor, E., Higuchi, N., Honorio, E., Jiménez, E., Keeling, H., Killeen, T. J., Lovett, J. C., Meir, P., Mendoza, C., Morel, A., Vargas, P. N., Patiño, S., Peh, K. S.-H., Cruz, A. P., Prieto, A., Quesada, C. A., Ramírez, F., Ramírez, H., Rudas, A., Salamão, R., Schwarz, M., Silva, J., Silveira, M., Ferry Slik, J. W., Sonké, B., Thomas, A. S., Stropp, J., Taplin, J. R. D., Vásquez, R., and Vilanova, E. (2010). Drought–mortality relationships for tropical forests. *New Phytologist*, 187:631–646.
- Pires, G. F. and Costa, M. H. (2013). Deforestation causes different subregional effects on the Amazon bioclimatic equilibrium. *Geophysical Research Letters*, 40:3618–3623.
- Pokhrel, Y. N., Fan, Y., and Miguez-Macho, G. (2014). Potential hydrologic changes in the Amazon by the end of the 21st century and the groundwater buffer. *Environmental Research Letters*, 9:084004.
- Rammig, A., Jupp, T., Thonicke, K., Tietjen, B., Heinke, J., Ostberg, S., Lucht, W., Cramer, W., and Cox, P. (2010). Estimating the risk of Amazonian forest dieback. *New Phytologist*, 187:694–706.
- Restrepo-Coupe, N., da Rocha, H. R., Huttyra, L. R., da Araujo, A. C., Borma, L. S., Christoffersen, B., Cabral, O. M., de Camargo, P. B., Cardoso, F. L., da Costa, A.

- C. L., Fitzjarrald, D. R., Goulden, M. L., Kruijt, B., Maia, J. M., Malhi, Y. S., Manzi, A. O., Miller, S. D., Nobre, A. D., von Randow, C., Sá, L. D. A., Sakai, R. K., Tota, J., Wofsy, S. C., Zanchi, F. B., and Saleska, S. R. (2013). What drives the seasonality of photosynthesis across the Amazon basin? A cross-site analysis of eddy flux tower measurements from the Brasil flux network. *Agricultural and Forest Meteorology*, 182–183:128 – 144.
- Reyer, C. P. O., Brouwers, N., Rammig, A., Brook, B. W., Epila, J., Grant, R. F., Holmgren, M., Langerwisch, F., Leuzinger, S., Lucht, W., Medlyn, B., Pfeifer, M., Steinkamp, J., Vanderwel, M. C., Verbeeck, H., and Villeda, D. M. (2015). Forest resilience and tipping points at different spatio-temporal scales: approaches and challenges. *Journal of Ecology*, 103:5–15.
- Rietkerk, M., Brovkin, V., van Bodegom, P. M., Claussen, M., Dekker, S. C., Dijkstra, H. A., Goryachkin, S. V., Kabat, P., van Nes, E. H., Neutel, A.-M., Nicholson, S. E., Nobre, C., Petoukhov, V., Provenzale, A., Scheffer, M., and Seneviratne, S. I. (2011). Local ecosystem feedbacks and critical transitions in the climate. *Ecological Complexity*, 8:223 – 228.
- Rockström, J., Falkenmark, M., Karlberg, L., Hoff, H., Rost, S., and Gerten, D. (2009). Future water availability for global food production: the potential of green water for increasing resilience to global change. *Water Resources Research*, 45(W00A1).
- Rozante, J. R. and Cavalcanti, I. F. A. (2008). Regional Eta model experiments: SALLJEX and MCS development. *Journal of Geophysical Research: Atmospheres*, 113(D17106).
- Rozante, J. R., Moreira, D. S., de Goncalves, L. G. G., and Vila, D. A. (2010). Combining TRMM and surface observations of precipitation: Technique and validation over South America. *Weather and Forecasting*, 25:885–894.
- Ruhoff, A. (2011). *Predicting evapotranspiration in tropical biomes using MODIS remote sensing data*. PhD thesis, Federal University of Rio Grande do Sul, Porto Alegre.
- Saatchi, S., Asefi-Najafabady, S., Malhi, Y., Aragão, L. E., Anderson, L. O., Myneni, R. B., and Nemani, R. (2013). Persistent effects of a severe drought on Amazonian forest canopy. *Proceedings of the National Academy of Sciences*, 110:565–570.
- Saatchi, S. S., Nelson, B., Podest, E., and Holt, J. (2000). Mapping land cover types in the Amazon basin using 1 km jers-1 mosaic. *International Journal of Remote Sensing*, 21:1201–1234.
- Salati, E., Dall’Olio, A., Matsui, E., and Gat, J. R. (1979). Recycling of water in the Amazon basin: an isotopic study. *Water Resources Research*, 15:1250–1258.

- Salazar, L. F., Nobre, C. A., and Oyama, M. D. (2007). Climate change consequences on the biome distribution in tropical South America. *Geophysical Research Letters*, 34(L09708).
- Samanta, A., Knyazikhin, Y., Xu, L., Dickinson, R. E., Fu, R., Costa, M. H., Saatchi, S. S., Nemani, R. R., and Myneni, R. B. (2012). Seasonal changes in leaf area of Amazon forests from leaf flushing and abscission. *Journal of Geophysical Research: Biogeosciences*, 117(G01015).
- Sampaio, G., Nobre, C., Costa, M. H., Satyamurty, P., Soares-Filho, B. S., and Cardoso, M. (2007). Regional climate change over eastern Amazonia caused by pasture and soybean cropland expansion. *Geophysical Research Letters*, 34(L17709).
- Savenije, H. H. (2004). The importance of interception and why we should delete the term evapotranspiration from our vocabulary. *Hydrological Processes*, 18:1507–1511.
- Scheffer, M. (2009). *Critical transitions in nature and society*. Princeton University Press. Princeton, U.S.A.
- Scheffer, M. and Carpenter, S. R. (2003). Catastrophic regime shifts in ecosystems: linking theory to observation. *Trends in ecology & evolution*, 18:648–656.
- Scheffer, M., Carpenter, S. R., Lenton, T. M., Bascompte, J., Brock, W., Dakos, V., Van De Koppel, J., Van De Leemput, I. A., Levin, S. A., Van Nes, E. H., Pascual, M., and Vandermeer, J. (2012). Anticipating critical transitions. *science*, 338:344–348.
- Scheffer, M., Holmgren, M., Brovkin, V., and Claussen, M. (2005). Synergy between small-and large-scale feedbacks of vegetation on the water cycle. *Global Change Biology*, 11:1003–1012.
- Sheffield, J., Goteti, G., and Wood, E. F. (2006). Development of a 50-year high-resolution global dataset of meteorological forcings for land surface modeling. *Journal of Climate*, 19:3088–3111.
- Sheffield, J., Wood, E. F., and Munoz-Arriola, F. (2010). Long-term regional estimates of evapotranspiration for Mexico based on downscaled isccp data. *Journal of Hydrometeorology*, 11:253–275.
- Sheffield, J., Wood, E. F., and Roderick, M. L. (2012). Little change in global drought over the past 60 years. *Nature*, 491:435–438.
- Shukla, J., Nobre, C., Sellers, P., et al. (1990). Amazon deforestation and climate change. *Science*, 247:1322–1325.



- Silvério, D. V., Brando, P. M., Balch, J. K., Putz, F. E., Nepstad, D. C., Oliveira-Santos, C., and Bustamante, M. M. (2013). Testing the Amazon savannization hypothesis: fire effects on invasion of a neotropical forest by native cerrado and exotic pasture grasses. *Philosophical Transactions of the Royal Society B: Biological Sciences*, 368(20120427).
- Sitch, S., Smith, B., Prentice, I. C., Arneth, A., Bondeau, A., Cramer, W., Kaplan, J., Levis, S., Lucht, W., Sykes, M. T., et al. (2003). Evaluation of ecosystem dynamics, plant geography and terrestrial carbon cycling in the LPJ dynamic global vegetation model. *Global Change Biology*, 9:161–185.
- Soares-Filho, B. S., Nepstad, D. C., Curran, L. M., Cerqueira, G. C., Garcia, R. A., Ramos, C. A., Voll, E., McDonald, A., Lefebvre, P., and Schlesinger, P. (2006). Modelling conservation in the Amazon basin. *Nature*, 440:520–523.
- Sombroek, W. (2001). Spatial and temporal patterns of Amazon rainfall: consequences for the planning of agricultural occupation and the protection of primary forests. *AMBIO: A Journal of the Human Environment*, 30:388–396.
- Spracklen, D., Arnold, S., and Taylor, C. (2012). Observations of increased tropical rainfall preceded by air passage over forests. *Nature*, 489:282–285.
- Staal, A., Dekker, S. C., Hirota, M., and van Nes, E. H. (2015). Synergistic effects of drought and deforestation on the resilience of the south-eastern Amazon rainforest. *Ecological Complexity*, 22:65–75.
- Staver, A. C., Archibald, S., and Levin, S. A. (2011). The global extent and determinants of savanna and forest as alternative biome states. *Science*, 334:230–232.
- Sudradjat, A., Brubaker, K., and Dirmeyer, P. (2002). Precipitation source/sink connections between the Amazon and La Plata river basins. In *AGU Fall Meeting Abstracts*, volume 1, page 0830. San Francisco, California, 6–10 December 2002.
- Trenberth, K. E. (1999). Atmospheric moisture recycling: Role of advection and local evaporation. *Journal of Climate*, 12:1368–1381.
- Tsonis, A. A., Swanson, K. L., and Roebber, P. J. (2006). What do networks have to do with climate? *Bulletin of the American Meteorological Society*, 87:585–595.
- Tsonis, A. A., Swanson, K. L., and Wang, G. (2008). On the role of atmospheric teleconnections in climate. *Journal of Climate*, 21:2990–3001.
- van der Ent, R. J., Savenije, H. H., Schaeffli, B., and Steele-Dunne, S. C. (2010). Origin and fate of atmospheric moisture over continents. *Water Resources Research*, 46(W09525).

- van der Ent, R. J. and Savenije, H. H. G. (2011). Length and time scales of atmospheric moisture recycling. *Atmospheric Chemistry and Physics*, 11:1853–1863.
- van der Ent, R. J., Tuinenburg, O. A., Knoche, H.-R., Kunstmann, H., and Savenije, H. H. G. (2013). Should we use a simple or complex model for moisture recycling and atmospheric moisture tracking? *Hydrology and Earth System Sciences*, 17:4869–4884.
- van der Ent, R. J., Wang-Erlandsson, L., Keys, P. W., and Savenije, H. H. G. (2014). Contrasting roles of interception and transpiration in the hydrological cycle. part 2: Moisture recycling. *Earth System Dynamics*, 5:471–489.
- van der Sleen, P., Groenendijk, P., Vlam, M., Anten, N. P., Boom, A., Bongers, F., Pons, T. L., Terburg, G., and Zuidema, P. A. (2014). No growth stimulation of tropical trees by 150 years of co2 fertilization but water-use efficiency increased. *Nature geoscience*, pages 24–28.
- van Nes, E. H., Hirota, M., Holmgren, M., and Scheffer, M. (2014). Tipping points in tropical tree cover: linking theory to data. *Global change biology*, 20:1016–1021.
- van Nes, E. H. and Scheffer, M. (2005). Implications of spatial heterogeneity for catastrophic regime shifts in ecosystems. *Ecology*, 86:1797–1807.
- Veenendaal, E. M., Torello-Raventos, M., Feldpausch, T. R., Domingues, T. F., Gerard, F., Schrodte, F., Saiz, G., Quesada, C. A., Djangbletey, G., Ford, A., Kemp, J., Marimon, B. S., Marimon-Junior, B. H., Lenza, E., Ratter, J. A., Maracahipes, L., Sasaki, D., Sonké, B., Zapfack, L., Villarroya, D., Schwarz, M., Yoko Ishida, F., Gilpin, M., Nardoto, G. B., Affum-Baffoe, K., Arroyo, L., Bloomfield, K., Ceca, G., Compaore, H., Davies, K., Diallo, A., Fyllas, N. M., Gignoux, J., Hien, F., Johnson, M., Mougou, E., Hiernaux, P., Killeen, T., Metcalfe, D., Miranda, H. S., Steininger, M., Sykora, K., Bird, M. I., Grace, J., Lewis, S., Phillips, O. L., and Lloyd, J. (2015). Structural, physiognomic and above-ground biomass variation in savanna–forest transition zones on three continents – how different are co-occurring savanna and forest formations? *Biogeosciences*, 12:2927–2951.
- Vera, C., Baez, J., Douglas, M., Emmanuel, C., Marengo, J., Meitin, J., Nicolini, M., Noguez-Paegle, J., Paegle, J., Penalba, O., et al. (2006a). The South American low-level jet experiment. *Bulletin of the American Meteorological Society*, 87:63–77.
- Vera, C., Higgins, W., Amador, J., Ambrizzi, T., Garreaud, R., Gochis, D., Gutzler, D., Lettenmaier, D., Marengo, J., Mechoso, C., et al. (2006b). Toward a unified view of the American monsoon systems. *Journal of Climate*, 19:4977–5000.

- Victoria, R. L., Martinelli, L. A., Mortatti, J., and Richey, J. (1991). Mechanisms of water recycling in the Amazon basin: isotopic insights. *Forestry and the Environment*, 20:384–387.
- Von Randow, C., Manzi, A., Kruijt, B., De Oliveira, P., Zanchi, F., Silva, R., Hodnett, M., Gash, J., Elbers, J., Waterloo, M., et al. (2004). Comparative measurements and seasonal variations in energy and carbon exchange over forest and pasture in South West Amazonia. *Theoretical and Applied Climatology*, 78:5–26.
- Walker, R., Moore, N. J., Arima, E., Perz, S., Simmons, C., Caldas, M., Vergara, D., and Bohrer, C. (2009). Protecting the Amazon with protected areas. *Proceedings of the National Academy of Sciences*, 106:10582–10586.
- Wang, K. and Liang, S. (2008). An improved method for estimating global evapotranspiration based on satellite determination of surface net radiation, vegetation index, temperature, and soil moisture. *Journal of Hydrometeorology*, 9:712–727.
- Wang, Y., Gozolchiani, A., Ashkenazy, Y., Berezin, Y., Guez, O., and Havlin, S. (2013). Dominant imprint of rossby waves in the climate network. *Physical Review Letter*, 111:138501.
- Wasserman, S. and Faust, K. (1994). *Social network analysis: Methods and applications*. Cambridge university press. Cambridge, England, 1994.
- Watts, D. J. (2002). A simple model of global cascades on random networks. *Proceedings of the National Academy of Sciences*, 99:5766–5771.
- Werth, D. and Avissar, R. (2002). The local and global effects of Amazon deforestation. *Journal of Geophysical Research: Atmospheres*, 107:55.
- White, A., Cannell, M. G., and Friend, A. D. (1999). Climate change impacts on ecosystems and the terrestrial carbon sink: a new assessment. *Global environmental change*, 9:21–30.
- Wiedermann, M., Donges, J. F., Heitzig, J., and Kurths, J. (2013). Node-weighted interacting network measures improve the representation of real-world complex systems. *Europhysics Letters*, 102(28007).
- Xu, L., Samanta, A., Costa, M. H., Ganguly, S., Nemani, R. R., and Myneni, R. B. (2011). Widespread decline in greenness of Amazonian vegetation due to the 2010 drought. *Geophysical Research Letters*, 38(L07402).
- Yamasaki, K., Gozolchiani, A., and Havlin, S. (2008). Climate networks around the globe are significantly affected by el niño. *Physical Review Letter*, 100:228501.

- Yin, L., Fu, R., Shevliakova, E., and Dickinson, R. E. (2013). How well can cmip5 simulate precipitation and its controlling processes over tropical South America? *Climate Dynamics*, 41:3127–3143.
- Zelazowski, P., Malhi, Y., Huntingford, C., Sitch, S., and Fisher, J. B. (2011). Changes in the potential distribution of humid tropical forests on a warmer planet. *Philosophical Transactions of the Royal Society of London A: Mathematical, Physical and Engineering Sciences*, 369:137–160.
- Zemp, D. C., Schleussner, C.-F., Barbosa, H., Van der Ent, R., Donges, J. F., Heinke, J., Sampaio, G., and Rammig, A. (2014a). On the importance of cascading moisture recycling in South America. *Atmospheric Chemistry and Physics*, 14:13337–13359.
- Zemp, D. C., Wiedermann, M., Kurths, J., Rammig, A., and Donges, J. F. (2014b). Node-weighted measures for complex networks with directed and weighted edges for studying continental moisture recycling. *Europhysics Letters*, 107(58005).
- Zhang, Y., Leuning, R., Hutley, L. B., Beringer, J., McHugh, I., and Walker, J. P. (2010). Using long-term water balances to parameterize surface conductances and calculate evaporation at 0.05 degree spatial resolution. *Water Resources Research*, 46(W05512).
- Zhou, C., Zemanová, L., Zamora, G., Hilgetag, C. C., and Kurths, J. (2006). Hierarchical organization unveiled by functional connectivity in complex brain networks. *Physical Review Letter*, 97(238103).
- Zhou, L., Tian, Y., Myneni, R. B., Ciais, P., Saatchi, S., Liu, Y. Y., Piao, S., Chen, H., Vermote, E. F., Song, C., et al. (2014). Widespread decline of congo rainforest greenness in the past decade. *Nature*, 509:86–90.